Master's thesis

NTNU
Norwegian University of Science and Technology
Faculty of Natural Sciences
Department of Biology

Yemima Tanudjaja

Early Warning Signs and Dynamics of H_2S Production in Recirculating Aquaculture System

Master's thesis in Ocean Resources
Supervisor: Murat V. Ardelan
Co-supervisor: Mathew K. Avarachen
June 2021

NTNU
Norwegian University of
Science and Technology

Yemima Tanudjaja

Early Warning Signs and Dynamics of H_2S Production in Recirculating Aquaculture System

Master's thesis in Ocean Resources
Supervisor: Murat V. Ardelan
Co-supervisor: Mathew K. Avarachen
June 2021

Norwegian University of Science and Technology
Faculty of Natural Sciences
Department of Biology

NTNU
Norwegian University of
Science and Technology

Abstract

The introduction of seawater, especially in post-smolt recirculating aquaculture system (RAS), has led to the formation of hydrogen sulfide (H_2S) which is one of the major challenges in RAS that has caused sudden mass fish mortality in recent years. Some preventive measures have been taken to reduce the occurrence of H_2S. However, a reliable system that can provide warning indicators indicating a situation leading to H_2S is needed. Study of oxidation-reduction (redox) reactions becomes important in determining some possible warning indicators for H_2S. According to the redox sequence, several electron acceptors can be used as warning signs, such as nitrate (NO_3^-), manganese (II) (Mn (II)), and iron (II) (Fe (II)) as their redox reactions precede the generation of H_2S. This study focuses on the potential of Mn (II) and Fe (II) to be the warning indicators for H_2S in RAS and the evaluation of their analysis methods. Furthermore, the development time of sulfidic condition in RAS as well as the total H_2S production potential from RAS were also assessed to provide a complete picture of H_2S generation in RAS.

In this study, the assessment of Mn (II) and Fe (II) as warning indicators for H_2S along with the production of H_2S from Atlantic salmon (*Salmo salar* L.) organic waste were conducted for 25 days under batch incubation consisting of two treatment conditions, with and without the addition of ~6 mM of nitrate. Fe (II) analysis was performed in flow injection with luminol based chemiluminescence (FIA-CL) and inductively coupled plasma mass spectrometry (ICP-MS), whereas Mn (II) concentrations were measured in ICP-MS only. The concentrations of H_2S were measured spectrophotometrically with methylene blue method. In addition, measurement of redox potential (E_h), pH, and dissolved O_2 were also carried out.

The addition of nitrate could inhibit the production of H_2S until day 15, while in the control (without nitrate addition), an increase in H_2S level was observed since day 2. The total H_2S production during 25 days of incubation ranged from 2.4–2.7 µM. In the nitrate treatment, the first increase in Mn (II) occurred from day 1, while the concentration of Fe (II) remained as low as the initial level until day 8 (measured with ICP-MS) and day 11 (measured with FIA-CL). In comparison to H_2S, Mn (II) increased well before H_2S formation, about 15 to 17 days earlier. On the other hand, Fe (II) was found to increase closer to H_2S production than Mn (II), around 7 to 9 days earlier. In the control, Mn (II) and Fe (II) contents were seen to increase from day 1 and day 2, respectively, overlapping with H_2S production.

The results demonstrates that both Mn (II) and Fe (II) can be used as warning indicators for H_2S formation, however, Fe (II) is considered to be a better indicator than Mn (II) because it occurs not too long before H_2S production. Despite measurement inaccuracies, FIA-CL is still reliable and considered more practical than ICP-MS to help system in RAS develop warning indicators for H_2S formation as it allows on-site application and more real time analysis.

Preface

I would like to express my gratitude to my supervisor, Professor Murat V. Ardelan, for his guidance, time, and positive motivation on this project. I would also like to thank my co-supervisors, Mathew Kuttivadakkethil Avarachen, for being a great mentor and contributing a lot of time and energy to this project. Also, to Nicolas Sanchez for teaching me patiently about FIA-CL instrument. To Anica Simic, for helping me prepare and deliver my ICP-MS samples. To Andre Meriac, for his partnership and support to this project.

I would also like to thank my teamwork: Clara Gansert, Bjørn Anda Estensen, and Magne Bjørnstad Vrangen, for the pleasant discussions, constant help and motivation throughout the project, and for being great and kind co-workers.

I am so grateful to be surrounded by many friendly people during my stay in Trondheim, Norway. Thanks to all the members of the Indonesian Student Association in Trondheim (PPIT) who made my stay in Trondheim enjoyable.

I am also very grateful to my parents and family for their love, support, and prayers. And finally, to Christopher Lawrence, to whom I am most grateful for his endless love, support, and motivation.

Table of Contents

List of Figures

List of Tables

List of Abbreviations (or Symbols)

CH_4	Methane
CO_2	Carbon dioxide
DNRA	Dissimilatory nitrate reduction to ammonia
DO	Dissolved Oxygen
DOC	Dissolved organic carbon
DOM	Dissolved organic matter
E_h	Redox potential
H_2O_2	Hydrogen peroxide
Fe	Iron
FIA-CL	Flow injection analysis with chemiluminescence
H_2S	Hydrogen sulfide
HCl	Hydrochloric acid
HNO_3	Nitric acid
HS^-	Bisulfide
ICP	Inductively coupled plasma
ICP-MS	Inductively coupled plasma mass spectrometry
K_2CO_3	Potassium carbonate
LC50	Lethal concentration 50
LMCT	Ligand-to-metal charge transfer
Mn	Manganese
N_2	Nitrogen gas
N_2O	Nitrous oxide
NH_4^+	Ammonium ion
NO_3^-	Nitrate
NOB	Nitrite oxidizing bacteria
O_2	Oxygen
RAS	Recirculating aquaculture system
Redox	Reduction-oxidation
ROS	Reactive oxygen species
S^{2-}	Sulfide
SO_4^{2-}	Sulfate
SRB	Sulfate reducing bacteria
TAN	Total ammonia nitrogen

1 Introduction

Recirculating aquaculture system (RAS) has been globally used to produce juvenile Atlantic salmon (salmon smolts) on land, especially in Norway, and has addressed major environmental concerns in ocean-based aquaculture and land-based flow-through systems. The advanced technology in RAS is beneficial not only to reduce environmental footprints by allowing more concentrated waste streams, but also to help maintain resources availability due to less water consumption and thus less energy usage to heat the water. In addition, full control over water quality and stability as well as better utilization of space and tank capacity complement the full potential benefits of RAS to become the major aquaculture industry in the future (Fjellheim et al., 2017).

In Norway, the more traditional freshwater RAS has been in operation for many years to rear Atlantic salmon to the smolt stage. Nowadays, there has been an expansion to raise post-smolts in RAS before releasing them into the sea. The goal is to reduce costs associated with permits or license fees (EY, 2019); shorten growth time in open cages which contributes to increasing production stability by minimizing biological risk and exposure to lice, parasites, and diseases, as well as reducing the risk of escapes (Ytrestøyl et al., 2020); and better utilization of maximum allowed biomass (MTB) that leads to higher production yields from each production site (Bjørndal and Tusvik, 2017). In addition, raising post-smolt salmon on land may significantly lower production time at sea and increase fish robustness, health, and growth rates due to better production control (Nofima, 2015).

Despite the extensive benefits of RAS, however, there are some challenges that are primarily related to water quality. Numerous factors circulating in the water ranging from biological, chemical, and physical conditions, such as bacteria, viruses, algae, fungi, ammonia, CO_2, O_2, temperature, pH, metals, organic matter, and salinity, influence the water quality and ultimately affect optimal conditions for fish growth and development. In comparison to traditional systems such as flow-through system and sea-cages, harmful substances and toxic metabolites from fish or bacteria may accumulate in RAS due to the recirculating water. This situation will lead to suboptimal condition for the fish, especially if the water treatment system is not carried out well (Fjellheim et al., 2017).

One of the major challenges in RAS is the risk of hydrogen sulfide (H_2S) production which is a serious threat to fish health and welfare. In recent years, there have been incidents of sudden mass fish mortality and a strong unpleasant odor around RAS area, especially in post-smolt production, caused by H_2S (Åtland and Stenberg, 2019). Utilization of seawater in post-smolt RAS triggers higher generation of H_2S by sulphate reducing bacteria (SRB) due to large amount of sulphate in seawater (~2700 mg/L), whereas in comparison, freshwater only contains 5–50 mg/L of sulphate (Boyd, 2014). In addition, RAS provides perfect condition for sulphate reduction since it is biologically very active and, therefore, potentially rich in organic matter, particles, biofilms, ammonia, and nitrates. This situation, along with proper microbial community, temperature, and pH of the water, facilitates anaerobic condition, which is the fundamental factor of H_2S production, and hence affect the quantity and production rate of H_2S (Muyzer and Stams, 2008).

H_2S has been shown to be extremely toxic to both freshwater and marine fish species with LC50 varying between species. The LC50 for most freshwater species is between 20–50 µg/L, equivalent to 0.6–1.5 µM (Smith and Oseid, 1974), while for marine fish, it ranges from 50–500 µg/L or 1.5–15 µM (Boyd, 2014). Acute exposure to 22–29 µM H_2S, which is equivalent to 0.75–0.99 mg/L H_2S, has been reported to cause significant stress and damage to the gill tissue of salmon smolts leading to reduced growth and susceptibility to disease. Furthermore, chronic exposure to 7.8 µM H_2S also leads to liver damage and reduced growth of salmon smolts (Kiemer et al., 1995).

Some preventive approaches have been taken to reduce the occurrence of H_2S in the water, such as performing good cleaning practices, establishing a good system design, and maintaining maximum allowed nitrate concentration to prevent the sulphate reduction. Nevertheless, since H_2S is a severe threat for the fish, the development of H_2S should be identified as early as possible. The study of oxidation-reduction (redox) reactions in RAS may be useful for determining some possible warning indicators for H_2S since the formation of H_2S involves the exchange of electrons between sulphate and accumulated organic matter under anaerobic condition (Weiner, 2007).

In general, redox reaction involves microorganisms, electron donors from organic carbon, and electron acceptors, such as O_2, NO_3^-, Mn (IV), Fe (III), SO_4^{2-}, and CO_2. It can occur under both aerobic and anaerobic condition, depending on the type of bacteria and availability of electron acceptors. In the absence of oxygen or under anaerobic condition, microbes use other electron acceptors to produce energy from organic matter in this following order: NO_3^-, Mn (IV), Fe (III), SO_4^{2-}, and CO_2. This order marks the highest to lowest energy obtained by the bacteria. This means that after NO_3^- disappears, Mn (IV) and Fe (III) will be the next preferred electron acceptor before SO_4^{2-} is reduced to produce H_2S (Weiner, 2007). The reduction of Mn (IV) and Fe (III) will release soluble Mn (II) and Fe (II), respectively. Therefore, an increase in the concentration of these ions is proposed as warning indicators for H_2S.

1.1 Recirculating Aquaculture System

Fish in RAS are reared in several fish tanks under a controlled environment regulated by several water treatment systems, which typically consist of mechanical filter, biofilter, CO_2 degasser, protein skimmer, and oxygen cones. Some RASs also include disinfection systems such as UV and ozone. Each component plays distinct and important roles to maintain the water quality and stability as close to optimum level as possible. Apart from fish, there are also heterotrophic bacteria living within the system. Both fish and heterotrophic bacteria consume O_2 and produce CO_2, ammonia, and particles, as a result of feeding and metabolism activities. Accumulation of these products will cause poor water condition which can be toxic to fish. Therefore, the water treatment system as in the RAS is needed to maintain optimal water quality levels (Fjellheim et al., 2017).

As the first treatment step, the mechanical filter aims to remove large particles (> 20 µm) from the water coming out of the fish tanks. The removal of large particles is important as it helps increase the work efficiency of further water treatment systems. Two commonly used mechanical filters are belt filter and drum filter. After being freed from large particles, the water usually moves into the biofilter to get total ammonia, both ionized (NH_4^+) and unionized form (NH_3), converted into nitrite (NO_2^-) and then into nitrate (NO_3^-). This process is known to be carried out by two groups of autotrophic nitrifying bacteria, namely ammonia oxidizing bacteria (AOB), such as *Nitrosomonas*, and nitrite oxidizing bacteria (NOB), such as *Nitrobacter.* Both ammonia and nitrite are very

toxic for the fish. They cause respiratory system disorders by disrupting gill physiological function and oxygen delivery, as well as interfering with fish osmoregulation and nervous system. Furthermore, ammonia, which is mainly present as NH_3 under higher pH, is more harmful to the fish than unionized form of ammonia (NH_4^+). Norwegian Food Safety Authority has set safety level of less than 2 mg/L TAN (total ammonia nitrogen), 2 µg/L NH_3-N, 0.1 mg/L nitrite-N (in freshwater), and 0.5 mg/L nitrite-N (in seawater). Meanwhile, nitrate is less toxic and therefore can be maintained at higher concentration of 100 mg/L nitrate-N maximum for post-smolt Atlantic salmon. Efficiency of biofilter is normally 90%. The water from the biofilter will contain low TAN and medium to high nitrate due to some denitrification processes of nitrate into N_2 gas by the bacteria in the biofilter under anaerobic condition (Fjellheim et al., 2017).

From the biofilter, the water is transferred to the degasser to remove CO_2 from the water. Many studies have shown that high concentration of CO_2 in the water disrupts the fish respiration by lowering the pH and consequently decreasing the maximum carrying capacity of hemoglobin to carry O_2 throughout the body of the fish. For Atlantic salmon, it is important to maintain the CO_2 concentration to be below 15 mg/L. The removal of CO_2 from the water is achieved by using an aerator such as trickling filter. The principle is to maintain the concentration gradient of the dissolved CO_2 in the water and the CO_2 in the surrounding air within the degasser. Since the CO_2 content inside and around the degasser are lower than in the water, the CO_2 from the water will be vented out of the water. The outcoming water from the degasser usually contain around 70–80% less CO_2 depending on the efficiency of the degasser (Fjellheim et al., 2017).

The next typical treatment step commonly used in marine RAS is removal of bacteria and smaller particles (< 20 µm) by using protein skimmer. The accumulation of smaller particles including bacteria may create anaerobic condition that is favorable for the opportunistic bacteria to grow and thus produce H_2S. The working principle of the protein skimmer is generating foam or bubbles that are used to capture and harvest smaller particles in the water. Furthermore, as both fish, heterotrophic, and nitrifying bacteria consume O_2 for their respiration and activity, the O_2 content in the water is thus significantly reduced. Therefore, as a final step before the water flows back into the fish tank, the O_2 is added up to 100–110% saturation to fulfill the fish O_2 requirement as assigned by NFSA (Norwegian Food Safety and Authority). Pressurized oxygen tanks or liquid oxygen tanks are commonly used to supply O_2 to the water in the RAS (Fjellheim et al., 2017).

It is important that water quality as well as interaction between water quality parameters, such as pH, O_2, TAN, metals, and H_2S, are monitored and maintained within the acceptable levels. In line with the increasing trend of post smolt salmon production on land, many RASs have used seawater in their production systems. However, the use of seawater poses different challenges to freshwater RAS, such as lower biofilter and degasser efficiency, formation of rest oxidants from ozone system, corrosion on RAS components, and higher possibility of H_2S formation due to higher sulphate concentration in seawater (2700 mg/L) compared to freshwater (2.2 mg/L) (Fjellheim et al., 2017; Boyd, 2014).

1.2 Hydrogen Sulfide (H_2S)

H_2S is an extremely toxic gas to humans and aquatic life. It exists as a colorless and flammable gas with a characteristic of strong rotten egg odor. Due to its higher density than air, which is 0.99 g/ml of H_2S compared to 0.00128 g/ml of air, H_2S tends to

accumulate in the bottom area of low O_2 environment (National Center for Biotechnology Information, 2020; Opphardt, 2003). It has a molecular weight of 34.08 g/mol (National Center for Biotechnology Information, 2020) and is soluble in water at 100 mM at 25°C (Calhoun et al, 1988) and 122 mM at 20°C (Li and Moore, 2008). In aqueous solution, it always equilibrates with its anions: bisulfide (HS^-) and sulfide (S^{2-}). The equilibrium reaction of H_2S is shown in the equation below (Li and Lancaster, 2013):

$$H_2S_{(g)} \rightleftharpoons H_2S_{(aq)} \rightleftharpoons HS^- + H^+ \rightleftharpoons S^{2-} + 2\ H^+$$

The aqueous form of H_2S is volatile, yet it is extremely water soluble which making it harder to aerate than CO_2. Moreover, the dissociation process of H_2S is highly dependent on pH. This means that the pH solution determines the concentration of $H_2S_{(aq)}$ (Yongsiri et al., 2004; Åtland and Stenberg, 2019). When the pH increases, the concentration of H_2S will be reduced significantly as it dissociates into HS^- and S^{2-}. Unlike H_2S and S^{2-} which are considerably toxic, HS^- is by nature not toxic. As shown in Figure 1.1, H_2S starts to dissociate at pH around 5 and fully forms HS^- at pH around 9. At pH 7, both H_2S and HS^- are in approximately equal proportions. Meanwhile S^{2-} starts to exist at pH above 11. The RAS, especially for smolt and post smolt salmon production, operates typically at pH between 6.2–7.8. This means that the H_2S fractions mainly exist in the form of H_2S and HS^- (Åtland and Stenberg, 2019).

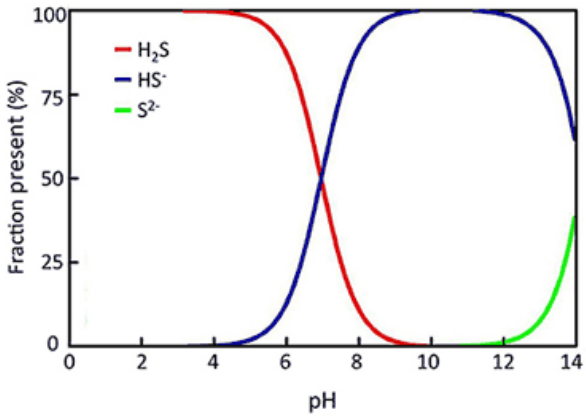

Figure 1.1: The equilibrium of H2S fractions at different pH (Åtland and Stenberg, 2019)

H_2S occurs naturally in many biological systems, such as culture ponds, municipal sewage, and industrial effluents, mainly from sulphate reduction under anaerobic environment and in the presence of accumulated organic matter, performed by sulphate reducing bacteria. These bacteria use oxygen from sulphate (SO_4^{2-}) as an electron acceptor to degrade organic matter and produce energy. Therefore, the sulphate concentration in the water, in addition to pH, temperature, and availability of organic matter, largely determines the H_2S production rate and concentration in the water. Generally, seawater contains higher sulphate than freshwater, which is around 2700 mg/L on average. Meanwhile, freshwater usually contains only 5–50 mg/L of sulphate. Increased use of seawater, such as in post smolt production, has a higher risk of H_2S formation (Boyd, 2014). However, the H_2S concentration in the water or sediment can decrease due to several further reactions, such as H_2S oxidation by bacterial sulfide oxidation, reaction with metal ions to form black precipitates of metal sulfides, such as iron-, and manganese sulfides, and diffusion from the sediment into the water as a gas phase (Zhang and Millero, 1993; Boyd, 2014).

Many studies have shown severe consequences of H_2S in fish. It interferes with the respiration system by inhibiting the release of oxygen leading to cellular anoxia which eventually blocks the ATP production (Kiemer et al., 1995). In addition, long term exposure to H_2S can reduce growth, fecundity, and swimming performance (Adelman and Smith, 1970; Oseid and Smith, 1972). The LC50 values of H_2S varies between fish species. A study has reported that the LC50 values of H_2S for several freshwater fish species are between 20–50 µg/L, equivalent to 0.6–1.5 µM (Smith and Oseid, 1974), while for marine fish are between 50–500 µg/L or 1.5–15 µM (Boyd, 2014). It has also been reported that an acute exposure to 22–29 µM H_2S, which is equal to 0.75–0.99 mg/L H_2S, resulted in significant stress and damage to the gill tissue of salmon smolts leading to reduced growth and susceptibility to disease. Furthermore, a chronic exposure to 7.8 µM H_2S had caused liver damage and decreased growth in salmon smolts although some signs of adaption were detected (Kiemer et al., 1995).

1.3 H_2S in RAS

There are several factors causing the H_2S formation in RAS apart from the natural sulphate content both in freshwater and seawater. These are stagnant water and sludge, dead zones or corners, thick biofilm, too low water flow that can lead to dirt sedimentation inside the pipe, infrequent pipe cleaning and flushing, and other technical problems that may cause water backlash around the sediments and release all the H_2S formed from the sediments (Yu and Bishop, 1998; Attramadal, 2020). In addition, at the end of the production cycle, when the fish are starving, ammonia production is reduced significantly. As a result, nitrate concentration in the water will decrease. This means there will be less nitrates available as electron acceptors to mediate the decomposition reaction of organic matter by anaerobic bacteria. Consequently, the H_2S concentration is usually higher at the end of the production cycle (Attramadal, 2020).

Approaches have been taken to prevent the H_2S formation. First, establishment of good system designs, such as good material coating, short and fewer number of pipes to avoid dead zones, as well as good water velocity and hydraulic retention time, have been put into practice to help secure the system from H_2S. Surveillance by using sensors in addition to routine cleaning and sediment removal has also been applied to reduce the risk of H_2S formation and support the early detection of H_2S. Under detectable H_2S condition, identifying sources, introducing clean water, maintaining high nitrate level above 40 mg/L, and increasing the pH of the water are usually taken as initial measure to deal with and save the fish from H_2S (Attramadal, 2020; Åtland and Stenberg, 2019).

1.4 Denitrification in RAS

As the biofilters continuously convert ammonia into nitrate, the amount of nitrate in RAS may accumulate and become harmful to fish. In the RAS, there are several denitrification mechanisms to prevent the accumulation of nitrates and maintain its concentration below their maximum limit in addition to heterotrophic denitrification when oxygen concentration drops to the critical level. Regulating water exchange rate is the main mechanism to dilute the nitrate from the system and maintain its level to around 100 mg NO_3-N/L. Typically, RAS consumes 300–400 L new water per kg feed per day to maintain the maximum allowed nitrate concentration (Fjellheim et al., 2017).

Nitrate can also be removed from the system through dissimilatory pathways which mostly takes place in anaerobic biofilters. This mechanism involves two groups of bacteria which produce different end products. One group of bacteria, namely

fermentative anaerobic bacteria, reduces nitrate to either nitrite or ammonia ($NO_3^- \rightarrow NO_2^- \rightarrow NH_4^+$) (this process is called dissimilatory nitrate reduction to ammonia (DNRA)), while the other group, mainly facultative anaerobes called denitrifiers, reduces nitrate to nitrogen gas (N_2) via nitrite ($NO_3^- \rightarrow NO_2^- \rightarrow NO \rightarrow N_2O \rightarrow N_2$) (the process is called denitrification) (van Rijn et al., 2006). Environmental conditions highly affect the ratio of N_2O to N_2 produced by the denitrifiers. Higher O_2 concentration, the presence of S^{2-}, and lower pH support the higher N_2O to N_2 ratio. This is because nitrous oxide reductase, which produces N_2, is more sensitive to these conditions which results in inhibition of N_2O conversion to N_2 (Amador and Loomis, 2018).

In the DNRA pathway, nitrate is used as an electron acceptor when the fermentative bacteria cannot reduce organic matter (fermentation). Meanwhile, in the denitrification, the bacteria will use nitrate as an electron acceptor when O_2 is not available (Tiedje, 1990). The majority of denitrifiers are heterotrophic denitrifiers that use organic carbon, such as alcohols, carbohydrates, amino acids, and fatty acids, as a source of carbon and electrons. Another denitrifying bacterium is autotrophic denitrifier which is prevalent in a reduced environment low in dissolved carbon. They will use reduced inorganic compounds, such as Fe (II), Mn (II), sulfide (S^{2-}), and CH_4 as electron donors and inorganic carbon as a carbon source (Korom, 1992).

The availability and type of organic carbon as well as the redox status of the aquatic environment affect how the reaction takes place and which groups of organisms are present. High C/N ratio leads to H_2S production and favors DNRA bacteria over denitrifiers (Tiedje, 1990). In contrary, low C/N ratio coupled with low O_2 condition, suboptimal pH, or high light intensities leads to incomplete reduction of nitrate, resulting in the accumulation of nitrite, nitric oxide (NO), and N_2O (van Rijn and Rivera, 1990).

In RAS, denitrification is mostly performed in anaerobic biofilters with the addition of proper amount of organic matter, such as sludge from the system or methanol. The utilization of organic matter in the denitrification proceeds as follows:

$$2C_{18}H_{19}O_9N + 13NO_3^- + 5H^+ = C_{18}H_{19}O_9N + 7N_2 + 12H_2O + 18CO_2$$

Through denitrification, the consumption of new water can reduce up to 30–40 L per kg feed per day (Fjellheim et al., 2017).

1.5 Reduction Oxidation (Redox) Reaction

The presence of microorganisms, organic matters, salts, metals, inorganic nonmetals, as well as their interaction with physical water quality, builds complex chemical and biological reactions in the water. Biodegradation or chemical breakdown of organic materials by microorganisms is one of the many important reactions happening in the water. This is done mainly through oxidation-reduction (redox) reactions which principally involve a series of processes of transferring electrons from organic carbons which function as electron donors to other compounds as electron acceptors. This process results in metabolic energy for the microbes, carbon, and other materials or elements that are used to sustain microbial growth (Weiner, 2007).

There are six basic elements for biodegradation to occur. They consist of microorganisms which are mainly bacteria; electron donors from organic carbon compounds that act as both food and carbon sources; electron acceptors such as O_2, NO_3^-, Mn (IV), Fe (III), SO_4^{2-}, and CO_2; carbon from organic carbon; nutrients such as nitrogen, phosphorus, calcium, magnesium, and iron; and environmental conditions including pH, temperature, salinity, oxygen content, etc. Redox reactions can occur under aerobic and anaerobic

conditions, depending on the availability of electron acceptors and type of bacteria. In the presence of sufficient oxygen, microbes use oxygen as an electron acceptor to oxidize organic carbon and transform it into carbon dioxide and water. In contrast, in the absence of oxygen or anaerobic condition, microbes use other electron acceptors, NO_3^-, Mn (IV), Fe (III), SO_4^{2-}, and CO_2, to convert organic carbon into water and carbon dioxide or methane. Moreover, the amount of energy produced from aerobic respiration is higher than anaerobic respiration (Weiner, 2007).

The preferences of electron acceptors used by microbes to oxidize organic matter follow the following order based on the energy produced and the availability of the electron acceptors: O_2, NO_3^-, Mn (IV), Fe (III), SO_4^{2-}, and CO_2. This order signifies the highest to lowest energy obtained by the bacteria from utilizing these electron acceptors to degrade organic matters. Since these bacteria obtain the greatest amount of energy from O_2, the aerobic respiration always takes place prior to the anaerobic respiration whenever adequate dissolved O_2 is accessible. When the oxygen is fully consumed, these microbes will use NO_3^-, Mn (IV), Fe (III), SO_4^{2-}, or CO_2, according to the availability of these electron acceptors in that sequence. This means that when NO_3^- disappears, Mn (IV) and Fe (III) will be the next preferred electron acceptor for anaerobic bacteria. After Mn (IV) and Fe (III) are no longer available, the anaerobic bacteria will reduce SO_4^{2-} and produce toxic H_2S (Weiner, 2007). The complete biodegradation reactions of each electron acceptors are shown in Table 1.1.

Process	Electron Acceptors	Complete Reactions
Aerobic respiration	O_2	$\{CH_2O\} + O_2 \rightarrow CO_2 + H_2O$
Denitrification	NO_3^-	$5\{CH_2O\} + 4NO_3^- + 4H^+ \rightarrow 5CO_2 + 2N_2 + 7H_2O$
Manganese reduction	Mn (IV)	$\{CH_2O\} + 2MnO_{2(s)} + 4H^+ \rightarrow CO_2 + 2Mn^{2+} + 3H_2O$
Iron reduction	Fe (III)	$\{CH_2O\} + 4Fe(OH)_{3(s)} + 8H^+ \rightarrow CO_2 + 4Fe^{2+} + 11H_2O$
Sulphate reduction	SO_4^{2-}	$2\{CH_2O\} + SO_4^{2-} + H^+ \rightarrow 2CO_2 + HS^- + 2H_2O$
Methanogenesis	CO_2	$2\{CH_2O\} \rightarrow CH_4 + CO_2$

Note: $\{CH_2O\}$ indicates the organic matters being degraded (Weiner, 2007)

Table 1.1 Electron acceptors and their complete biodegradation reactions

Furthermore, the energy released during the redox reaction has a correlation with redox potential (E_h). If less energy is released during the redox reaction, the value of redox potential becomes more negative. In other words, as biodegradation progresses towards more anaerobic condition, the redox potential of the water decreases to as low as –500 mV. Therefore, the value of redox potential indicates which electron acceptors are being used in the biodegradation redox reaction. Anaerobic biodegradation starts to occur when the redox potential is at +740 mV and the O_2 level is reduced to less than 0.5 mg/L. In this state, anaerobic biodegradation begins with denitrification process. This process proceeds well at pH between 6.2–10.2 and E_h between –200 mV and +665 mV. After nitrate/nitrite has been depleted, the reduction of Mn (IV) to Mn (II) will initiate, followed by the reduction of Fe (III) to Fe (II). Both Mn (II) and Fe (II) are soluble in water. The reduction of Mn (IV) occurs at E_h +520 mV, while Fe (III) initiates at lower E_h –50 mV. The available SO_4^{2-} is also used as an electron acceptor when no more dissolved O_2, NO_3^-, Mn (IV), are Fe (III) are available. The SO_4^{2-} reduction occurs at pH 7 and E_h –200 mV (Weiner, 2007).

1.6 Manganese in Seawater

Manganese (Mn) is an important micronutrient and a potential redox reactant, especially for marine microbial communities. It exists mainly in three oxidation states which are widely distributed in global ocean: soluble Mn (II), soluble Mn (III)-ligand complexes, and solid Mn (IV) oxides (Hansel, 2017). Each oxidation state has different tendency to donate or accept electrons in its participation to mediate redox reaction with both organic and inorganic compounds and to recycle many bioactive elements, such as carbon, nitrogen, oxygen, sulfur, and iron. The solid Mn (III/IV) oxides and aqueous Mn (III)-ligand complexes are two of the strongest natural oxidants in seawater that also participate in the biodegradation reaction. However, Mn (III) is an intermediate product in the oxidation of Mn (II) to Mn (IV). Not only donating electron, Mn (III)-ligand complexes also accept electrons. This property makes Mn (III) a very reactive compound (Oldham et al., 2019). Meanwhile, the soluble Mn (II) has tendency to be oxidized to Mn (IV) which is predominantly performed by microorganism. This biological Mn (II) oxidation occurs relatively fast compared to chemical Mn (II) oxidation (Tebo, et al., 2004).

Mn (IV), which can exist as solid oxide, oxyhydroxide, and hydroxide, are favored under aerobic, high pH, and high E_h condition, while Mn (II) is formed in the absence of O_2 and under low pH and E_h condition. However, Mn (II) can persist as Mn^{2+} cation in naturally oxygenated waters (Tebo, et al., 2004). The soluble Mn (III), which is unstable and acts both as an electron acceptor and donor, exists in the suboxic zone or at the oxic/anoxic sediment interface and is rapidly disproportionated at pH below 7 to solid Mn (IV) oxide at oxic zone and to soluble Mn (II) at anoxic zone. In the presence of suitable ligand (L), Mn (III) is stabilized by the ligand and form Mn (III)-L complex (Trouwborst et al., 2006). Due to the characteristic of their preferred condition, the distribution of each Mn species varies across seawater depth. In surface waters, Mn (III)-L complexes dominates the concentration of Mn, whereas Mn (IV) oxide is found abundantly at bottom ocean waters (Oldham et al., 2019). Figure 1.2 shows the equilibrium diagram of dissolved Mn activity as a function of pH and E_h.

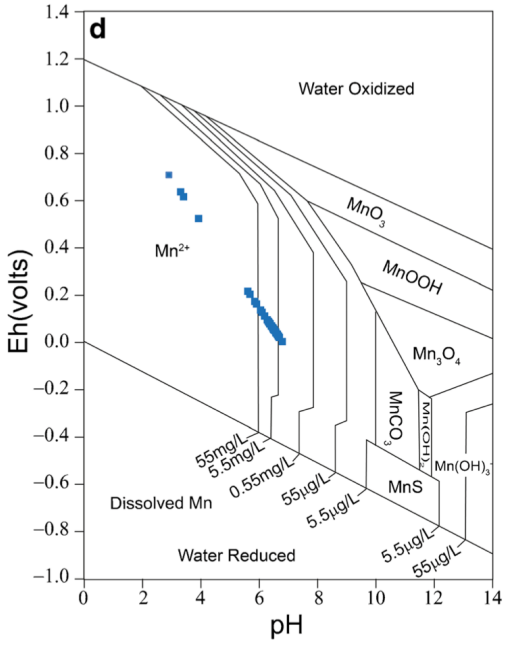

Figure 1.2: Equilibrium diagram of dissolved Mn activity as a function of pH and Eh (Hem, 1985; Khozyem et al., 2019)

In seawater, Mn is mainly supplied by continuous input of atmospheric dust. Other sources of Mn into the ocean are river (Aguilar-Islas and Bruland, 2006), sediments (Middag et al., 2013), melting sea ice, and hydrothermal vents (Middag et al., 2011). The concentration and oxidation states of Mn also varies across the water column. In the surface waters, Mn exists in small concentrations with soluble Mn predominates due to photochemical reduction of Mn (IV) particulate by dissolved organic compounds (Sunda et al. 1983). However, regardless of the speciation, the concentration of Mn in the euphotic zone can decrease due to uptake by phytoplankton to assist the photosynthesis; and removal of dissolved Mn (II) by oxidation to Mn (IV) or other oxidation states followed by subsequent adsorption by particles that continuously sink to the bottom water (Sunda, 1994). Conversely, since the formation of Mn (IV) is mainly performed by manganese oxidizing bacteria, which are photo-inhibited, Mn (IV) particulates are found mainly below the photic zone (Chapin, 1990).

Determination of Mn (II) in seawater can be achieved by exploiting Mn (II) to catalyze the oxidation of 7,7,8,8-tetracyanoquinodimethane (TCNQ) in an alkaline solution that produces light. The principle is to measure photon emission rate resulting from chemiluminescent reaction which is proportional to the Mn (II) concentration. This principle has been appropriately adapted for flow-injection analysis system in order to develop a rapid and reliable method of Mn (II) determination in sea water (Chapin et al., 1991).

1.7 Iron in Seawater

Iron is a reactive trace metal element existing at significantly low concentration in the oceans. In aqueous solution, iron occurs in two oxidation states, trivalent or ferric form (Fe (III)) and divalent or ferrous form (Fe (II)). Fe (III) exists predominantly in the ocean in complex form with inorganic and organic materials and is subject to hydrolysis resulting in formation of various Fe (III) oxyhydroxide precipitates. Meanwhile, Fe (II) occupies most of dissolved iron state in natural water exposed to the atmosphere (pH 5.0–8.0 and E_h 0.3–0.5 V). Especially at alkaline pH, ferrous is more soluble than ferric iron (Santana et al., 2005; King and Farlow, 2000).

Both ferrous and ferric iron can exist in various states in aqueous solution and have a tendency to create stable soluble complex ions with organic or inorganic materials, such as oxide, hydroxide, chloride, fluoride, phosphate, sulphate, and carbonic ions. In terms of Fe (III), the most common species is ferric hydroxide ($Fe(OH)_3$) which has a very low solubility, yet can be ionized to become $Fe(OH)_2^+$, FeO^+, $FeOH^{2+}$, Fe^{3+}, FeO_2^-, or FeO_4^{2-}. Meanwhile, as for Fe (II), species such as Fe^{2+} (most frequent form), $FeCl^-$, and $FeSO_4$, turn out to be quite stable than other ferrous species such as $Fe(OH)_2$, $FeOH^+$, $FeCO_3$, and $Fe(CO_3)_2^{2-}$. These unstable Fe (II) species are rapidly oxidized by atmospheric oxygen (O_2) and hydrogen peroxide (H_2O_2) into Fe (III) under pH and E_h condition of natural water (Santana et al., 2005; King and Farlow, 2000).

Lifetime, amount, and species of iron in the water at equilibrium are strongly influenced by the amount of oxidant and water chemistry variables, which include pH, redox potential (E_h), temperature, light intensity, salinity, dissolved O_2, reactive oxygen species (ROS), and organic matters. pH affects the ion activities and thus establish hydroxide complexes as well as solid hydroxides. Regarding Fe (II) oxidation, strong acid or low pH will slow down the oxidation reaction of Fe (II). A stability-field diagram related to pH and E_h for aqueous ferric-ferrous system is shown in Figure 1.3 (Hem and Cropper, 1959).

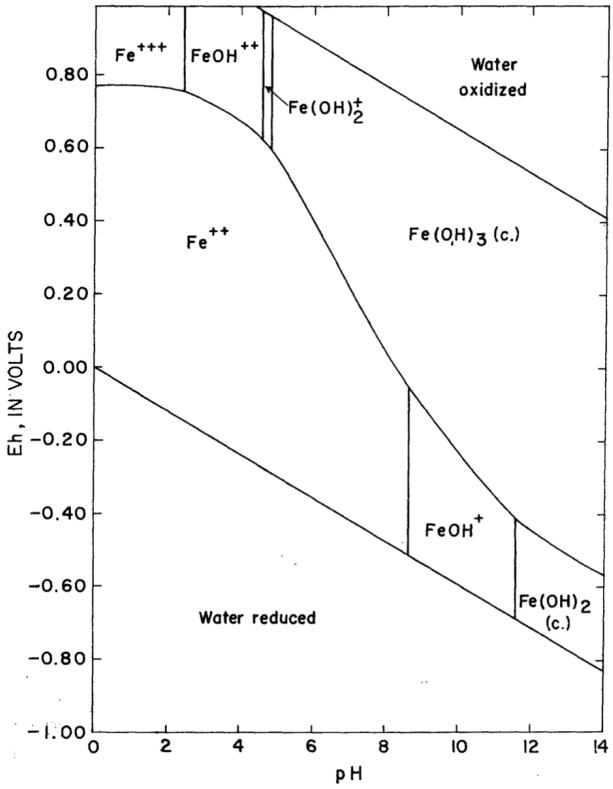

Figure 1.3: Stability field diagram for aqueous ferrous-ferric system (Hem and Cropper, 1959)

In addition to its chemical forms, iron can also be classified according to its particle size into particulate (PFe) (>0.45 μm), dissolved (dFe) (<0.45 μm), soluble (sFe) (<0.02 μm) and colloidal iron (cFe) (0.02–0.45 μm) (von der Heyden and Roychoudhury, 2015). Each fraction can form complexes with both inorganic and organic particles. In the ocean, a large portion of inorganic particulates and colloidal iron exist as hydroxides or oxides (Kuma et al., 1996). In terms of dissolved iron, the colloidal fraction comprises 90% of the dissolved form of iron in coastal waters and less than 10% in pelagic region (Bergquist et al., 2007).

The major form of iron in the oceans that controls the concentration and distribution of dissolved iron is the complex Fe (III)-binding ligands (Hunter and Boyd, 2007). In natural waters, most of the dissolved iron forms complex with organic ligands, such as humic acid or detritus materials generally produced by bacteria or phytoplankton. These organic ligands help to increase the solubility of Fe (III) (Gledhill and Buck, 2012). The occurrence of dissolved iron, which largely in the Fe (II) form, increases in low E_h and O_2 or reducing environments, as in decaying organic sediments (Chever et al., 2015). de Baar and de Jong (2001) noted that dissolved iron concentration in the Southern Ocean varied from 0.03–0.5 nM, whereas higher concentrations (0.3–1.4 nM) were found at deeper depths. In general, dissolved iron concentration in the photic zone of the open ocean is typically 0.5–1 nM (Misumi et al., 2014). Moreover, Fe (II) concentration is expected to be much higher in freshwater, around up to 50 mg/L or 0.9 mM (van Beek et al., 2021).

Dissolved iron in the photic zone originates from both external and in-situ sources, which include atmospheric aerosols, vertical mixing and upwelling, river and bottom sediments, and biogenic recycling of cellular iron (Wells et al., 1994). The primary source of iron introduction into the open ocean is atmospheric aerosols or airborne dust which are

assembled from terrestrial particles (Moore and Braucher, 2008). In coastal waters, substantial iron input comes from riverine sources and bottom sediments in the form of organic and inorganic complexes (Wells et al., 1994). Vertical water mixing through upwelling is an important iron supply in atmospheric remote area. In the bottom sediment, iron can be bound to both inorganic and organic substances, especially phosphate (PO_4). In the deeper anoxic sediment, iron may be dissolved due to reduction process which causes ligands such as phosphate to be released and diffused into the water column (Slomp et al., 1996). Marine microorganisms also play a role in iron remineralization supply to the photic zone (Schmidt, 2016).

Iron exhibits scavenging characteristics which establishes a concentration gradient that decreases with increasing seawater age and depth. In the open ocean, dissolved iron is constantly recycled and removed from the dissolved pool through particle scavenging and biological uptake by phytoplankton (Moore and Braucher, 2007). In addition, intermediate- and deep-water irons are mainly adsorbed onto both biotic and abiotic particles, which then settle in the bottom sediment. This process leads to iron depletion in the surface water (Wells et al., 1994), which subsequently makes iron a limiting micronutrient for marine primary production as it is an essential element required for photosynthesis (Geider and Laroche, 1994), N_2 fixation (Moore et al., 2009), and building structure and maintaining productivity of marine microbial community (Tagliabue et al., 2017).

The major process regulating the iron cycling in the aqueous environment is reduction and oxidation (redox) reaction. Iron reduction, which usually happens in more acidic water, is induced by several processes which consist of photochemical reduction of Fe (III)-binding ligands (both organic and inorganic ligands) (Miller et al., 1995); reduction by Fe (III) reducing bacteria within anoxic sediments containing organic carbon (Swanner et al., 2018); reduction by hydrogen sulfide (H_2S) (Afonso and Stumm, 1992); and photochemical and enzymatic reduction in the presence of oxygen by photo-produced reactive oxygen species ($^{\bullet}O_2^-$) and bacteria, such as *Cyanobacteria* (Kranzler et al., 2011). Fe (III) bound to organic ligands, such as oxalic, citric, carboxylic, and tartaric acids, has been shown to be more photo-reactive than Fe (III) bound to inorganic ligands (Kuma et al., 1992). The photochemical reductive pathway of Fe (III) known as ligand-to-metal charge transfer (LMCT) involves electron transfer from Fe (III)-binding ligands to photoexcited Fe (III) surface atom, resulting in dissolution of Fe (II) into the solution (Barbeau et al., 2001).

As opposed to Fe (III), Fe (II) which is more soluble and labile kinetically than Fe (III), undergoes rapid oxidation predominantly performed by O_2, superoxide radicals ($^{\bullet}O_2^-$), hydrogen peroxide (H_2O_2), and hydroxyl radical ($^{\bullet}OH$). The oxidation reaction with H_2O_2, which is produced photochemically by the favor of sunlight from $^{\bullet}O_2^-$, which possibly comes from dissolved organic matter, is another dominant Fe (II) oxidation pathway in the surface seawater besides O_2. Therefore, the presence of light is also an essential factor enhancing the rate of both iron reduction and oxidation. In deeper seawater, the H_2O_2 concentration will be lower due to insufficient light penetration, and thus the Fe (II) oxidation will be dominated by O_2 (Wells et al., 1994). Furthermore, higher organic matter will also intensify the oxidation of Fe (II) by leading towards more anoxic state. However, the complex formation of Fe (II) with organic materials can reduce the oxidation rate of Fe (II) (Ramos et al., 2016).

1.8 Determination of Fe (II) and Mn (II) in Seawater

1.8.1 Determination of Fe (II) with FIA-CL

Flow injection analysis with chemiluminescence detection (FIA-CL) is a rapid and sensitive analytical technique that is widely used to determine various ions or compounds capable of forming reactive oxygen species (ROS) in aqueous solutions. This technique benefits from light generated by chemical reaction, predominantly between luminol (5-amino-2,3-dihydro-1,4-phthalazinedione) and ROS (Borman et al., 2009). The principle of FIA with luminol based chemiluminescence is the intensity of light emitted from the oxidation of luminol by ROS resulting from the oxidation of analytes, such as Fe^{2+}, PO_4^{3-}, Co^{2+}, Cr^{2+}, Cu^{2+}, NO_3^-, and H_2O_2, is proportional to the concentration of the analytes. The general oxidation reaction of luminol that produces light is shown in Figure 1.4 (Rose and Waite, 2001).

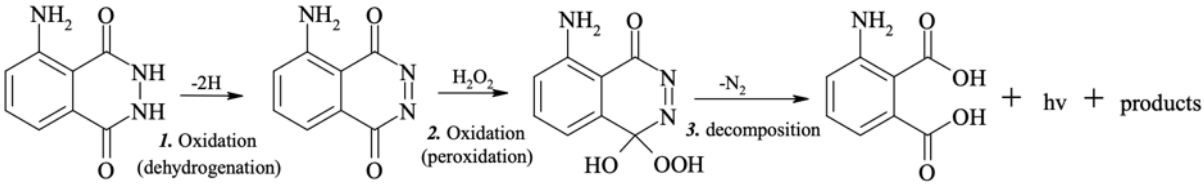

Figure 1.4: The general chemical reaction of luminol with aqueous Fe (II) to produce chemiluminescence (Borman et al., 2009)

In Fe (II) determination, Fe (II) will be oxidized and produced H_2O_2 which will catalyze the second stage of luminol oxidation as shown in Figure 1.4. Therefore, Fe (II) is not a direct catalyst but plays a role in producing oxidants that escalates the oxidation of luminol (Rose and Waite, 2001).

The presence of other species, such as fulvic acid, dissolved organic carbon (DOC) or dissolved organic matter (DOM), and redox-active metals, may reduce the sensitivity of the Fe (II) analysis with FIA-CL (Pullin and Cabaniss, 2001; O' Sullivan et al., 1995). These interferences, especially organic chelators, form complex coordination with Fe (II) and stabilize iron against oxidation by O_2 (Santana et al., 2000; Theis and Singer, 1974). This condition will lead to lower signal caught by FIA detector due to slower formation of the ROS required for the chemiluminescence of luminol. Furthermore, low pH also interferes with the signal by either enhancing or depressing the chemiluminescence formation. It enhances the signal by slowing down the pre-injection oxidation of Fe (II), resulting in more H_2O_2 that oxidize luminol in the mixing chamber. In addition, the acid can also overcome the buffer capacity of the luminol solution, which consequently will disrupt luminol dehydrogenation process (step 1) and decrease the signal, especially at nanomolar concentration of Fe (II). The detection limit of Fe (II) with FIA-CL in both marine and freshwater can be as low as sub-nanomolar concentration which is an advantage over other iron analysis methods (Croot and Laan, 2002).

Analysis with FIA-CL begins with injection of a liquid sample into a continuous liquid carrier stream. The injected sample is then dispersed in a carrier solution and flowed into a mixing coil where the sample mixes with reagent. The process is then followed by the signal detection on the detector before being washed out of the system (Harvey, 2019).

The basic components of FIA system consist of reagent, carrier, injection valve, pump, reaction coil, and detector or photon counter as shown in Figure 1.5. Specifically, the injection valve is used to introduce a sample solution into carrier stream; the pump

works to propel carrier, reagent, and sample stream through a narrow tubing; and the reaction coil is a part where sample disperses and mixes with reagent (Harvey, 2019).

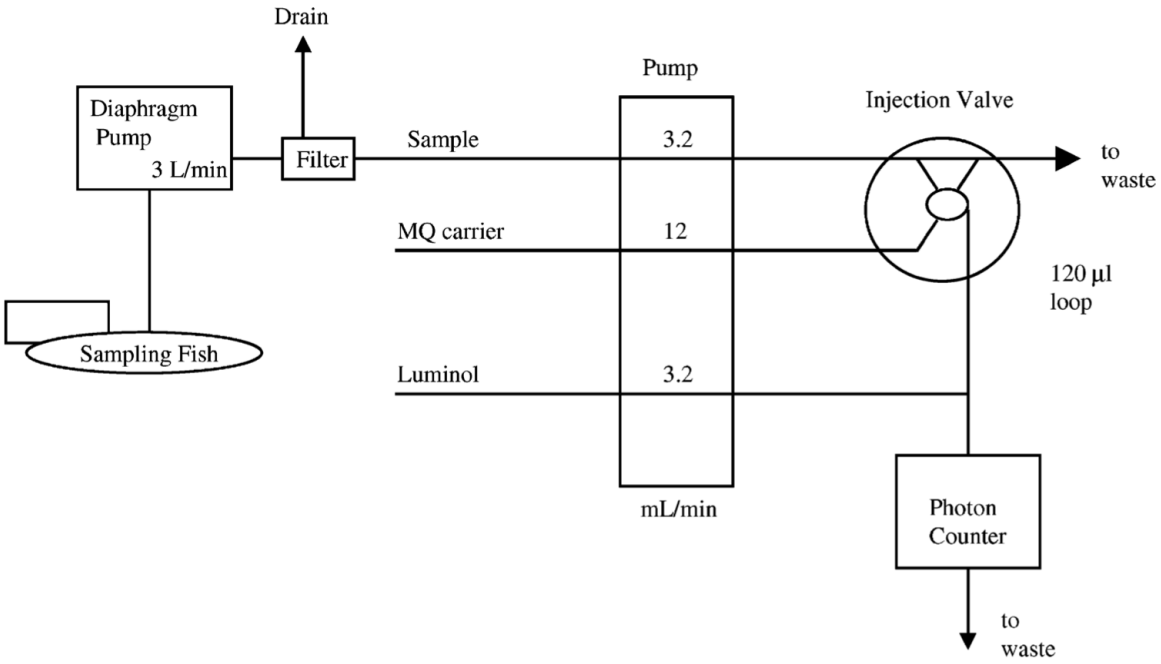

Figure 1.5: Schematic FIA diagram (Croot and Laan, 2002)

Typical output from the detector consists of a maximum peak or height (H) and an area of the peak related to the analyte concentration. The time between sample injection and the maximum peak is the time span (T) during which the chemical reaction takes place. The duration of one sample cycle is usually less than 30 seconds. The volume of injected sample ranges from 1–200 µL. Figure 1.6 shows a typical detector response of FIA system (Harvey, 2019).

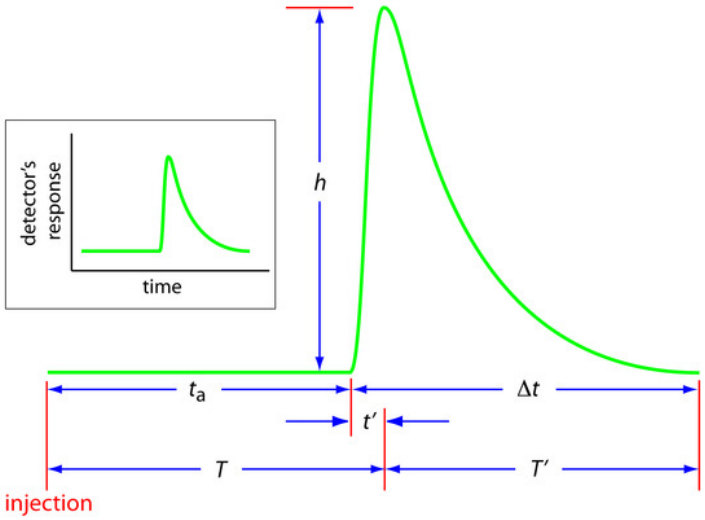

Figure 1.6: Typical FIA output from detector as a function of time (Harvey, 2019)

1.8.2 Determination of Mn (II) and Fe (II) with ICP-MS

Inductively coupled plasma mass spectrometry (ICP-MS) is an analytical technique designed to analyze multi elements simultaneously, primarily in liquid samples, at trace levels. It is advantageous since it only needs low sample volume, simple sample preparation, short analysis time, and high precision and sensitivity. However, it is expensive and requires a high level of chemical purity and staff expertise (Wilschefski and Baxter, 2019).

The principle of ICP-MS is that ionizing the sample to produce small polyatomic ions that can be detected and translated into the concentration of these ions. Dilution of the sample with an acid, such as nitric acid or hydrochloric acid, or an alkali, such as ammonium hydroxide is required prior to analysis. ICP-MS cannot distinguish different chemical species of an element. In terms of Fe and Mn, ICP-MS measures all dissolved Fe and Mn in the sample, not specifically Mn (II) and Fe (II) (Wilschefski and Baxter, 2019).

There are six fundamental components of ICP-MS: sample introduction system (nebulizer, spray chamber), inductively coupled plasma (ICP), interface, ion optics, mass analyzer and detector. Nebulizer is a tool to aerosolize the liquid samples before being introduced to the ICP. From nebulizer, the sample then enters the spray chamber to smooth out the aerosol droplets by selectively filters out the larger droplets. This is an important step because ICP cannot efficiently dissociate larger droplets (>10 μm in diameter). The sample is then atomized and ionized by high temperature in the ICP which is then transferred to the interface and ion optics region where the ions are focused and directed into the mass analyzer and finally measured by the detector (Wilschefski and Baxter, 2019).

1.9 Objectives

The general aims of this project are to study redox reactions in RAS, evaluate the dynamics of H_2S generation in RAS, and assess the potential of Mn (II) and Fe (II) to be the warning indicators for H_2S in RAS.

The specific goals are:

- To investigate development time of sulfidic condition in RAS under predetermined nitrate (NO_3^-) concentration
- To estimate the total H_2S production potential from RAS within that fixed nitrate concentration
- To assess potential of Mn (II) and Fe (II) as warning indicators for H_2S within RAS by using ICP-MS and FIA-CL instrument.

1.10 Hypothesis

The hypotheses of this project are:

- The type of organic matters in RAS (labile or recalcitrant) and the amount of biodegradable organic matters determine the total potential for H_2S formation.
- The development time of sulfidic condition and net "release" potential for H_2S in the system is determined by the balance of electron donor and alternative electron acceptors.
- Mn (II) and Fe (II) can be used as warning indicators for H_2S formation
- Mn (II) will be detected prior to Fe (II) and therefore is better indicator

2 Materials and Methods

2.1 Materials

The experiment was performed at Norwegian University of Science and Technology (NTNU) on February 11th to March 8th, 2021. This experiment is part of NOFIMA's CtrlAQUA WATERQUAL 2021 project and involved 4 master students with different topic of interests related to H_2S production from recirculating aquaculture system. The topics consisted of investigation on nitrous oxide production, denitrification processes, nutrient (nitrate (NO_3^-), nitrite (NO_2^-), ammonia (NH_4^+), and phosphate (PO_4^{3-})) changes, reduced metal (Mn (II) and Fe (II)) formation, and dissolved organic carbon (DOC) characterization.

The sludge from fish organic waste collected from RAS facilities at NOFIMA was delivered to NTNU in a frozen state to preserve its initial condition.

2.2 Fish Organic Waste Collection

The fish organic waste used in this experiment originated from Atlantic salmon (*Salmo salar* L.) farming operated under recirculating aquaculture system (RAS) in grow-out hall 3 Nofima Sunndalsøra. The fish rearing system where the sludge was collected from involved two octagonal tanks with volume capacity of 100 m^3 each, total biomass of about 7500 kg (or 1500 fish per tank with an average weight of 2.5 kg/fish), total feed load of 60 kg/day, make-up water flow of 100 L/min which corresponds to an exchange rate of about 45% of the system volume/day, and water recirculation flow of 5700 L/min. The actual temperature and pH on the day of sampling was 13.2°C and 7.3, respectively. Samples of fish organic waste were collected at swirl separators and frozen prior to use for the H_2S production experiments.

2.3 Experimental Design and Sampling

The experimental design consisted of two conditions: without nitrate addition, which was referred as control, and with nitrate addition. For each treatment, approximately 5% of well-mixed sludge (~30 ml) were transferred to a pre-washed dark bottle with the volume capacity of 595 ml. Into the bottle allocated for the nitrate treatment, about 2 ml of 1.75 M $NaNO_3$ solution were added. This nitrate addition aimed to attain ~6 mM or ~82 mg/L of NO_3-N (the maximum allowed concentration of NO_3-N in salmon farm is 100 mg/L) (Fjellheim et al., 2017). All bottles were then filled up with filtered seawater to its maximum volume in order to prevent the air space, and then kept at 12°C.

Each bottle was designed to be sampled only once throughout the whole experimental period. Duplicates were set up for each bottle. Samplings were conducted 19 times throughout the experimental period which was done within 25 days. The sampling interval varied between treatment depending on the H_2S production pattern on each treatment. Daily sampling was carried out when H_2S was observed to be constantly increasing. Meanwhile, sampling was performed every second day when H_2S concentration was relatively similar to the previous measurement.

All the bottles were shaken twice a day, at 10:00 AM (an hour prior to sampling) and at 15:00 PM. The bottles were shaken properly to keep water column mixed with the sediments, create water circulation, and release some of the compounds in the sediment into the water column to detect the compounds produced both in water column and sediments. The sampling procedure for all analysis was done by siphoning to prevent the O_2 entrance.

2.4 Acid Washing Procedure

Prior to sampling and analysis, the tubing, syringe, and 50 ml centrifuge plastic tubes were acid washed to ensure the complete removal of trace metals and secure an accurate and precise trace metal analysis. The cleaning procedures started by immersing these plastics in approximately 3.6 M ultra-pure nitric acid (HNO_3) for at least an hour. Following that, they were rinsed six times with Milli-Q water. The first three rinsing steps were done by adding a very small amount of Milli-Q water and allowing the water to be in contact with all the inner surface of the plastics. The purpose is to prevent the sudden pH increase that may cause the re-adsorption of metal to the plastic surface. The last three steps were done by rinsing them with gradual increase of Milli-Q water up to full volume capacity.

2.5 Chemical Analysis

2.5.1 Hydrogen Sulfide (H_2S)

The H_2S determination method referred to Cline (1969). This method uses diamine as a reagent and zinc acetate (10%) to preserve samples. Diamine solution was made by dissolving 0.8 g *N,N*-di-methyl-p-phenylenediamine and 1.2 g $FeCI_3*6H_2O$ in 200 ml diluted HCl (100 ml of concentrated HCl (37%) and 100 ml of Milli-Q water). Zinc acetate (10%) was not used since samples were directly analyzed.

The H_2S analysis began by transferring around 45 ml of supernatants into 50 ml centrifuge plastic tubes and then were centrifuged at 4500 rpm for 20 minutes. 3.2 ml of diamine reagent were then added into 40 ml of sample. The mixture was then kept in the dark for 30 minutes to allow color development. After 30 minutes, the mixture was swirled slightly and diluted with Milli-Q water to obtain 1/10, 1/100, and 1/1000 dilution. These dilutions were made by adding 18 ml of Milli-Q water into 2 mL of the mixture. To get 1/10 dilution, the mixture was taken from the initial reaction, meanwhile 1/100 and 1/1000 dilution were obtained from 1/10 and 1/100 dilution, respectively. Afterwards, all dilutions were measured in a spectrophotometer at 665 nm wavelength using a 5 cm cuvette. Milli-Q water was used as reference or blank to zero the spectrophotometer. The spectrophotometer used was Jenway 6715 UV/vis spectrophotometer. The sample's supernatant without any addition of diamine was also measured as background noise.

Due to COVID situation, sodium sulfide (Na_2S) standard could not arrive in time, therefore standard curve for measuring the actual H_2S concentration in the samples could not be derived. The conversion of H_2S absorbance to concentration (mM) was carried out by either using a molar extinction coefficient of 95000 M^{-1} cm^{-1} (Cenens and Schoonheydt, 1988) and Beer–Lambert equation : $A = \varepsilon \times c \times l$, where A is the absorbance, ε is the molar extinction coefficient, c is the concentration of methylene blue, and l is the cuvette path length in cm (Li, 2015); or by referring to previous standard curve made by Cline (1969): $y = 0.674x + 0.032$ ($R^2 = 0.999$), where y is the

concentration of S^{2-} in mg/L and x is the absorbance. In this thesis, the previous standard curve was chosen to represent approximate H_2S concentration in the samples.

2.5.2 Fe (II) in FIA-CL

For metal analysis, around 100 ml of supernatants were transferred into two 50 ml metal-free centrifuge plastic tubes and then filtered through 0.2 μM Sartobarn-Sartorious filtering cartridge. Since both Mn (II) and Fe (II) are dissolved metals, this process is essential to ensure the removal of other metal forms that may interfere further steps of analysis (USA. Department of Environment and Natural Resources Division of Water Resources., 2015).

The Fe (II) content in the sample was first determined by flow injection with luminol based chemiluminescence (FIA-CL) developed by FeLume Waterville Analytical, (Waterville, ME) with photomultiplier photon counter detector. The software used was Labview run FIA version 2.03. The instrument's general setting was performed at 5 samples per second with timing parameters of 40 seconds for loading and 40 seconds for elution 1. In addition to the samples, the main components of FIA system consisted of combined carrier of Milli-Q water and luminol reagent which flowed through peristaltic pump tubing into detector. The reagent and sample flowed at the same speed of 2 ml/min, meanwhile the combined carrier flow was 8 ml/min. The internal peristaltic pump tubing diameter of carrier, reagent, and sample were 1.85 mm, 1.3 mm, and 1.3 mm, respectively.

To prepare 1 L of luminol reagent, 10 ml of luminol stock solution (0.1 M) were made by mixing 0.13 g of Luminol ($C_8H_7N_3O_2$) and 0.53 g of potassium carbonate (K_2CO_3) with 10 ml of Milli-Q water. This mixture was then shaken vigorously until all the luminol and K_2CO_3 fully dissolved. Afterwards, this 10 ml of luminol stock solution were dissolved in a solution made of 940 ml of Milli-Q water, 40 ml of supra pure ammonia (>25%), and 10 ml of supra pure or higher grade concentrated HCl (Q-HCl ~8M (Quartz-distilled, sub-boiled)).

To determine the concentration of Fe (II) in the samples, the calibrations were made within the concentration range of 0.2 to 150 nm and performed on the same day as sample analysis. The Fe (II) standards for calibration consist of primary (50 mM ammonium iron (II) sulphate), secondary (50 μM ammonium iron (II) sulphate), and tertiary standards (1 μM ammonium iron (II) sulphate). The primary standard was prepared by dissolving 0.392 g of ammonium iron (II) sulphate ($Fe(NH)_4(SO)_4)_2 \cdot 6H_2O$) in 30 μL Q-HCl and then filled up with Milli-Q water up to 30 ml. The acid will decrease the pH and keep the Fe in the reduced form. The primary standard was kept in a 30 ml HDPL Nalgene bottle covered with aluminium foil and stored for a maximum of one month. The secondary standard was made by diluting 50 μL of primary standard in 50 μL of Q-HCl and 49.95 ml of Milli-Q water. The secondary standard was kept in a 60 ml HDPL dark Nalgene bottle for a maximum of 3 days. The tertiary standard was used for additions to calibrations. It was prepared in dark Nalgene bottle just before the calibrations by diluting 1 ml of secondary standard into 49 ml of aged seawater (seawater that had been stored in the dark for at least 24 hours at in-situ temperatures in order to oxidize all Fe (II)) (Croot and Laan, 2002).

2.5.3 Mn (II) and Fe (II) in ICP-MS

In addition to FIA-CL, ICP-MS technique was also used to determine the concentration of Fe (II) and Mn (II). ICPMS was used to detect all soluble Fe and Mn and to evaluate the increase of these trace metals over time as a result of the reduction of MnO and FeO(OH) in relation to H_2S.

As the Mn (II) and Fe (II) analysis in ICP-MS were not performed immediately after filtration, to keep the soluble Fe and Mn in the solution, to keep both Fe (II) and Mn (II) in the reduced and soluble phase, and to avoid adsorption on the wall of sample bottles and precipitation, samples were acidified with ultra-pure 3.6 M HNO_3 to pH less than 2 (1.7–2). This pH condition preserves those metals in its dissolved state (Mn (II) and Fe (II)) (Ohio. Office of Research and Development, United States Environmental Protection Agency., 1994; Fitzsimmons and Boyle, 2012). The amount of 3.6 M HNO_3 added was around 90–120 μl for every 15 ml of samples, determined in advance by adding a certain amount of acid on a certain volume of samples.

Prior to measurement, all samples were adjusted to contain 0.1 M HNO_3. This was done by adding 10 ml of Milli-Q water and 104 μl of concentrated HNO_3 into 500 μl of sample, followed by a dilution to 15 ml (or equal to 15.041 g). All samples were then delivered to SINTEF Ocean Trondheim for ICP-MS measurements. The samples were measured by an Agilent 8800 Triple Quadrupole ICP-MS (Agilent Technologies, USA) with ISIS (Integrated Sample Introduction System), SPS4 autosampler (Agilent Technologies, USA) and a standard sample introduction system (Micro Mist glass concentric nebulizer, quartz double pass spray chamber, quartz torch with 2.5 mm id and standard nickel cones). No gas and O_2 modes were used in this method. This ICP-Tuning conditions are shown in Table 2.1.

Parameter	Value
RF Power	1550 W
RF Matching	1.80 V
Sample depth	8.0 mm
Nebulizer Gas Flow	1.05 L/min
Option Gas Flow	0.0 L/min
Make Up Gas Flow	0.0 L/min
Nebulizer Pump	0.1 rps
S/C Temp	2°C
Cell tuning modes	NoGas and O2
O_2 Flow Rate	30%
Scan Type	MS/MS
Replicate/peak pattern/sweeps	4/3/30

Table 2.1 Agilent 8800 Series Triple Quadrupole ICP-MS System parameters

2.5.4 pH, Redox Potential, and Dissolve O_2 (DO)

For pH, redox potential, and dissolved O_2 measurement, ~30 ml supernatants were poured into beaker glass and measured immediately using wtw ph/ion 340i pH meter and LDOTM HQ20 Portable Dissolved Oxygen Meter, and Mettler Toledo P14805-DXK-S8/120 Redox Potential Meter.

2.6 Statistical Analysis

Since some replications were missing in this experiment due to limited number of samples, any statistical analysis, especially ANOVA, could not be performed in this thesis. In order to cover the overall picture of the redox sequence development, more sample were required than expected, therefore some replicates were omitted to complete the experiment.

3 Results

3.1 H_2S Development

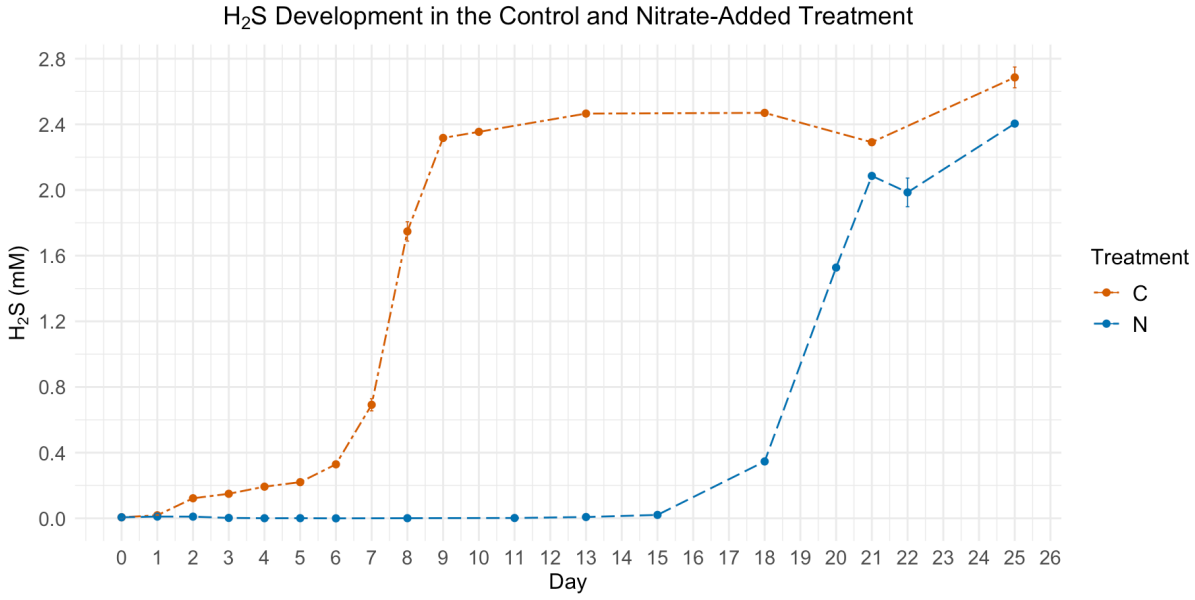

Figure 3.1: H_2S development in the control and nitrate-added treatment

The production of H_2S in the control samples (without nitrate addition) and nitrate-added samples for 25 days of observation are shown in Figure 3.1. Each line represents different sample conditions. The initial H_2S concentration was around 6.39 ± 1.94 mM, which indicates that some H_2S might have been produced within the sludge since the sludge was collected.

As shown in Figure 3.1, slow increases in H_2S from the control samples were observed during the first 6 days. Obviously, the increase was started from day 2, providing the H_2S level to 0.12 ± 0.01 mM which is considered very high compared to the LC50 value of H_2S for marine fish species (1.5–15 µM). After the constant small rises until day 6, significant increases occurred and lasted up to day 9 as presented by steep line during this period. Subsequently, from day 9 to day 21, the H_2S concentration appeared to be constant at around 2.3 mM. However, at the final day, the H_2S was slightly increase significantly to 2.69 ± 0.09 mM.

A different H_2S situation was observed in the nitrate-added samples. The generation of H_2S was relatively slower compared to the control as indicated by steady line during the first 15 days. This implies the capability of nitrate, in this case was ~6 mM or ~82 mg/L NO_3-N, to maintain low H_2S level until day 15. The first increase was detected on day 18 giving a high H_2S level to 0.35 mM. Following this, constant significant increases depicted by steep figure occurred throughout the rest of the experiment days allowing the formation of H_2S as high as 2.40 ± 0.01 mM on day 25. However, this was still lower than the H_2S content in the control samples on the last day.

Overall, the control produced higher H_2S content than the nitrate-added treatment over the entire experimental period. Furthermore, Figure 3.1 points out clearly that both

control and nitrate-added samples had rapid considerable increase when H_2S began to develop. In addition, the same concentrations of H_2S were formed in the control samples 12–14 days earlier than the nitrate-added samples. As an example of comparison, the H_2S concentration on day 6 in the control (0.33 ± 0.02 mM) was comparable to nitrate-added samples on day 18 (0.35 mM), and H_2S content of the control on day 8 (1.75 ± 0.08 mM) was close to the nitrate-added samples on day 20 (1.53 mM).

3.2 Metal Analysis (Manganese and Iron)

3.2.1 Fe (II) Measured in FIA-CL

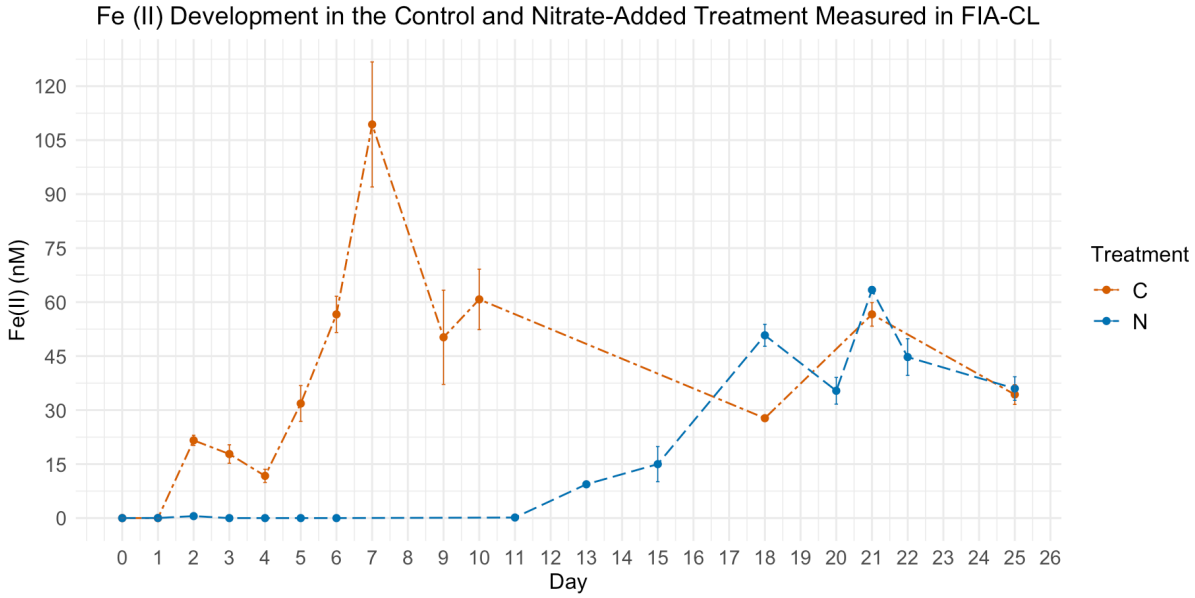

Figure 3.2: Fe (II) development in the control and nitrate-added treatment measured in FIA-CL

Figure 3.2 shows the dynamics of Fe (II) generation of the control and nitrate-added samples measured in FIA instrument. The Fe (II) values of both treatments are distinguished by different lines and were measured 60 minutes after sampling. The waiting time between sampling and measurement may have reduced the actual concentration of Fe (II) generated in each condition.

Overall, each treatment exhibited a different Fe (II) formation time and pattern throughout the experimental period even though there were similarities in the Fe (II) levels of the two treatments on the first two days. The control was able to yield higher Fe (II) concentration (109.36 ± 34.74 nM on day 7) than the nitrate-added system (63.38 ± 1.27 nM on day 21). It was also observed that there was a delay of about 14 days in the nitrate-added samples to form the maximum recorded Fe (II) content in comparison to the control.

The detection of Fe (II) was first observed in the control samples on day 2 (21.6 ± 2.82 nM) which was followed by slight declines on the next two days and increases thereafter until it peaked on day 7 (109.36 ± 34.74 nM). The peak implied a maximum Fe (II) concentration recorded by the instrument. Following this, the Fe (II) level declined significantly to 50.23 ± 26.17 nM on day 9 and then fluctuated throughout the rest of the experiment (see red line in Figure 3.2) within the range between 27.75 ± 0.31 nM and 60.76 ± 16.78 nM.

The noticeable increase in the trendline of the nitrate-added samples after a long constant minor level of Fe (II) was first observed on day 13 (9.39 nM). This increase continued gradually until first peak was noticed on day 18 (50.78 ± 4.31 nM). However, after day 18, the Fe (II) formation seemed to be unstable as shown by a decrease on day 20 (35.37 ± 5.24 nM) (although it was not statistically significant) and an increase back on day 21 (63.38 ± 1.27 nM) forming a second peak. On the final day, the Fe (II) level reduced to 36.00 ± 5.67 nM. This value was similar to that of the control samples (34.33 ± 4.75 nM).

3.2.2 Total Dissolved Mn and Fe Measured in ICP-MS

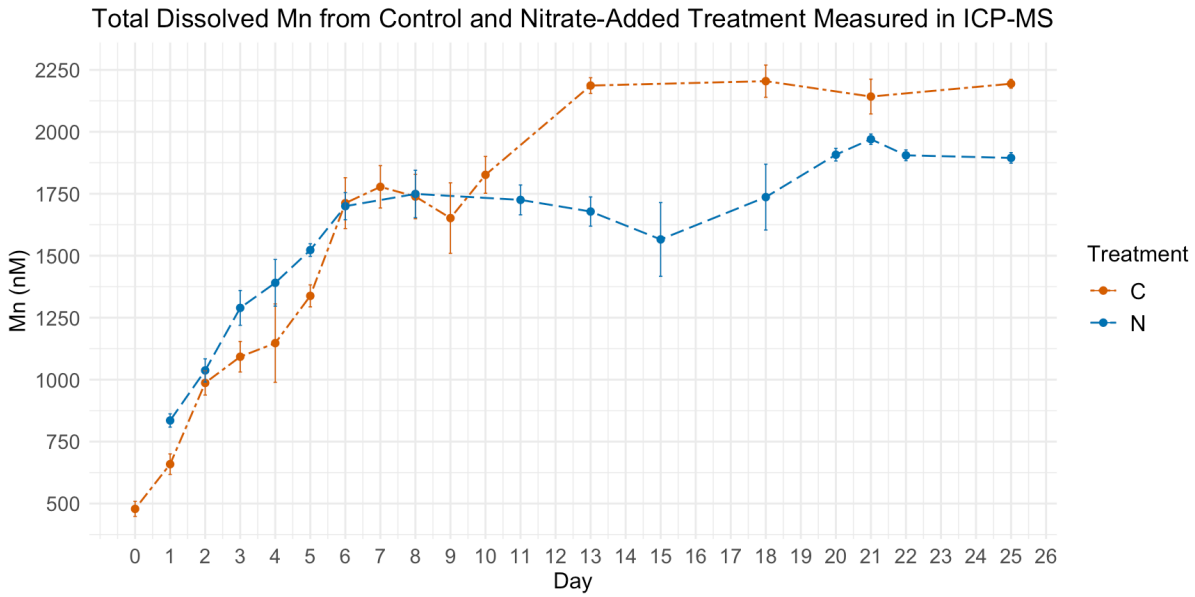

Figure 3.3: Total dissolved Mn in the control and nitrate-added treatment measured in ICP-MS

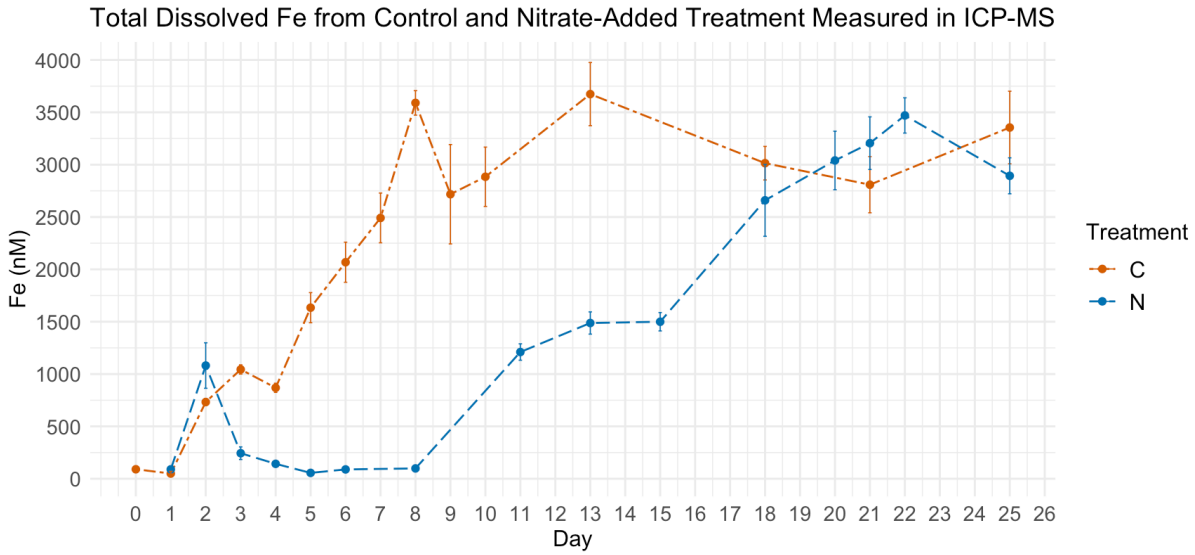

Figure 3.4: Total dissolved Fe in the control and nitrate-added treatment measured in ICP-MS

Figure 3.3 and 3.4 shows daily development of dissolved manganese and iron in the control and nitrate-added treatment measured in ICP-MS. The concentration of each

metal is considered an approximate as metal preservation for each sample was not carried out within the same time calculated from the time of sampling. Each value was subtracted from the value of dissolved Mn and Fe contained in the seawater used as a sludge medium. Each line with a different color represents each treatment as stated on each figure.

Based on Figure 3.3, it is visible that the initial total dissolved Mn was already high at 478.49 ± 74.19 nM. It is also seen that the gradual increase in dissolved Mn concentration in both treatments already started since day 1. This increase lasted similarly in both treatment for the first 6 days with the nitrate treatment showing a slightly higher concentration until day 6. After day 6, the Mn development in each treatment began to proceed differently. In the control, the concentration of Mn increased very slightly from 1712.22 ± 205.05 nM to 1778.07 ± 170.94 nM then followed by a decrease to a slight extent and a large increase until day 13. After day 13, the Mn concentration remained constant for the rest of the experiment at around 2200 nM.

In the nitrate treatment, after day 6, there was a constant period at ~1725 nM for about 7 days followed by a small decline on day 15 and an increase thereafter leading to a final constant Mn concentration at ~1900 nM. This increase lasted until day 21 giving the highest Mn concentration recorded at 1970.15 ± 29.64 nM.

There was a similar situation in the dissolved Mn development in both control and nitrate treatment where a constant final period was expected after a second increase. However, the nitrate treatment took longer to reach the maximum stable Mn level compared to the control. The final total dissolved Mn concentration in the nitrate treatment was also lower than in the control which was probably due to the lower ratio of organic matter to available electron acceptor in the nitrate treatment.

Based on Figure 3.4, the development of Fe was different in each treatment. In the control treatment, the initial dissolved Fe level was 90.36 ± 64.5 nM. This concentration began to increase on day 2 and continued gradually until day 8 with the Fe concentration reaching almost its highest level at 3590.29 ± 234.08 nM. Following day 8, the Fe levels seemed to fluctuate within 2700 to 3700 nM. The highest Fe level was observed on day 13 with Fe content of 3674.11 ± 426.64 nM.

In contrast, in the nitrate treatment, the concentration of dissolved Fe appeared to change minimally during the first 8 days. The concentration fluctuated slightly between 49 to 250 nM with an exception on day 2 where a spike was observed at 1081.20 ± 433.86 nM. In this period, Fe levels remained mostly at around 90 nM. The first Fe increase in the nitrate treatment was detected after day 8, precisely on day 11 because no sampling was done on day 9 and 10. This increase took place slowly until day 15 followed by a larger increase afterwards which continued until day 22 where Fe level was found to be the highest in the nitrate treatment (3470.32 ± 291.97 nM). On the last day, Fe level was found to decrease to 2893.57 ± 297.46 nM.

The maximum dissolved Fe content was observed to be similar in both treatments. However, the nitrate treatment took 14 days longer to reach the maximum Fe concentration than the control.

3.3 The Comparison between H_2S, Mn (II), and Fe (II) Formation

3.3.1 H_2S in comparison with Fe (II) Measurement in FIA-CL

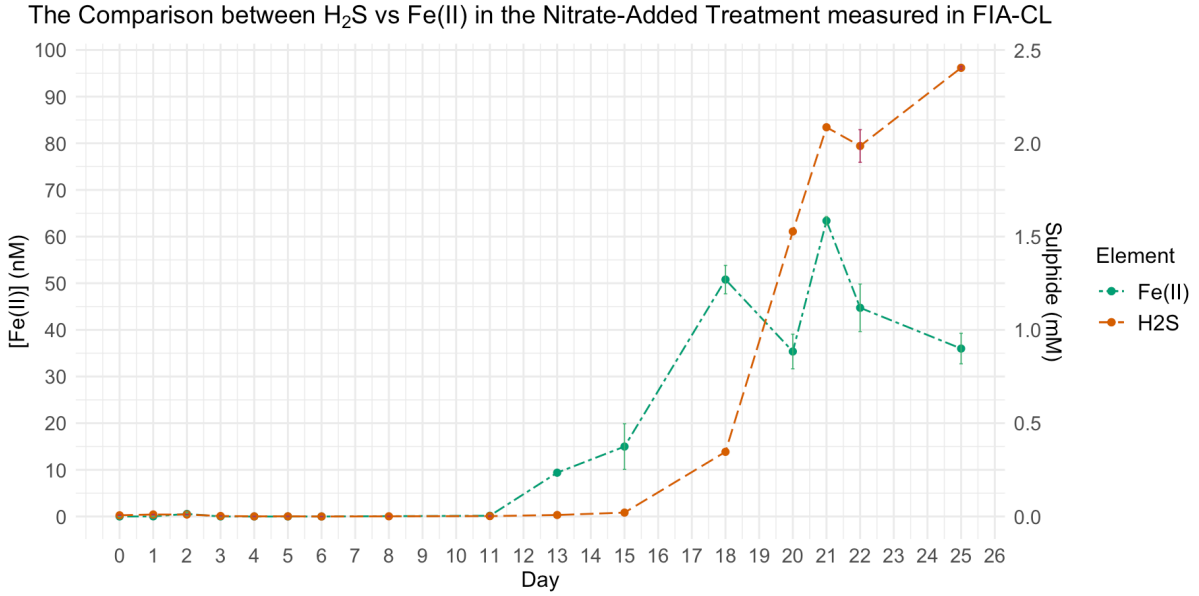

Figure 3.5: The comparison between H_2S and Fe (II) in the nitrate-added treatment measured in FIA-CL

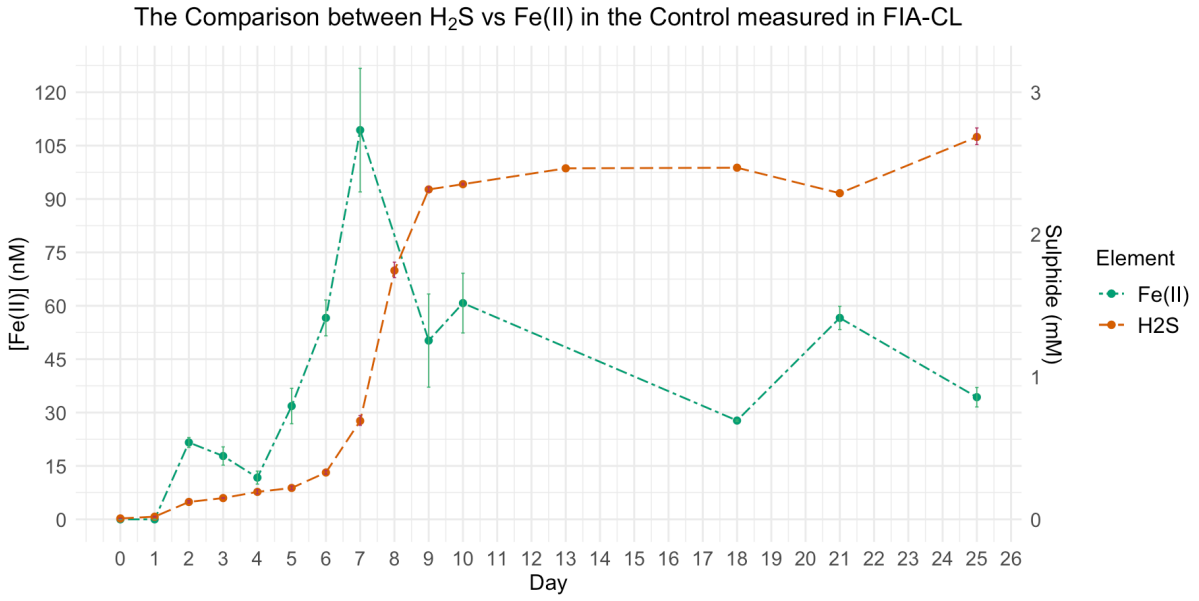

Figure 3.6: The comparison between H_2S and Fe (II) in the control measured in FIA-CL

Figure 3.5 and 3.6 present direct comparisons between Fe (II) and H_2S formation of the control and nitrate-added treatment, respectively. The green lines represent Fe (II), whereas the red lines indicate H_2S.

In the nitrate-added samples, the first Fe (II) signal was captured on day 13 (9.39 nM), whereas the significant increases in H_2S were first detected on day 18. These data point out that Fe (II) was formed earlier than H_2S with a time between these two events of approximately 5 days. When the H_2S formation initiated on day 18, the Fe (II) content

had increased about 5 times of its level on day 13 (50.78 ± 4.31 nM). As the H_2S level grew higher, the Fe (II) became unstable, and the level tended to decrease.

However, not all results from the nitrate treatment were relevant for the control samples. The development of H_2S in the control had started since day 1, while the first Fe (II) signal was just detected on day 2. The slow yet steady increase in H_2S during the first 6 days was accompanied by the unstable formation of Fe (II). However, entering day 5, the concentration of Fe (II) began to increase extensively until it reached its peak on day 7. When Fe (II) peaked, H_2S was found to rise significantly and even more considerably in the following two days, meanwhile Fe (II) level was found to decrease significantly after the peak. As H_2S reached its constant level from day 9 to almost the final experimental day, the Fe (II) level fluctuated with the maximum level found to be 60.76 ± 16.78 nM.

3.3.2 H_2S in comparison with Fe (II) and Mn (II) Measurement in ICP-MS

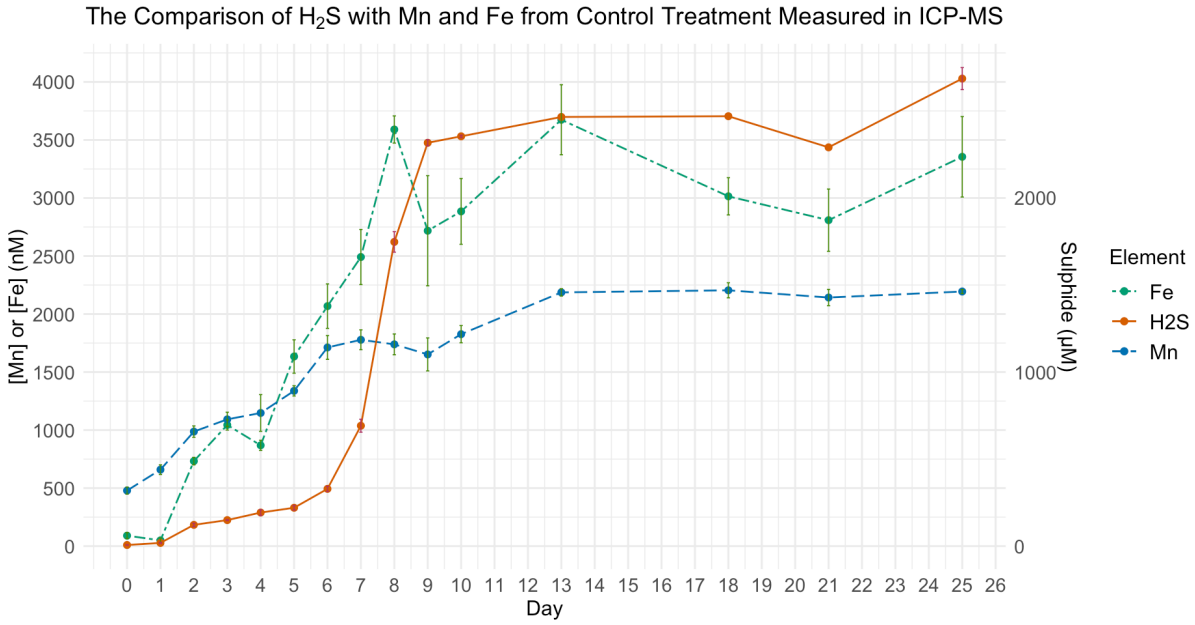

Figure 3.7: The comparison between H2S, dissolved Mn, and dissolved Fe measured in ICP-MS in the control treatment

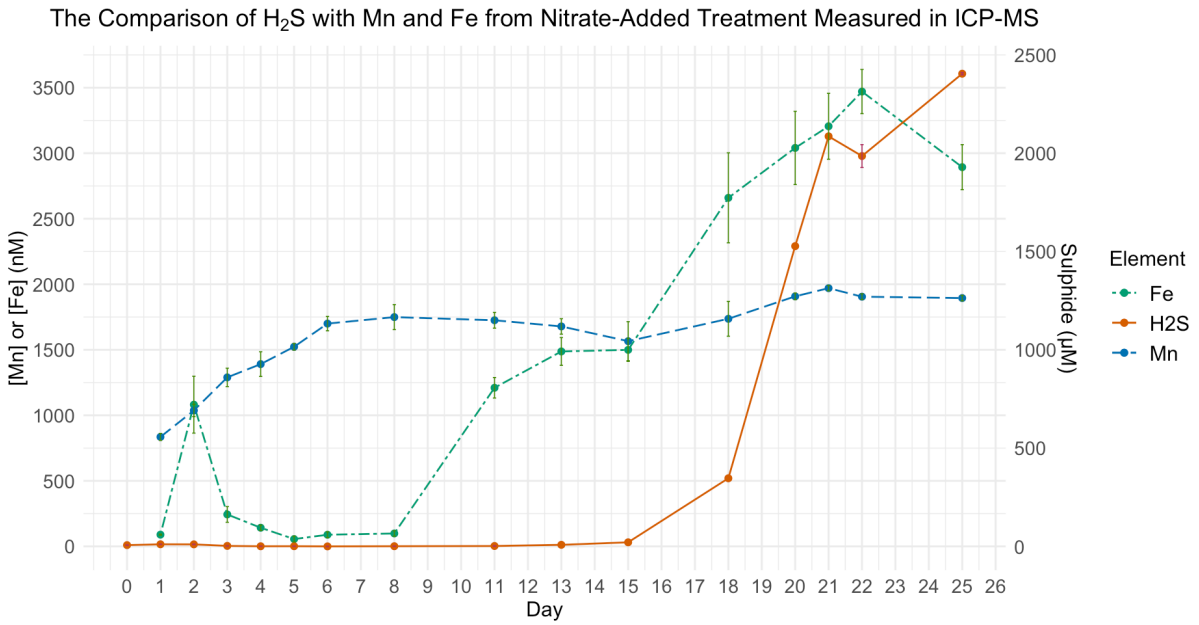

Figure 3.8: The comparison between H_2S, dissolved Mn, and dissolved Fe measured in ICP-MS in the nitrate-added treatment

Figures 3.7 and 3.8 show comparison between the formation of H_2S, dissolved Mn, and dissolved Fe measured in ICP-MS throughout the experimental period in the control and nitrate-added treatment, respectively. Each line represents each element as stated on each figure legend.

As shown in Figure 3.7, the formation of Mn and Fe in the control overlapped with the formation of H_2S since day 1. Along with the increase and slow development in H_2S from day 1 to day 6, the concentration of both Mn and Fe also increased. From this figure, the Fe concentration clearly increased more rapidly than Mn during this period. After day 6, as H_2S started to grow more significantly, the Fe concentration continued to increase while Mn formation began to slow down. When H_2S peaked on day 9, the Fe level was found to fall after reaching its peak on day 8. Mn was also found to be slightly reduced as H_2S reached its peak. Since the H_2S level began to remain unchanged on day 9 onwards, the Fe level fluctuated between 2800–3700 nM whereas Mn level increased slightly to 2186.65 ± 44.79 nM and then remained constant. Since H_2S increase was observed in the control as early as day 1, it was difficult to assess the potential of Mn and Fe as early signs of H_2S development.

As shown in Figure 3.8, the assessment of Fe and Mn potential as indicators for H_2S formation was clearer and easier in the nitrate treatment as H_2S formation was inhibited until day 15, allowing a clearer picture of the Mn and Fe development before H_2S production.

The results from ICP-MS of the nitrate treatment (Figure 3.8) showed that the increase in Mn concentration was detected since day 1, while the increase in Fe level was observed after day 8. In terms of Mn, the increase happened slowly and gradually until day 6 followed by a constant period at ~1750 nM and a slight increase to ~2000 nM from day 18 to 21 or when H_2S concentration started to increase significantly. In terms of Fe, after day 8, the increase in Fe level seemed to slow down especially on day 11 to 15. However, when the H_2S concentration started to increase significantly, the Fe (II) formation also accelerated until day 22 giving the maximum Fe value of 3470.32 ±

291.97 nM. On the last day, when the H_2S concentration reached its maximum level, the Fe concentration dropped to 2893.57 ± 297.46 nM.

Based on the ICP-MS results, the increase in dissolved Fe was first detected on day 11 as no sampling were done on day 9 and 10. This Fe increase was found to occur ~9 days after the first Mn increase and ~7 days before the first increase in H_2S on day 18.

3.4 pH

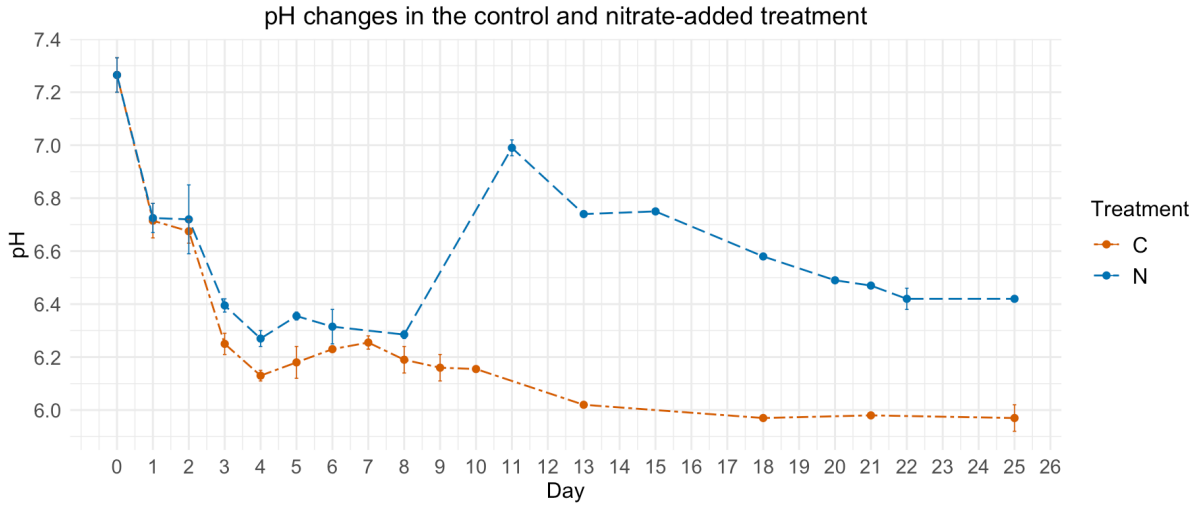

Figure 3.9: pH changes in the control and nitrate-added treatment

pH is an important attribute that changes during redox reaction. The changes in pH in the control and nitrate-added systems are shown in Figure 3.9. Both control and nitrate-added treatments had neutral initial pH of around 7.26 ± 0.09. However, this neutral pH did not last long. The pH on the first two days was lower than day 0 for both treatments, which was around 6.7. On day 3 and 4, the pH dropped even lower to 6.27 ± 0.04 in the nitrate treatment and 6.13 ± 0.03 in the control (data from day 4). This pH level on day 4 were found to be the lowest peak for nitrate treatment, whereas for control, this pH was the lowest before it went lower on day 13.

After day 4, the pH of the control samples increased slightly to 6.26 ± 0.04 on day 7 and then dropped back down to pH around 6 on day 13 which remained constant for the rest of the experiment. Meanwhile in the nitrate treatment, the pH seemed to be constant from day 4 to day 8 before increasing to 6.99 ± 0.04 on day 11. Following this, the pH gradually became more acidic as the experiment reached its final stage with the final pH of 6.42 on the last day. Overall, the control samples had lower pH than the nitrate-added samples, indicating the more acidic condition in the control samples.

3.5 Redox Potential (E_h)

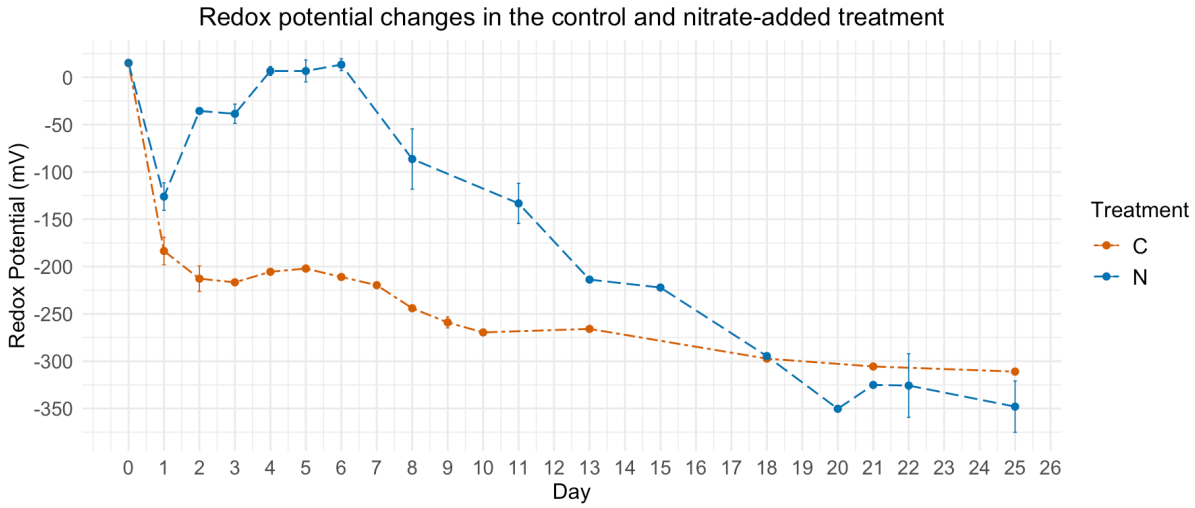

Figure 3.10: Redox potential changes in the control and nitrate-added treatment

Figure 3.10 shows the redox potential dynamics of the control and nitrate-added conditions for 25 days of observation. The initial E_h of the two treatments was 15.05 ± 1.91 mV. On the first day, both treatments already had significant reduction to negative value, −183.60 ± 20.65 mV in the control and a higher value in the nitrate treatment (−126.10 ± 20.51 mV). However, after experiencing steep decline on day 1, these two conditions behaved differently. The E_h in the control tended to decrease slightly but continuously, while in the nitrate treatment, there was a gradual increase back to the initial value before experiencing a significant decrease.

After constant value between −200 to −225 mV until day 6, the E_h of the controls started to decrease again on day 7. This reduced to around −270 mV that lasted from day 10 to day 13 and then became lower to −311.00 ± 2.40 mV on the final day.

In the condition with nitrate, after dropping significantly on the first day, the E_h value gradually increased back to around its initial value. The peak of this increase was observed on day 6 with the value of 13.30 ± 8.77 mV. A continuous decrease happened after the peak until day 20. Day 11, that marked the last negligible Fe (II) level in the nitrate condition before an increase in concentration was detected, demonstrated a redox value close to the value on day 1 (−133.30 ± 29.98 mV). In comparison to the control, the E_h of the nitrate treatment from day 2 to day 11 were significantly higher. However, higher values than the control continued only until day 18. The E_h values on day 18, when first H_2S increase in the nitrate samples was also detected, was -294.6 mV. On day 20 to day 25 the E_h of the nitrate treatment was lower than that of the control, between −325 to −350 mV.

3.6 Dissolved Oxygen

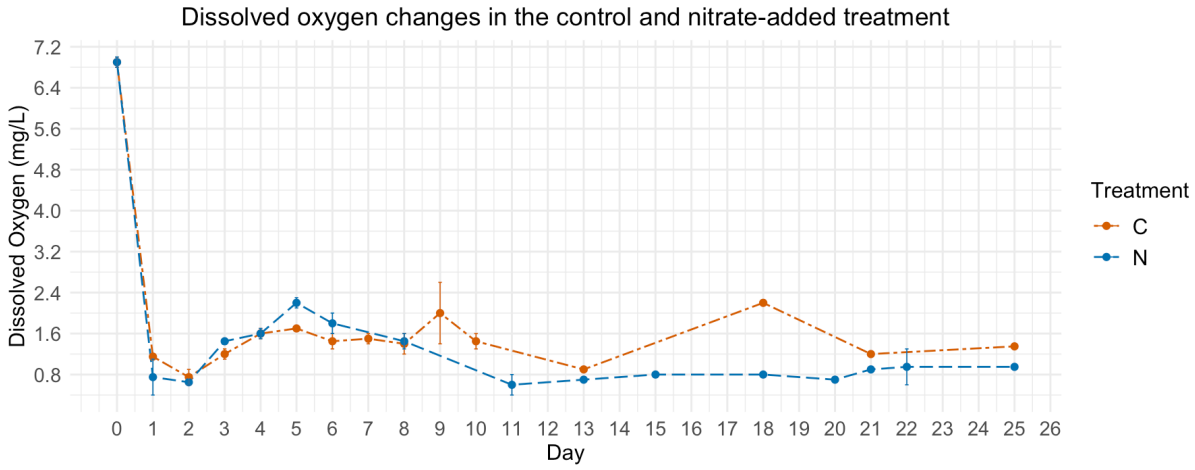

Figure 3.11: Dissolved oxygen changes in the control and nitrate-added treatment

Figure 3.11 showed the dissolved O_2 (DO) measurement from both control and nitrate treatments. However, the results seemed to be unreliable since DO measurements were not carefully conducted under minimized O_2 condition. Therefore, some O_2 from open air might have entered the system and interfered the DO measurement leading to fluctuated O_2 level as shown in Figure 3.11.

4 Discussions

4.1 H_2S Development

This study showed that the addition of ~6 mM of nitrate could postpone H_2S formation until day 15. It suggests that the presence and concentration of electron acceptors, which in this study was tested with nitrate, affect the initiation time of H_2S generation. This result corresponds to the previous studies showing that the activity of sulphate-reducing bacteria (SRB) is inhibited by aerobic conditions through the addition of nitrate or oxygen (Bentzen et al., 1995; Dilling and Cypionka, 1990). The mechanisms of nitrate to inhibit sulfide production involves: (1) oxidation of sulfide back to sulphate (Mohanakrishnan et al., 2008); (2) stimulating the growth of autotrophic denitrifying and sulfide-oxidizing bacteria, especially in environments with a high ratio of nitrate to carbon content and sulphate rich, which were capable to use sulfide as electron donors in the denitrification process and therefore suppress the sulfide production (García De Lomas et al., 2006); and (3) producing nitrite that also stimulates sulfide oxidation and inhibits the reduction of sulfite (SO_3^{2-}) to sulfide (HS^-) (Mohanakrishnan et al., 2008; Barton and Hamilton, 2007).

In the nitrate treatment, the first increase in H_2S concentration was observed on day 18. Interrelated study focusing on denitrification process in this project showed that nitrate (NO_3^-) was fully consumed on day 6, whereas nitrite (NO_2^-) as an intermediate product of NO_3^- reduction to NH_4^+, lasted longer until day 10 before being completely depleted on day 11. There was approximately 4 days after the nitrite was fully used up until the sulphate reduction began to resume on day 15. This is in accordance with the results of previous studies that have also shown inhibitory effect of nitrate and nitrite on sulfide generation. When both nitrate and nitrite were fully consumed, Mohanakrishnan et al. (2008) and Jiang et al. (2010) observed a gradual recovery of sulphate reduction up to the maximum initial sulfide level before the addition of nitrate, which varied depending on the type and amount of organic matter and the abundance of electron acceptors.

On the last day, the H_2S concentration in the addition of nitrate (2.40 ± 0.01 mM) was recorded lower than the control (2.70 ± 0.09 mM) yet was similar to the control on day 10 (2.35 ± 0.01 mM). The recovery of sulphate reduction was initiated in the nitrate-added samples on day 15. This means it took about 10 days to reach H_2S level similar to the one in the control on day 10, indicating a similar H_2S production rate to that of the control. This is in line with earlier studies on H_2S production rate. Two related studies by Mohanakrishnan et al. (2008) and Jiang et al. (2010) found a similar H_2S production rate in sewer system to reach initial H_2S level after the termination of nitrite supply into the system.

The lower H_2S level on the last day might be an indication that the H_2S production in the nitrate-added samples was still ongoing. In addition, a slight increase in H_2S level in the control on the last day might also be a sign of ongoing sulfide production. It is suspected that more time might be needed to reach the maximum H_2S production in both treatments. Similar study demonstrated that the maximum H_2S level obtained from rainbow trout organic waste in 35 g/L salinity was 159.1 mg/L or equal to 4.68 mM, almost double the highest H_2S level observed in this study. However, organic matters

concentration, sulphate concentration, and salinity level might affect the maximum H_2S production, but the main driver here is organic matter (Letelier-Gordo et al., 2020).

4.2 Manganese (II) and Iron (II) Development

4.2.1 Manganese (II) Development

According to the results from ICP-MS, the initial Mn concentration after the addition of sludge was relatively high (478.49 ± 74.19 nM) compared to typical concentration of Mn from coastal seawater or river, for example around 1.7 nM in East China Sea and 39.3 nM from Changjiang river water (Wang et al., 2016). Studies have shown that Mn concentration is significantly higher in the presence of organic matter than the typical Mn concentration in the seawater. Even an increase in the concentration of various Mn fractions was found as more organic matter was added into the system (Samiei and Bostani, 2016). Yakushev et al. (2009) demonstrated that Mn was found to be bound in stable complexes with organic matter or phosphorus-containing compounds at significant concentrations at an average of 0.5–1 nM.

The increase in Mn concentration in both treatments started on day 1 and continued until around day 6. Based on the redox sequence and the resulting free energy, Mn reduction occurs after NO_3^- reduction because lower free energy is produced from Mn reduction (Stumm and Morgan, 1996). However, this project also pointed out that NO_3^- reduction also lasted until day 6 (Estensen, 2021), which implies that the Mn (IV) or (III) and NO_3^- reduction overlapped. This is possible because the free energy produced by the reduction of Mn (ΔG = -3090 to -2920 kJ/mol) is close to the denitrification (ΔG = -3030 kJ/mol). In addition, differences in the oxidation state of Mn affect the amount of energy produced (Burdige, 1993). This situation has also been observed by previous studies showing that the reduction of Mn occurred before complete denitrification in the pelagic sediments (Klinkhammer et al., 1980).

In Figure 3.3, it is seen that dissolved Mn concentration was higher in the nitrate treatment than in the control during the first 6 days. Since NO_3^- is reduced prior to Mn, the dissolved Mn concentration should be lower in the nitrate treatment than in the control, especially during the first 6 days when NO_3^- was still present. However, the addition of sodium nitrate solution to the nitrate treatment may have some Mn as a contaminant leading to the higher dissolved Mn concentration in the nitrate treatment. Furthermore, the longer time to acidify the control samples might have caused the dissolved Mn to be re-oxidized to Mn (IV) in the presence of O_2, thus lowering the concentration of dissolved Mn in the control samples.

Different situation of dissolved Mn concentration after day 6 may be related to redox potential (E_h) and pH conditions. Since the redox value was considerably lower in the control than in the nitrate treatment, indicating more anoxic condition especially from day 6 to 13, the dissolved Mn level in the control started to increase earlier on day 9 (pH was ~6.2), whereas in the nitrate treatment, there was a stable period until day 15 (pH was ~6.75) before the Mn level started to increase to a certain extent and eventually stabilized. This is in accordance with Stumm and Morgan (1996) who explained that the redox equilibrium activity of Mn depends on E_h, pH, and temperature. The lower the E_h and pH, the more Mn (II) is reduced. Moreover, the lower pH, the reduction of Mn starts to take place at higher redox value. As both E_h and pH in the control and nitrate-added treatment reached constant especially during the last few days, the Mn concentration also became stable indicating the equilibrium state of the reduction process.

4.2.2 Iron (II) Development

The results from ICP-MS showed that the initial concentration of dissolved Fe was 90.36 ± 64.5 nM. This level is considered high compared to the typical dissolved iron concentration in the coastal water, for example around 13.4–43.4 nM in summer period and 5.6–107 nM in spring period in Jiaozhou Bay (Yellow Sea, China) (Su et al., 2016). According to Sjöstedt et al. (2013) and Boyd and Ellwood (2010), Fe can form complexes with dissolved organic matter (DOM) that causes an increase in the solubility of Fe. In this study, the sludge added also likely contributed to high amount of DOM to which Fe (III) could bind to and become soluble, leading to the high initial concentration of dissolved Fe.

However, on day 0 and 1, FIA-CL could not detect the presence of Fe (II) in both treatments. This might be an indication of the absence of Fe (II) formation on the first day, therefore it can be concluded that the dissolved Fe detected in ICP-MS most likely came from Fe (III). Nevertheless, there is uncertainty since the samples were not analyzed immediately after sampling which might have caused Fe (II) to be oxidized, thus causing Fe (II) undetected in FIA-CL. Furthermore, all samples on day 0 and 1 were centrifuged before filtration to facilitate the filtration step. According to Croot and Laan (2002), one of the most essential factors determining the rate of Fe (II) oxidation is temperature. Their studies have shown that high temperatures lead to an exponential decrease in the half-life of Fe (II) due to high oxidation rates. Since centrifugation generates heat, it is presumed that most of the Fe (II) generated in the samples may also have been oxidized. Therefore, in order to prevent the rapid oxidation of Fe (II) due to high temperatures and to allow the detection of Fe (II), especially when Fe (II) were actually still low, the centrifugation step was omitted from the procedure from day 2 onwards.

Although ICP-MS measures both dissolved Fe (III) and Fe (II), the increase in Fe concentration was caused by Fe (II) resulting from the reduction of Fe (III) in both particulate and dissolved form. Fe (II) in the control were detected in both FIA-CL and ICP-MS on day 2. On the other hand, the addition of nitrate was able to delay the formation of Fe (II) until day 8 according to the ICP-MS results (see Figure 3.4). These results correlate with the research conducted by Liu et al. (2016) who found that nitrate could suppress the production of dissolved Fe (II) as more efficient energy was produced from nitrate reduction.

The first formation of Fe (II) in the nitrate treatment was observed on day 11 in ICP-MS and on day 13 in FIA-CL. However, there was also an observed spike observed in ICP-MS on the second day which was most likely to be contamination from the surrounding air or surfaces that might have had contact with the samples. This is confirmed by the recovery of dissolved Fe concentration after the second day. As this project also pointed out that nitrate and nitrite were fully used up on day 11 (Estensen, 2021), it was obvious that Fe (III) reduction happened once nitrate and/or nitrite were no longer available. According to Weiner (2007), nitrate (NO_3^-), as an electron acceptor, can produce more energy for bacteria compared to Fe (III). Therefore, nitrate reduction happened before Fe (III) reduction. Furthermore, nitrate can also cause the oxidation of Fe (II) back to Fe (III) in the presence of organisms capable of oxidizing of Fe (II) by using nitrate as an electron acceptor. This will retain iron in its oxidized form (Fe (III)) (Weber et al., 2006).

The late detection of Fe (II) in FIA-CL confirmed the sensitivity of Fe (II) to oxidation. The samples for ICPMS analysis were preserved to keep Fe (II) in the reduced form, while for the analysis in FIA-CL, there was no sample preservation that allowed Fe (II) to

be oxidized to Fe (III). In addition, the measurement in FIA-CL was conducted later than the sample preservation time for ICP-MS, which might have caused Fe (II) to be fully oxidized and therefore could not be detected in FIA-CL on day 11.

As Fe (II) began to form, it was seen that the development of Fe (II) took place gradually until a peak was formed on day 8 in the control and on day 22 in the nitrate treatment based on the ICP-MS results (see Figure 3.4). This condition suggests that the system was progressing toward more anaerobic condition as more Fe (II) was produced (Stumm and Morgan, 1996). However, changes in pH and redox potential (E_h) during this period were different between treatments. The pH and E_h in the control tended to be constant, which was around pH 6.2 and E_h between −200 to −250 mV (observed from day 4 to 8). Meanwhile, in the nitrate-added samples, both pH and E_h seemed to decrease, from pH 7 to 6.4 and E_h −133.3 to around −325 mV (observed from day 11 to 22). This large E_h reduction started when nitrate and nitrite were completely consumed on day 11. This situation is in line with the previous study by Frindte et al. (2015) who also observed a rapid and significant drop in E_h when nitrate was fully depleted from the sediment-water interface. Typically, at pH 7–8, when the concentration of Mn (II) and Fe (II) rises further, the E_h ranges from −240 to −100 mV (Stumm and Morgan, 1996). In this study, the lower E_h observed when Fe (II) were at peaks might indicate a deeper anoxic condition.

Furthermore, based on the results from ICP-MS, it took 14 days longer for the nitrate treatment to reach the Fe peak (day 22) compared to the control (day 8). The longer time for the nitrate treatment to reach the peak is due to the high Eh that hindered the reduction of Fe (III). In addition, the increase in pH also slows down the rate of Fe (III) reduction (Stumm and Morgan, 1996). This situation was observed in the nitrate treatment on day 11 to 15 when pH increased from ~6.3 on day 8 to ~7 on day 11 and then remained constant at ~6.75 on day 13 and 15.

According to the FIA-CL results, the Fe (II) peak in the control and nitrate treatment were detected on day 7 (as no measurement were done on FIA-CL on day 8) and day 18, respectively. The Fe (II) peak in the control was similar to the result from ICP-MS which was on day 8, while in the nitrate treatment, the result was significantly different from the ICP-MS result which was on day 22. Pullin and Cabaniss (2001) and O' Sullivan et al. (1995) have demonstrated that the presence of dissolved organic matter can reduce the detection sensitivity of Fe (II) in FIA-CL by forming complex coordination with Fe (II) thereby stabilizing Fe (II) against oxidation. Later study concluded that FIA-CL is not suitable for measuring Fe (II) content in the presence of high dissolved organic matter, especially when Fe (II) content is high (Borman et al., 2009). This condition will lead to a lower signal captured by FIA-CL detector due to slower formation of reactive oxygen species required for the chemiluminescence of luminol. In addition, lower pH also affects the sensitivity of FIA-CL by overcoming the buffer capacity of the luminol solution, thereby disrupting luminol dehydrogenation process and consequently lowering the signal (Croot and Laan, 2002). These reasons may also explain the lower concentration of Fe (II) produced in FIA-CL compared to ICP-MS (see Figure 3.2 and 3.4).

4.3 The Comparison between Fe (II), Mn (II), and H_2S Development

In correlation with H_2S, Fe (II) in the nitrate-added samples could be detected in FIA-CL 5 days earlier than H_2S and 7 days earlier in ICP-MS. Meanwhile, Mn (II) started to increase on day 1, 17 days before the first H_2S production. In the control, the generation

of Mn (II) and Fe (II) overlapped with the H_2S production. The situation in the nitrate treatment is in accordance with the theory of the redox reaction sequence that states that the reduction of Mn (IV) and Fe (III) precedes the reduction of sulphate due to the more efficient energy produced (Weiner 2007; Stumm and Morgan, 1996). In the control, however, since the H_2S formation happened on day 1, it was difficult to evaluate the redox reaction that took place before sulphate reduction.

Before the appearance of H_2S, the level of Fe (II) showed a gradual increase in both treatments. However, when H_2S appeared, the Fe (II) level began to decrease and became unstable. The decrease and stability seemed to be lower in FIA-CL than ICP-MS. The concentration of Mn (II) also increased when the H_2S level was increasing or had reached its high stable content as happened in the control. In contrast to Fe (II), Mn (II) tends to be stable after increasing. The fluctuating Fe (II) condition in the presence of H_2S can be attributed to sulfide. Under reduced conditions, Fe (II) can react with sulfide and form iron sulfide precipitates such as FeS or FeS_2 (Nielsen et al., 2005). In contact with O_2, Fe (II) can be rapidly oxidized back to Fe (III) (Wells et al., 1994). When Fe (III) interacts with sulfide, there will be redox reaction between Fe (III) (as electron donor) and sulfide (as electron acceptor), forming Fe (II) and sulphate (Nielsen et al., 2005). Another process that may also contribute to the Fe (II) instability is complexation with organic matter that can decrease Fe (II) oxidation rate thus causing lower signal detection in FIA-CL (Ramos et al., 2016).

Despite the less accurate Fe (II) measurement due to complexation with organic matter, FIA-CL is still reliable to give early warning sign for H_2S formation. This is possible because the issue with unstable signal production was most likely indicated when Fe (II) concentration was about to increase or was still at low level and when there was an increase in the production of H_2S. In addition, on site and real time analysis is essential for RAS to detect increases in soluble Mn and Fe. As ICP-MS took longer procedure and time for analysis than FIA-CL, FIA-CL is considered to be more suitable for on-site detection technique.

4.4 pH

Both treatments showed a decrease in pH since day 1 from 7.26 $\pm$ 0.09 on the day 0 to ~6.7 on day 1 which was most likely related to CO_2 production from biodegradation of organic matter through redox reactions. In water, CO_2 will react with water and form carbonic acid (H_2CO_3) which can dissociate into bicarbonate (HCO_3^-) and carbonate (CO_3^{2-}) to reach an equilibrium state. This dissociation liberates proton (H^+) which will lower the pH of the water. Since the experiment was a closed system, CO_2 tended to accumulate and cause further pH reduction (Stumm and Morgan, 1996). This situation was seen on day 3 and 4 where the pH decreased further to 6.13 $\pm$ 0.03 in the control and 6.27 $\pm$ 0.04 in the nitrate treatment. This might also be an indication that the systems were progressing towards anaerobic state.

A slight increase in pH was observed in the controls on day 4 to 7. This increase in pH was probably due to a decrease in Fe (III) and Mn (IV) as an increase in Fe (II) concentration was also observed in this period. Soetaert et al. (2007) showed that the proton (H^+) consumption in decreasing Fe (III) and Mn (IV) at all pH ranges far exceeds the production of dissolved inorganic carbon, which mainly is CO_2, thereby increasing the pH. Meanwhile, the pH on the nitrate treatment on day 4 to 7 appeared to be constant as

around pH 6 to 7, negatively charged substances are generally produced (ΣCO_2) and consumed (ΣNO_3^-) in equal proportion (Soetaert et al., 2007).

During the period when H_2S started to grow in the control, particularly from day 7 to 13, the pH decreased slightly to ~6 which then remained constant for the rest of the experiment. This small reduction in pH might be induced by more CO_2 production compared to the total sulphate consumption (ΣSO_4^{2-}) within this particular pH range (6–7) (Soetaert et al., 2007). In the nitrate treatment, a pH spike to around neutral pH was observed on day 11 after a short constant period at pH ~6.3. This increase in pH is suspected to be due to the dissimilatory nitrate reduction to ammonia (DNRA) which might have produced ammonia that lowered the pH.

4.5 Redox Potentials (E_h)

The initial redox potential (E_h) in this study was considerably lower (15.05 ± 1.91 mV) than the typical E_h under aerobic condition which is 300–700 mV (pH 7) (DeLaune and Reddy, 2005). According to DeLaune and Reddy (2005), this initial E_h value indicates the stage of Fe (III) reduction. In most studies of redox chemistry, the initial E_h value has always been above above 200 mV (Bell, 1969; Bailey and Beauchamp, 1971; Włodarczyk et al., 2007; Gardiner and James, 2012). There are several possible reasons that determine the value of E_h. Gardiner and James (2012) demonstrated that the amount of organic matter and the number of electron acceptors affect the E_h value. Their study showed that more organic matters and electron acceptors (nitrate) led to a lower E_h. This also indicates that more redox reactions are taking place in the system. Therefore, the low initial E_h in this study was probably due to low O_2 content and the high amount of organic matter in the system.

The control had considerable reduction in E_h from day 1 which tended to decrease slowly and gradually afterwards. On day 1, when the small H_2S production was first spotted, the E_h reduced extensively to −183.60 ± 20.65 mV followed by a slight decrease to ~ −225 mV on day 7 and further reduction to ~ −300 mV on day 18 which then lasted until the final day. This redox situation was also observed in a similar experiment by Bailey and Beauchamp (1971). He found that the E_h decreased significantly in the first few days of the experiment followed by a constant E_h of about −300 mV until the end of the experiment. According to DeLaune and Reddy (2005), the E_h between −100 to −200 mV at pH 7 indicates the formation of H_2S. Meanwhile, at −300 mV, methane production through the reduction of CO_2 begins.

In the nitrate treatment, although a sharp reduction also occurred on day 1, the E_h value recovered gradually to around the initial value before decreasing again on day 6. A similar situation was also observed by Bell (1969) and Yamane and Sato (1964) who found that after O_2 depletion, the E_h dropped rapidly, followed by slight increase. In their study, they concluded that the production of hydrogen gas (H_2) from the decomposition of organic matter distorts the redox equilibrium leading to redox instability. In this study, as nitrates were completely consumed on day 6, the E_h started to decrease continuously until day 20 before reaching stability at ~ −350 mV. This continuous decrease implies that the redox reaction occurred under more anaerobic condition. On day 18, when the first H_2S rise was detected, the E_h value of around −300 mV indicated further redox reaction of methanogenesis taking place in the system.

5 Conclusions

The addition of ~6 mM of nitrate to the system containing 5% of fish organic waste could prevent the formation of H_2S until day 15 compared to a system without nitrate addition (day 2). This result demonstrates that addition of nitrate increases the number of electron acceptor which affects the balance between electron donors and electron acceptors thereby prolonging the initiation of sulfidic condition. When the system reaches sulfidic condition, the total production potential of H_2S is around 2.4–2.7 mM observed within 25 days with a slightly lower concentration in the nitrate-added system.

Both Mn (II) and Fe (II) can be used as indicators as they are produced before H_2S. In addition, it is true that Mn (II) is detected before Fe (II), however, Mn (II) increased well before H_2S formation, about 15 to 17 days earlier. On the other hand, Fe (II) was found to increase closer to H_2S production than Mn (II), around 7 to 9 days earlier. Therefore, it is concluded that Fe (II) is a better indicator than Mn (II) as it occurs not too long before H_2S production.

FIA-CL is considered more practical and suitable than ICP-MS to assist system in RAS to develop warning indicators for H_2S formation as it as it allows on-site application, more real time analysis, and short procedures. However, the results in this study indicate some issues with the FIA-CL results regarding measurement accuracy due to the high amount of organic matter and rapid oxidation during the period after sampling to before analysis. Interestingly, this study has also pointed out that organic matter is not an issue when the Fe (II) concentration is minor as well as there is no H_2S production, as the signal interferences occur because of complexation between Fe with organic matter or sulfides. In addition, it is also possible to reduce oxidation by performing in-line measurement under cold temperatures as this will decrease the rate of Fe (II) oxidation (Croot and Laan, 2002).

FIA-CL also allows to selectively measure Mn (II) concentration. However, since it was not feasible for a person to measure both Mn (II) and Fe (II) simultaneously in one FIA-CL instrument, Mn (II) measurement in FIA-CL were not carried out in this project. For further research, it is possible to use FIA-CL to detect Mn (II) and Fe (II) as a warning indicator for H_2S formation in RAS by involving several people to collaborate. Moreover, to achieve better results, more samples can be prepared in advance to provide a better statistical approach of the results.

References

Adelman, I. R. and Smith, L. L., (1970). Effect of hydrogen sulfide on Northern pike eggs and sac fry. *Transactions of the American Fisheries Society.* **99**(3), 501–509.

Afonso, M. D. S. and Stumm, W., (1992). Reductive dissolution of iron(III) (hydr)oxides by hydrogen sulfide. *Langmuir* [online]. **8**, 1671–1675. [Viewed 10 April 2021]. Available from: doi: 10.1021/la00042a030.

Aguilar-Islas, A. and Bruland, K., (2006). Dissolved manganese and silicic acid in the Columbia River plume. *Marine Chemistry* [online]. **101**(3–4), 233–247. [Viewed 2 June 2021]. Available from: doi: 10.1016/j.marchem.2006.03.005.

Amador, J. A. and Loomis, G., (2018). *Soil-based Wastewater Treatment.* Madison: American Society of Agronomy, Soil Science Society of America, and Crop Science Society of America.

Attramadal, K., (2020). *Marine RAS and H_2S* [PowerPoint presentation]. February. [Viewed 27 February 2020]. Available from: https://ntnu.blackboard.com.

Bailey, L. D. and Beauchamp, E. G., (1971). Nitrate Reduction, and Redox Potentials Measured with Permanently and Temporarily Placed Platinum Electrodes In Saturated Soils. *Canadian Journal of Soil Science*. **51**, 51–5.

Barbeau, K., Rue, E. L., Bruland, K. W. and Butler, A., (2001). Photochemical cycling of iron in the surface ocean mediated by microbal iron(III)-binding ligands. *Nature* [online]. **413**(6854), 409–413. [Viewed 10 April 2021]. Available from: doi: 10.1038/35096545.

Barton, L. L. and Hamilton, W. A., (2007). *Sulphate-reducing bacteria: environmental and engineered systems*. New York: Cambridge University Press.

Bell, R. G., (1969). Studies on the decomposition of organic matter in flooded soil. Soil Biology and Biochemistry [online]. **1**(2), 105–116. [Viewed 23 May 2021]. Available from: doi: 10.1016/0038-0717(69)90001-7.

Bentzen, G., Smith, T. A., Bennett, D., Webster, N. J., Reinholt, F., Sletholt, E. and Hobson, J., (1995). Controlled dosing of nitrate for prevention of H2S in a sewer network and the effects on the subsequent treatment processes. *Water Science and Technology* [online]. **31**(7), 293–302. [Viewed 18 May 2021]. Available from: doi: 10.1016/0273-1223(95)00346-O.

Bergquist, B., Wu, J. and Boyle, E., (2007). Variability in oceanic dissolved iron is dominated by the colloidal fraction. *Geochimica et Cosmochimica Acta* [online]. **71**(12), 2960–2974. [Viewed 6 April 2021]. Available from: doi: 10.1016/j.gca.2007.03.013

Bjørndal, T. and Tusvik, A., (2017). *Land based farming of salmon: economic analysis.* Working Paper Series 1, Norwegian University of Science and Technology Ålesund.

Borman, C. J., Sullivan, B. P., Eggleston, C. M. and Colberg, P. J. S., (2009). The Use of Flow-Injection Analysis with Chemiluminescence Detection of Aqueous Ferrous Iron

in Waters Containing High Concentrations of Organic Compounds. *Sensors* [online]. **9**(6), 4390-4406. [Viewed 12 April 2021]. Available from: doi: 10.3390/s90604390.

Boyd, C. E., (2014). Hydrogen Sulfide Toxic, But Manageable. *Global Aquaculture Advocate* [online]. March/April 2014, 35–36. [Viewed 2 February 2020]. Available from: https://aquafishcrsp.oregonstate.edu/sites/aquafishcrsp.oregonstate.edu/files/boyd2014hydrogensulfide_gaa.pdf.

Boyd, P. W. and Ellwood, M. J., (2010). The biogeochemical cycle of iron in the ocean. *Nature Geoscience* [online]. **3**, 675–682. [Viewed 5 June 2021]. Available from: doi: 10.1038/ngeo964.

Burdige, D. J., (1993). The biogeochemistry of manganese and iron reduction in marine sediments. *Earth-Science Reviews* [online]. **35**, 249–284. [Viewed 4 June 2021]. Available from: https://uol.de/f/5/inst/icbm/ag/mbgc/Publikation/Burdige_Fe_Mn_reduction_Earth_Sci_Rev_1993.pdf.

Calhoun, D. B., Englander, S. W., Wright, W. W. and Vanderkooi, J. M., (1988). Quenching of room temperature protein phosphorescence by added small molecules. *Biochemistry* [online]. **27**(22), 8466–8474. [Viewed 12 August 2020]. Available from: doi:10.1021/bi00422a026.

Cenens, J. and Schoonheydt, R. A., (1988). Visible Spectroscopy of Methylene Blue on Hectorite, Laponite B, and Barasym in Aqueous Suspension. *Clays and Clay Minerals* [online]. **36**(3), 214-224. [Viewed 8 June 2021]. Available from: doi: 10.1346/CCMN.1988.0360302.

Chapin, T. P., (1990). *Determination of Manganese in Seawater by Flow Injection Analysis with Chemiluminescence Detection.* Master thesis, San Jose State University, California, USA. [Viewed 14 August 2020]. Available from: doi: 10.31979/etd.spg4-fe7e.

Chapin, T. P., Johnson, K. S. and Coale, K. H., (1991). Rapid determination of manganese in seawater by flow-injection analysis with chemiluminescence detection. *Analytica Chimica Acta*. **249**, 469–478.

Chever, F., Rouxel, O. J., Croot, P. L., Ponzevera, E., Wuttig, K. and Auro, M., (2015). Total dissolvable and dissolved iron isotopes in the water column of the Peru upwelling regime. *Geochimica et Cosmochimica Acta* [online]. **162**, 66–82. [Viewed 9 April 2021]. Available from: doi: 10.1016/j.gca.2015.04.031.

Cline, J. D., (1969). Spectrophotometric determination of hydrogen sulphide in natural waters. *Limnology and Oceanography* [online]. **14**, 454–458. [Viewed 27 January 2021]. Available from: doi: https://doi.org/10.4319/lo.1969.14.3.0454.

Croot, P. L. and Laan, P., (2002). Continuous shipboard determination of Fe(II) in polar waters using flow injection analysis with chemiluminescence detection. *Analytica Chimica Acta* [online]. **466**(2), 261-273. [Viewed 12 April 2021]. Available from: doi: 10.1016/S0003-2670(02)00596-2.

de Baar, H. J. W. and de Jong, J. T. M., (2001). Distributions, sources and sinks of iron in seawater. In: D. Turner and K. A. Hunter, eds. *Biogeochemistry of Iron in Seawater*. New York: Wiley. pp. 123–253.

DeLaune R. D. and Reddy, K. R., (2005). Redox Potentials. In: D. Hillel, ed. *Encyclopedia of Soils in the Environment.* New York: Elsevier Ltd. pp. 366–371.

Dilling, W. and Cypionka, H., (1990). Aerobic respiration in sulfate-reducing bacteria. *FEMS Microbiology Letters*, **71**, 123–128.

Estensen, B. J., (2021). Redox reactions in the oxic-anoxic water column interface. Master thesis, Norwegian University of Science and Technology, Trondheim, Norway. [Unpublished].

EY., (2019). *The Norwegian Aquaculture Analysis 2019* [online]. UK: EYGM Limited. [Viewed 2 February 2020]. Available from: https://assets.ey.com/content/dam/ey-sites/ey-com/no_no/topics/fiskeri-og-sjømat/norwegian-aquaculture-analysis_2019.pdf.

Fitzsimmons, J. N. and Boyle, E. A., (2012). An intercalibration between the geotraces goflo and the mitess/vanes sampling systems for dissolved iron concentration analyses (and a closer look at adsorption effects. *Limnology and Oceanography: Methods* [online]. **10**(6):437–450. [Viewed 27 January 2021]. Available from: doi: 10.4319/lom.2012.10.437.

Fjellheim, A. J., Hess-Erga, O., Attramadal, K., and Vadstein, O., (2017). *Recycling of water in hatchery production - Background booklet for courses in recycling technology for hatchery production*. Serial number: 7107-2017. ISBN number: 978-82-577-6842-3.

Frindte, K., Allgaier, M., Grossart, H.-P. and Eckert, W., (2015) Microbial Response to Experimentally Controlled Redox Transitions at the Sediment Water Interface. *PLoS ONE* [online]. **10**(11), e0143428. [Viewed 18 May 2021]. Available from: doi: 10.1371/journal.pone.0143428.

García de Lomas, J., Corzo, A., Gonzalez, J. M., Andrades, J. A., Iglesias, E. and Montero, M. J., (2006). Nitrate promotes biological oxidation of sulfide in wastewaters: experiment at plant-scale. *Biotechnology & Bioengineering* [online]. **93**(4), 801–11. [Viewed 18 May 2021]. Available from: doi: 10.1002/bit.20768.

Gardiner, D. T. and James, S., (2012). Wet Soil Redox Chemistry as Affected by Organic Matter and Nitrate. *American Journal of Climate Change*, **1**, 205–209. [Viewed 19 May 2021]. Available from: doi: 10.4236/ajcc.2012.14017.

Geider, R. J. and Laroche, J. (1994). The role of iron in phytoplankton photosynthesis, and the potential for iron-limitation of primary productivity in the sea. *Photosynthesis Research* [online]*.* **39**(3), 275–301. [Viewed 10 April 2021]. Available from: doi: 10.1007/BF00014588.

Gledhill, M. and Buck, K. N., (2012). The organic complexation of iron in the marine environment: a review. *Frontiers in Microbiology* [online]. **3**, 69. [Viewed 9 April 2021]. Available from: doi: 10.3389/fmicb.2012.00069.

Hansel, C. M., (2017). Manganese in Marine Microbiology. *Advances in microbial physiology* [online]. **70**, 37–83. [Viewed 14 August 2020]. Available from: doi: 10.1016/bs.ampbs.2017.01.005.

Harvey, D., (2019). Flow Injection Analysis [online]. *Chemistry Libretexts.* [Viewed 2 April 2021]. Available from: https://chem.libretexts.org/@go/page/5589.

Hem, J. D., (1985). Study and interpretation of the chemical characteristics of natural water. In: U.S. Geological Survey Water-Supply Paper 2254, 3rd edition. USA: United States Government Printing Office.

Hem, J. D. and Cropper, W. H., (1959). Survey of Ferrous-Ferric Chemical Equilibria and Redox Potentials. In: U.S. Geological Survey. *Chemistry of Iron in Natural Water* [online]. Washington: U.S. G.P.O. [Viewed 6 April 2021]. Available from: doi: 10.3133/wsp1459A.

Hunter, K. A. and Boyd, P. W., (2007). Iron-binding ligands and their role in the ocean biogeochemistry of iron. *Environmental Chemistry* [online]. **4**(4), 221–232, [Viewed 9 April 2021]. Available from: doi: 10.1071/EN07012.

Jiang, G., Gutierrez, O., Sharma, K. R. and Yuan, Z., (2010). Effects of nitrite concentration and exposure time on sulfide and methane production in sewer systems. *Water Research* [online]. **44**(14), 4241–51. [Viewed 18 May 2021]. Available from: doi: 10.1016/j.watres.2010.05.030.

Khozyem, H., Hamdan, A., Tantawy, A. A., Emam, A. and Elbadry, E., (2019). Distribution and origin of iron and manganese in groundwater: case study, Balat-Teneida area, El-Dakhla Basin, Egypt. *Arabian Journal of Geosciences* [online]. **12**, 523. [Viewed 6 June 2021]. Available from: doi: 10.1007/s12517-019-4689-1.

Kiemer, M. C. B., Black, K. D., Lussot, D., Bullock, A. M. and Ezzi, I., (1995). The effects of chronic and acute exposure to hydrogen sulphide on Atlantic salmon (*Salmo salar* L.). *Aquaculture* [online]. **135**, 311–327. [Viewed 19 May 2021]. Available from: doi: 10.1016/0044-8486(95)01025-4.

King, D. W. and Farlow, R., (2000). Role of carbonate speciation on the oxidation of Fe(II) by H2O2. *Marine Chemistry*. **70**, 201–209.

Klinkhammer, G. P., (1980). Early diagenesis in sediments from the eastern equatorial Pacific, II. Pore water metal results. *Earth and Planetary Science Letters*. **49**(1), 81-101. 10.1016/0012-821X(80)90151-X

Korom, S. F., (1992). Natural denitrification in the saturated zone: a review. *Water Resources Research* [online]. **28**(6), 1657–1668. [Viewed 8 April 2021]. Available from: doi: 10.1029/92WR00252.

Kranzler, C., Lis, H., Shaked, Y. and Keren, N., (2011). The role of reduction in iron uptake processes in a unicellular, planktonic cyanobacterium. *Environmental Microbiology* [online]. **13**(11), 2990–2999. [Viewed 10 April 2021]. Available from: doi: 10.1111/j.1462-2920.2011.02572.x.

Kuma, K., Nakabayashi, S., Suzuki, Y., Kudo, I. and Matsunaga, K., (1992). Photo-reduction of Fe(II) by dissolved organic substances and existence of Fe(II) in seawater during spring blooms. *Marine Chemistry* [online]. **37**(1–2), 15–27. [Viewed 10 April 2021]. Available from: 10.1016/0304-4203(92)90054-E.

Kuma, K., Nishioka, J. and Matsunaga, K., (1996). Controls on iron(iii) hydroxide solubility in seawater; the influence of ph and natural organic chelators. *Limnology and Oceanography* [online]. **41**(3), 396–407. [Viewed 6 April 2021]. Available from: https://aslopubs.onlinelibrary.wiley.com/doi/pdf/10.4319/lo.1996.41.3.0396.

Letelier-Gordo, C. O., Aalto, S. L., Suurnäkki, S. and Pedersen, P. B., (2020). Increased sulfate availability in saline water promotes hydrogen sulfide production in fish organic waste. *Aquaculture Engineering* [online]. **89**, 102062. [Viewed 18 May 2021]. Available from: doi: 10.1016/j.aquaeng.2020.102062.

Li, L. and Moore, P. K., (2008). Putative biological roles of hydrogen sulfide in health and disease: a breath of not so fresh air?. *Trends in Pharmacological Sciences* [online]

29(2), 84–90. [Viewed 12 August 2020]. Available from: doi: 10.1016/j.tips.2007.11.003.

Li, Q. and Lancaster, J. R. Jr, (2013). Chemical foundations of hydrogen sulfide biology. *Nitric Oxide* [online]. **35**, 21–34. [Viewed 12 August 2020]. Available from: doi: 10.1016/j.niox.2013.07.001.

Li, Z., (2015). Quantification of hydrogen sulfide concentration using methylene blue and 5,5'-dithiobis(2-nitrobenzoic acid) methods in plants. *Methods in Enzymology* [online]. **554**C, 101-110. [Viewed 8 June 2021]. Available from: doi: 10.1016/bs.mie.2014.11.031.

Liu, F.-J., Huang, B.-Q., Li, S.-X., Zheng, F.-Y. and Huang, X.-G., (2016). Effect of nitrate enrichment and diatoms on the bioavailability of Fe(III) oxyhydroxide colloids in seawater. *Chemosphere* [online]. **147**, 105–113. [Viewed 18 May 2021]. Available from: doi: 10.1016/j.chemosphere.2015.12.098.

Middag, R., de Baar, H., Klunder, M. and Laan, P., (2013). Fluxes of dissolved aluminum and manganese to the Weddell Sea and indications for manganese co-limitation, *Limnology and Oceanography* [online]. **58**(1), 287–300. [Viewed 2 June 2021]. Available from: doi: 10.4319/lo.2013.58.1.0287.

Middag, R., de Baar, H., Laan, P. and Klunder, M., (2011). Fluvial and hydrothermal input of manganese into the Arctic Ocean [online]. *Geochimica et Cosmochimica Acta* [online]. **75**(9), 2393–2408. [Viewed 2 June 2021]. Available from: doi: 10.1016/j.gca.2011.02.011.

Miller, W. L., King, D. W., Lin, J. and Kester, D. R., (1995). Photochemical redox cycling of iron in coastal seawater. *Marine Chemistry* [online]. **50**, 63–77. [Viewed 10 April 2021]. Available from: doi: 10.1016/0304-4203(95)00027-O.

Misumi, K., Lindsay, K., Moore, J. K., Doney, S. C., Bryan, F. O., Tsumune, D. and Yoshida, Y., (2014). The iron budget in ocean surface waters in the 20th and 21st centuries: projections by the community earth system model version 1. *Biogeosciences* [online]. **11**, 33–55. [Viewed 9 April 2021]. Available from: doi: 10.5194/bg-11-22-2014.

Mohanakrishnan, J., Gutierrez, O., Meyer, R. L. and Yuan, Z., (2008). Nitrite effectively inhibits sulfide and methane production in a laboratory scale sewer reactor. *Water Research* [online]. **42**(14), 3961–71. [Viewed 18 May 2021]. Available from: doi: 10.1016/j.watres.2008.07.001.

Moore, J. K. and Braucher, O. (2007). Observations of dissolved iron concentrations in the World Ocean: implications and constraints for ocean biogeochemical models. *Biogeosciences Discuss* [online]. **4**, 1241–1277. [Viewed 10 April 2021]. Available from: https://bg.copernicus.org/preprints/4/1241/2007/bgd-4-1241-2007.pdf

Moore, J. K. and Braucher, O., (2008). Sedimentary and mineral dust sources of dissolved iron to the world ocean. *Biogeosciences* [online]. **5**(3), 631–656. [Viewed 9 April 2021]. Available from: doi: 10.5194/bg-5-631-2008.

Moore, C. M., Mills, M. M., Achterberg, E. P., Geider, R. J., La Roche, J., Lucas, M. I., McDonagh, E. L., Pan, X., Poulton, A. J., Rijkenberg, M. J. A., Suggett, D. J., Ussher, S. J. and Woodward, E. M. S., (2009). Large-scale distribution of Atlantic nitrogen fixation controlled by iron availability. *Nature Geoscinces* [online]. **2**, 867–871. [Viewed 10 April 2021]. Available from: doi: 10.1038/ngeo667.

Muyzer, G. and Stams, A. J. M., (2008). The ecology and biotechnology of sulphate-reducing bacteria. *Nature Reviews Microbiology* [online]. **6**, 441–454. [Viewed 2 February 2020]. Available from: doi: 10.1038/nrmicro1892.

National Center for Biotechnology Information., (2020). PubChem Compound Summary for CID 402, Hydrogen sulfide [online]. *PubChem*. [Viewed 12 August 2020]. Available from: https://pubchem.ncbi.nlm.nih.gov/compound/Hydrogen-sulfide.

Nielsen, A. H., Lens, P., Vollertsen, J. and Hvitved-Jacobsen, T., (2005). Sulfide-iron interactions in domestic wastewater from a gravity sewer. *Water Research* [online]. **39**(12), 2747–2755. [Viewed 18 May 2021]. Available from: doi: 10.1016/j.watres.2005.04.048.

Nofima., (2015). Potential for high salmon survival in future aquaculture systems [online]. *Nofima*. [Viewed 2 February 2020]. Available from: https://nofima.no/en/nyhet/2014/11/potential-for-high-salmon-survival- in-future-aquaculture-systems/.

O' Sullivan, D. W. Hanson, A. K., Jr. and Kester, D. R., (1995). Stopped flow luminol chemiluminescence determination of Fe(II) and reducible iron in seawater at subnanomolar levels. *Marine Chemistry* [online]. **49**, 65-77. [Viewed 12 April 2021]. Available from: doi: 10.1016/0304-4203(94)00046-G.

Ohio. Office of Research and Development, United States Environmental Protection Agency., (1994). *Method 200.7, Revision 4.4: Determination of Metals and Trace Elements in Water and Wastes by Inductively Coupled Plasma-Atomic Emission Spectrometry* [online]. pp. 200.7-22. [Viewed 27 January 2021]. Available from: https://www.epa.gov/sites/production/files/2015-08/documents/method_200-7_rev_4-4_1994.pdf.

Oldham, V. E., Lamborg, C. H. and Hansel, C. M., (2019). The Spatial and Temporal Variability of Mn Speciation in the Coastal Northwest Atlantic Ocean. *Journal of Geophysical Research: Oceans* [online]. **125**(1). [Viewed 14 August 2020]. Available from: doi: 10.1029/2019JC015167.

Opphardt, C. E., (2003). DENSITY Applications with Gases [online]. *Virtual Chembook Elmhurst College.* [Viewed 12 August 2020]. Available from: http://chemistry.elmhurst.edu/vchembook/123Adensitygas.html.

Oseid, D. M. and Smith, L. L., (1972). Swimming endurance and resistance to copper and malathion of bluegills treated by long-term exposure to sublethal levels of hydrogen sulfide. *Transactions of the American Fisheries Society*. **4**, 620–625.

Pullin, M. J. and Cabaniss, S. E., (2001). Colorimetric flow-injection analysis of dissolved iron in high DOC waters. *Water Research* [online]. **35**, 363-372. [Viewed 12 April 2021]. Available from: doi: 10.1016/s0043-1354(00)00259-1.

Ramos, G. S., Casiano J. M. S. and Dávila M. G., (2016). Effect of ocean warming and acidification on the Fe(II) oxidation rate in oligotrophic and eutrophic natural waters. *Biogeochemistry* [online]. **128**, 19–34. [Viewed 10 April 2021]. Available from: doi: 10.1007/s10533-016-0192-x.

Rose, A. L. and Waite, T. D., (2001). Chemiluminescence of luminol in the presence of iron(II) and oxygen: Oxidation mechanism and implications for its use. *Analytical Chemistry* [online]. **73**(24), 5909-5920. [Viewed 12 April 2021]. Available from: doi: 10.1021/ac015547q.

Samiei, M. and Bostani, A., (2016). Manganese Fractionation in Soils after Application of Municipal Solid Wastes Compost in Two Consecutive Years. *Applied and Environmental Soil Science* [online]. **2016**, Article ID 5202789. [Viewed 4 June 2021]. Available from: doi: 10.1155/2016/5202789.

Santana-Casiano, J. M., Davila, M. G., Rodriguez, M. J. and Millero, F.J., (2000). The effect of organic compounds in the oxidation kinetics of Fe(II). *Marine Chemistry* [online]. **70**(1–3), 211–222. [Viewed 12 April 2021]. Available from: doi: 10.1016/S0304-4203(00)00027-X.

Santana-Casiano, J. M., Davila, M. G. and Millero, F. J., (2005). Oxidation of nanomolar levels of Fe(II) with oxygen in natural waters*. Environmental Science & Technology* [online]*.* **39**(7), 2073–2079. [Viewed 6 April 2021]. Available from: doi: 10.1021/es049748y.

Schmidt, K., Schlosser, C., Atkinson, A., Fielding, S., Venables, H. J., Waluda, C. M. and Achterberg, E. P., (2016). Zooplankton gut passage mobilizes lithogenic iron for ocean productivity. *Current Biology* [online]. **26**(19), 2667–2673. [Viewed 9 April 2021]. Available from: doi: 10.1016/j.cub.2016.07.058.

Sjöstedt, C., Persson, I., Hesterberg, D., Kleja, D. B., Borg, H., and Gustafsson, J. P., (2013). Iron speciation in soft-water lakes and soils as determined by EXAFS spectroscopy and geochemical modelling. *Geochimica et Cosmochimica Acta* [online]. **105**, 172 – 186. [Viewed 5 June 2021]. Available from: doi: 10.1016/j.gca.2012.11.035.

Slomp, C. P., Epping, E. H. G., Helder, W. and Raaphorst, W. Van., (1996). A key role for iron-bound phosphorus in authigenic apatite formation in North Atlantic continental platform sediments. *Journal of Marine Research*. **54**, 1179–1205.

Smith, L. L. and Oseid, D. M., (1974). Effect of hydrogen sulfide on development and survival of eight freshwater fish species. In: J. H. S. Blaxter, ed. *The Early Life History of Fish* [online]*.* Heidelberg: Springer Berlin Heidelberg. pp. 417–430. [Viewed 19 May 2021]. Available from: doi: 10.1007/978-3-642-65852-5_34.

Soetaert, K., Hofmann, A. F., Middelburg, J. J., Meysman, F. J. R. and Greenwood, J., (2007). The effect of biogeochemical processes on pH. *Marine Chemistry* [online] **105**, 30–51. [Viewed 23 May 2021]. Available from: doi: 10.1016/j.marchem.2006.12.012.

Stumm, W. and Morgan, J. J., (1996). *Aquatic Chemistry, Chemical Equilibria and Rates in Natural Waters.* 3rd ed. New York: John Wiley & Sons, Inc.

Su, H., Yang, R., Pižeta, I., Omanović, D., Wang, S. and Li, Y., (2016). Distribution and Speciation of Dissolved Iron in Jiaozhou Bay (Yellow Sea, China). *Frontiers in Marine Science* [online]. **3**, 99. [Viewed 11 June 2021]. Available from: doi: 10.3389/fmars.2016.00099.

Sunda, W., Huntsman, S. and Harvey, G. (1983). Photoreduction of manganese oxides in seawater and its geochemical and biological implications. *Nature* [online]. **301**, 234–236. [Viewed 14 August 2020]. Available from: doi: 10.1038/301234a0.

Sunda, W. G., (1994). Trace Metal/Phytoplankton Interactions in the Sea. In: G. Bidoglio and W. Stumm, eds. *Chemistry of Aquatic Systems: Local and Global Perspectives. EUROCOURSES (Chemical and Environmental Science)* [online]*.* vol 5. Dordrecht:

Springer. pp. 213–247. [Viewed 14 August 2020]. Available from: doi: 10.1007/978-94-017-1024-4_9.

Swanner, E. D., Maisch, M., Wu, W. and Kappler, A., (2018). Oxic Fe(III) reduction could have generated Fe(II) in the photic zone of Precambrian seawater. *Scientific Reports* [online]. **8**, 4238. [Viewed 10 April 2021]. Available from: doi: 10.1038/s41598-018-22694-y.

Tagliabue, A., Bowie, A. R., Boyd, P. W., Buck, K. N., Johnson, K. S. and Saito, M. A., (2017). The integral role of iron in ocean biogeochemistry. *Nature* [online], **543** (7643), 51–59. [Viewed 10 April 2021]. Available from: doi: 10.1038/nature21058.

Tebo, B. M., Bargar, J. R., Clement, B. G., Dick, G. J., Murray, K. J., Parker, D., Verity, R. and Webb, S. M., (2004). Biogenic manganese oxides, properties and mechanisms of formation. *Annual Review of Earth and Planetary Sciences* [online]. **32**, 287–328. [Viewed 14 August 2020]. Available from: doi: 10.1146/annurev.earth.32.101802.120213.

Theis, T. L. and Singer, P. C., (1974). Complexation of iron(II) by organic matter and its effect on iron(II) oxygenation. *Environmental Science & Technology*. **8**, 596–573.

Tiedje, J. M., (1990). Ecology of denitrification and dissimilatory nitrate reduction to ammonia. In: A. J. B. Zehnder, ed. *Biology of Anaerobic Microorganisms.* New York: Wiley. pp. 179– 244.

Trouwborst, R. E., Clement, B. G., Tebo, B. M., Glazer, B. T. and Luther, G. W. 3rd., (2006). Soluble Mn(III) in suboxic zones. *Science* [online]. **313**(5795), 1955–1957. [Viewed 14 August 2020]. Available from: doi: 10.1126/science.1132876.

USA. Department of Environment and Natural Resources Division of Water Resources., (2015). *Summary of North Carolina Surface Water Quality Standards 2007-2014* [online]. [Viewed 27 January 2021]. Available from: https://files.nc.gov/ncdeq/documents/files/Summary%20of%20NC%20standards_Tri%20Rev%20Report_May_4_2015.pdf.

van Beek, C. G. E. M., Cirkel, D. G., de Jonge, M. J. and Hartog, N., (2021). Concentration of Iron(II) in Fresh Groundwater Controlled by Siderite, Field Evidence. *Aquatic Geochemistry* [online]. **27**, 49–61. [Viewed 6 June 2021]. Available from: doi: 10.1007/s10498-020-09390-y.

van Rijn, J., Rivera, G. (1990). Aerobic and anaerobic biofiltration in an aquaculture unit: nitrite accumulation as a result of nitrification and denitrification. *Aquacultural Engineering* [online]. **9**(4), 1–18. [Viewed 8 April 2021]. Available from: doi: 10.1016/0144-8609(90)90017-T.

van Rijn, J., Tal., Y. and Schreier, H. J., (2006). Denitrification in recirculating systems: Theory and applications. *Aquaculture Engineering* [online]. **34**(3), 364–376. [Viewed 12 August 2020]. Available from: doi: 10.1016/j.aquaeng.2005.04.004.

von der Heyden, B. and Roychoudhury, A., (2015). A review of colloidal iron partitioning and distribution in the open ocean. *Marine Chemistry*. **177**. [Viewed 6 April 2021]. Available from: doi: 10.1016/j.marchem.2015.05.010.

Wang, Z. W, Ren, J. L., Jiang, S., Liu, S. M., Xuan, J. L. and Zhang, J., (2016). Geochemical behavior of dissolved manganese in the East China Sea: Seasonal variation, estuarine removal, and regeneration under suboxic conditions.

Geochemistry, Geophysics, Geosystems [online]. **17**(2), 282–299. [Viewed 11 June 2021]. Available from: doi: 10.1002/2015GC006128.

Weber, K. A., Urrutia, M. M., Churchill, P. F., Kukkadapu, R. K. and Roden, E. E., (2006). Anaerobic redox cycling of iron by freshwater sediment microorganisms. *Environmental Microbiology* [online]. **8**(1), 100–113. [Viewed 18 May 2021]. Available from: doi: 10.1111/j.1462-2920.2005.00873.x.

Weiner, E. R., (2007). *Applications of Environmental Aquatic Chemistry: A Practical Guide.* 2nd ed. Boca Raton: CRC Press.

Wells, M. L., Price, N. M. and Bruland, K. W., (1994). Iron chemistry in seawater and its relationship to phytoplankton: a workshop report. *Marine Chemistry* [online]. **48**, 157–182. [Viewed 9 April 2021]. Available from: https://websites.pmc.ucsc.edu/~kbruland/Manuscripts/WELLS/WellsBrulandPriceMarChem1995.pdf.

Wilschefski, S. C. and Baxter, M. R., (2019). Inductively Coupled Plasma Mass Spectrometry: Introduction to Analytical Aspects. *The Clinical Biochemist Reviews* [online]. **40**(3): 115 – 133. [Viewed 11 June 2021]. Available from: doi: 10.33176/AACB-19-00024.

Włodarczyk, T., Szarlip, P., Brzezińska, M., Kotowska, U., (2007). Redox potential, nitrate content and pH in flooded Eutric Cambisol during nitrate reduction. Research In Agricultural Engineering, **53**(1), 20–28. [Viewed 19 May 2021]. Available from: doi: 10.17221/2132-RAE.

Yakushev, E., Pakhomova, S., Sørensona, K. and Skeia, J., (2009). Importance of the different manganese species in the formation of water column redox zones: Observations and modelling. *Marine Chemistry* [online]. **117**(1–4), 59 – 70. [Viewed 4 June 2021]. Available from: doi: 10.1016/j.marchem.2009.09.007.

Yamane, I. and Sato, K., (1964). Decomposition of glucose and gas formation in flooded soil. *Soil Science and Plant Nutrition*, **10**(3), 35-41. [Viewed 23 May 2021]. Available from: doi: 10.1080/00380768.1964.10431125.

Yongsiri, C., Hvitved-Jacobsen, T. and Vollertsen, J., (2004). Effect of Temperature on Air-Water Transfer of Hydrogen Sulfide. *Journal of Environmental Engineering* [online]. **130**(1). [Viewed 12 August 2020]. Available from: doi: 10.1061/(ASCE)0733-9372(2004)130:1(104).

Ytrestøyl , T., Takle, H., Kolarevic, J., Calabrese, S., Timmerhaus, G., Rosseland, B. O., Teien, H. C., Nilsen, T. O., Handeland, S. O., Stefansson, S. O., Ebbesson, L. O. E. and Terjesen, B. F., (2020). Performance and welfare of Atlantic salmon, Salmo salar L. post-smolts in recirculating aquaculture systems: Importance of salinity and water velocity. *Journal of the World Aquaculture Society* **51**, 2 [online]. [Viewed 19 May 2021]. Available from: doi: https://doi.org/10.1111/jwas.12682.

Yu, T. and Bishop, P. L., (1998). Stratification of microbial metabolic processes and redox potential change in an aerobic biofilm studied using microelectrodes. *Water Science and Technology* [online], **37**(4), 195–198. [Viewed 12 August 2020]. Available from: doi: 10.1016/S0273-1223(98)00104-8.

Zhang, J. Z. and Millero, F. J., (1993). The products from the oxidation of H_2S in seawater. *Geochimica et Cosmochimica Acta* [online]. **57**(8), 1705–1718. [Viewed 12 August 2020]. Available from: doi: 10.1016/0016-7037(93)90108-9.

Åtland, Å. and Stenberg, S. K., (2019). Water quality. In: B. Hjeltnes, B. Bang-Jensen, G. Bornø, A. Haukaas and C. S. Walde, eds. *The Health Situation in Norwegian Aquaculture 2018*. Norway: Norwegian Veterinary Institute 2019. pp. 96–99.

Appendices

Appendix 1: Fe (II) Raw Data from FIA-CL Measurement

Appendix 2: ICP-MS Results

Appendix 3: H_2S Measurement

Appendix 4: pH, Redox Potential, and Dissolved O_2

Appendix 1: Fe (II) Raw Data from FIA-CL Measurement

Date	Day	Sam-ple	Repli-cation	Samp-ling Time	Analy-sis Time	Time Differ-ence	Area	Maximum Height	Equation of Max Height vs Time for Extrapolation	Max height from extrapolation (t=60)	Calibration (Max Height vs Fe (II) Conc)	Fe (II) (nm) (t=60)
11-Feb-21	D0	1C	1	10:45	12:49	2:04:00	0.00	0.00		0.00		0.00
11-Feb-21	D0	1C	1	10:45	12:51	2:06:00	0.00	0.00		0.00		0.00
11-Feb-21	D0	1C	2	10:45	12:53	2:08:00	0.00	0.00		0.00		0.00
11-Feb-21	D0	1C	2	10:45	12:55	2:10:00	0.00	0.00		0.00		0.00
11-Feb-21	D0	1C	3	10:45	12:57	2:12:00	0.00	0.00		0.00		0.00
11-Feb-21	D0	1C	3	10:45	13:00	2:15:00	0.00	0.00		0.00		0.00
11-Feb-21	D0	2C	1	10:55	13:02	2:07:00	0.00	0.00		0.00		0.00
11-Feb-21	D0	2C	1	10:55	13:04	2:09:00	0.00	0.00		0.00		0.00
11-Feb-21	D0	2C	2	10:55	13:06	2:11:00	0.00	0.00		0.00		0.00
11-Feb-21	D0	2C	2	10:55	13:08	2:13:00	0.00	0.00		0.00		0.00
11-Feb-21	D0	2C	3	10:55	13:10	2:15:00	474.50	220		0.00		0.00
11-Feb-21	D0	2C	3	10:55	13:12	2:17:00	350.68	212		0.00		0.00
11-Feb-21	D0	1C	1	10:45	14:19	3:34:00	0.00	0.00		0.00		0.00
11-Feb-21	D0	1C	1	10:45	14:21	3:36:00	0.00	0.00		0.00		0.00
11-Feb-21	D0	1C	2	10:45	14:23	3:38:00	0.00	0.00		0.00		0.00
11-Feb-21	D0	1C	2	10:45	14:25	3:40:00	0.00	0.00		0.00		0.00
11-Feb-21	D0	1C	3	10:45	14:28	3:43:00	0.00	0.00		0.00		0.00
11-Feb-21	D0	1C	3	10:45	14:30	3:45:00	0.00	0.00		0.00		0.00
11-Feb-21	D0	2C	1	10:55	14:32	3:37:00	0.00	0.00		0.00		0.00
11-Feb-21	D0	2C	1	10:55	14:34	3:39:00	0.00	0.00		0.00		0.00
11-Feb-21	D0	2C	2	10:55	14:36	3:41:00	0.00	0.00		0.00		0.00
11-Feb-21	D0	2C	2	10:55	14:38	3:43:00	0.00	0.00		0.00		0.00
11-Feb-21	D0	2C	3	10:55	14:40	3:45:00	0.00	0.00		0.00		0.00
11-Feb-21	D0	2C	3	10:55	14:42	3:47:00	0.00	0.00		0.00		0.00

Date	Day	Sam-ple	Repli-cation	Samp-ling Time	Analy-sis Time	Time Differ-ence	Area	Maximum Height	Equation of Max Height vs Time for Extrapolation	Max height from extrapolation (t=60)	Calibration (Max Height vs Fe (II) Conc)	Fe (II) (nm) (t=60)
12-Feb-21	D1	1C	1	11:23	14:23	3:00:00	0.00	0.00		0.00		0.00
12-Feb-21	D1	1C	1	11:23	14:25	3:02:00	0.00	0.00		0.00		0.00
12-Feb-21	D1	1C	2	11:23	14:27	3:04:00	0.00	0.00		0.00		0.00
12-Feb-21	D1	1C	2	11:23	14:29	3:06:00	0.00	0.00		0.00		0.00
12-Feb-21	D1	2C	1	11:35	14:31	2:56:00	0.00	0.00		0.00		0.00
12-Feb-21	D1	2C	1	11:35	14:33	2:58:00	0.00	0.00		0.00		0.00
12-Feb-21	D1	2C	2	11:35	14:35	3:00:00	0.00	0.00		0.00		0.00
12-Feb-21	D1	2C	2	11:35	14:38	3:03:00	0.00	0.00		0.00		0.00
12-Feb-21	D1	1C	1	11:23	15:44	4:21:00	0.00	0.00		0.00		0.00
12-Feb-21	D1	1C	1	11:23	15:46	4:23:00	0.00	0.00		0.00		0.00
12-Feb-21	D1	1C	2	11:23	15:48	4:25:00	0.00	0.00		0.00		0.00
12-Feb-21	D1	1C	2	11:23	15:50	4:27:00	0.00	0.00		0.00		0.00
12-Feb-21	D1	2C	1	11:35	15:52	4:17:00	0.00	0.00		0.00		0.00
12-Feb-21	D1	2C	1	11:35	15:54	4:19:00	0.00	0.00		0.00		0.00
12-Feb-21	D1	2C	2	11:35	15:57	4:22:00	0.00	0.00		0.00		0.00
12-Feb-21	D1	2C	2	11:35	15:59	4:24:00	0.00	0.00		0.00		0.00
12-Feb-21	D1	1N	1	11:47	15:07	3:20:00	0.00	0.00		0.00		0.00
12-Feb-21	D1	1N	1	11:47	15:09	3:22:00	0.00	0.00		0.00		0.00
12-Feb-21	D1	1N	2	11:47	15:11	3:24:00	0.00	0.00		0.00		0.00
12-Feb-21	D1	1N	2	11:47	15:13	3:26:00	0.00	0.00		0.00		0.00
12-Feb-21	D1	2N	1	12:00	15:15	3:15:00	797.87	272		0.00		0.05
12-Feb-21	D1	2N	1	12:00	15:17	3:17:00	755.59	320		0.00		0.05
12-Feb-21	D1	2N	2	12:00	15:19	3:19:00	584.28	260		0.00		0.05
12-Feb-21	D1	2N	2	12:00	15:21	3:21:00	567.62	272		0.00		0.05
12-Feb-21	D1	1N	1	11:47	16:24	4:37:00	0.00	0.00		0.00		0.00

Date	Day	Sam-ple	Repli-cation	Samp-ling Time	Analy-sis Time	Time Differ-ence	Area	Maximum Height	Equation of Max Height vs Time for Extrapolation	Max height from extrapolation (t=60)	Calibration (Max Height vs Fe (II) Conc)	Fe (II) (nm) (t=60)
12-Feb-21	D1	1N	1	11:47	16:26	4:39:00	0.00	0.00		0.00		0.00
12-Feb-21	D1	1N	2	11:47	16:28	4:41:00	0.00	0.00		0.00		0.00
12-Feb-21	D1	1N	2	11:47	16:31	4:44:00	0.00	0.00		0.00		0.00
12-Feb-21	D1	2N	1	12:00	16:33	4:33:00	0.00	0.00		0.00		0.00
12-Feb-21	D1	2N	1	12:00	16:35	4:35:00	0.00	0.00		0.00		0.00
12-Feb-21	D1	2N	2	12:00	16:37	4:37:00	395.75	456		0.00		0.05
12-Feb-21	D1	2N	2	12:00	16:39	4:39:00	343.95	456		0.00		0.05
12-Feb-21	D1	2N	1	12:00	16:41	4:41:00	395.75	456		0.00		0.05
12-Feb-21	D1	2N	1	12:00	16:43	4:43:00	343.95	456		0.00		0.05
13-Feb-21	D2	1C	1	11:22	13:51	2:29:00	51,261.24	9408	y = 21853.78 - (88.87*x)	16,521.58	y = 298.91 + (813.33*x)	19.95
13-Feb-21	D2	1C	1	11:22	13:53	2:31:00	43,320.46	7620	y = 21853.78 - (88.87*x)	16,521.58	y = 298.91 + (813.33*x)	19.95
13-Feb-21	D2	1C	2	11:22	13:55	2:33:00	42,543.97	8648	y = 24660.568 - (106.279*x)	18,283.83	y = 298.91 + (813.33*x)	22.11
13-Feb-21	D2	1C	2	11:22	13:57	2:35:00	37,582.10	7940	y = 24660.568 - (106.279*x)	18,283.83	y = 298.91 + (813.33*x)	22.11
13-Feb-21	D2	2C	1	11:30	13:59	2:29:00	49,155.77	8076	y=20940.143 - (86.491*x)	15,750.68	y = 298.91 + (813.33*x)	19.00
13-Feb-21	D2	2C	1	11:30	14:01	2:31:00	48,282.61	7844	y=20940.143 - (86.491*x)	15,750.68	y = 298.91 + (813.33*x)	19.00
13-Feb-21	D2	2C	2	11:30	14:04	2:34:00	66,350.97	10428	y = 27466.379 - (109.259*x)	20,910.84	y = 298.91 + (813.33*x)	25.34
13-Feb-21	D2	2C	2	11:30	14:06	2:36:00	66,300.89	10632	y = 27466.379 - (109.259*x)	20,910.84	y = 298.91 + (813.33*x)	25.34
13-Feb-21	D2	1N	1	11:38	14:14	2:36:00	826.33	356	y = exp (6.724707 - 0.006072*x)	578.47	y = 38.26 + (905.45*x)	0.60
13-Feb-21	D2	1N	1	11:38	14:16	2:38:00	472.91	288	y = exp (6.724707 - 0.006072*x)	578.47	y = 38.26 + (905.45*x)	0.60
13-Feb-21	D2	1N	2	11:38	14:18	2:40:00	0.00	0.00		0.00		0.00
13-Feb-21	D2	1N	2	11:38	14:21	2:43:00	0.00	0.00		0.00		0.00
13-Feb-21	D2	2N	2	11:45	14:27	2:42:00	1,201.83	944	y = 1982.610 - (8.293*x)	1,485.03	y = 38.26 + (905.45*x)	1.60
13-Feb-21	D2	2N	2	11:45	14:29	2:44:00	725.69	304	y = 1982.610 - (8.293*x)	1,485.03	y = 38.26 + (905.45*x)	1.60
13-Feb-21	D2	1C	1	11:22	14:38	3:16:00	20,523.54	4040	y = 21853.78 - (88.87*x)	16,521.58	y = 298.91 + (813.33*x)	19.95
13-Feb-21	D2	1C	1	11:22	14:40	3:18:00	24,571.64	4668	y = 21853.78 - (88.87*x)	16,521.58	y = 298.91 + (813.33*x)	19.95

Date	Day	Sam-ple	Repli-cation	Samp-ling Time	Analy-sis Time	Time Differ-ence	Area	Maximum Height	Equation of Max Height vs Time for Extrapolation	Max height from extrapolation (t=60)	Calibration (Max Height vs Fe (II) Conc)	Fe (II) (nm) (t=60)
13-Feb-21	D2	1C	2	11:22	14:42	3:20:00	13,190.07	3136	y = 24660.568 - (106.279*x)	18,283.83	y = 298.91 + (813.33*x)	22.11
13-Feb-21	D2	1C	2	11:22	14:44	3:22:00	15,618.41	3460	y = 24660.568 - (106.279*x)	18,283.83	y = 298.91 + (813.33*x)	22.11
13-Feb-21	D2	2C	1	11:30	14:46	3:16:00	24,116.29	4272	y=20940.143 - (86.491*x)	15,750.68	y = 298.91 + (813.33*x)	19.00
13-Feb-21	D2	2C	1	11:30	14:48	3:18:00	20,187.87	3544	y=20940.143 - (86.491*x)	15,750.68	y = 298.91 + (813.33*x)	19.00
13-Feb-21	D2	2C	2	11:30	14:50	3:20:00	34,002.14	5796	y = 27466.379 - (109.259*x)	20,910.84	y = 298.91 + (813.33*x)	25.34
13-Feb-21	D2	2C	2	11:30	14:53	3:23:00	29,773.93	5108	y = 27466.379 - (109.259*x)	20,910.84	y = 298.91 + (813.33*x)	25.34
13-Feb-21	D2	1N	1	11:38	15:01	3:23:00	263.17	248	y = exp (6.724707 - 0.006072*x)	578.47	y = 38.26 + (905.45*x)	0.60
13-Feb-21	D2	1N	1	11:38	15:03	3:25:00	392.78	236	y = exp (6.724707 - 0.006072*x)	578.47	y = 38.26 + (905.45*x)	0.60
13-Feb-21	D2	1N	2	11:38	15:05	3:27:00	0.00	0.00		0.00		0.00
13-Feb-21	D2	1N	2	11:38	15:07	3:29:00	0.00	0.00		0.00		0.00
13-Feb-21	D2	2N	2	11:45	15:14	3:29:00	513.30	268	y = 1982.610 - (8.293*x)	1,485.03	y = 38.26 + (905.45*x)	1.60
13-Feb-21	D2	2N	2	11:45	15:16	3:31:00	359.82	228	y = 1982.610 - (8.293*x)	1,485.03	y = 38.26 + (905.45*x)	1.60
14-Feb-21	D3	1C	1	11:21	13:09	1:48:00	118,985.47	31,508.00	y = 97845.54 - (615.81*x)	60,896.94	y = -2272.1 + (3050.9*x)	20.71
14-Feb-21	D3	1C	1	11:21	13:11	1:50:00	121,662.68	29,984.00	y = 97845.54 - (615.81*x)	60,896.94	y = -2272.1 + (3050.9*x)	20.71
14-Feb-21	D3	1C	2	11:21	13:13	1:52:00	118,985.47	31,508.00	y = 92693.90 - (548.81*x)	59,765.30	y = -2272.1 + (3050.9*x)	20.33
14-Feb-21	D3	1C	2	11:21	13:15	1:54:00	121,662.68	29,984.00	y = 92693.90 - (548.81*x)	59,765.30	y = -2272.1 + (3050.9*x)	20.33
14-Feb-21	D3	2C	1	11:33	13:18	1:45:00	82,133.65	12,384.00	y = exp (11.03607 - 0.01295*x)	28,540.23	y = -2272.1 + (3050.9*x)	10.10
14-Feb-21	D3	2C	1	11:33	13:20	1:47:00	82,368.96	20,348.00	y = exp (11.03607 - 0.01295*x)	28,540.23	y = -2272.1 + (3050.9*x)	10.10
14-Feb-21	D3	2C	2	11:33	13:22	1:49:00	128,975.99	30,316.00	y = 91550.61 - (544.91*x)	58,856.01	y = -2272.1 + (3050.9*x)	20.04
14-Feb-21	D3	2C	2	11:33	13:24	1:51:00	134,854.78	33,160.00	y = 91550.61 - (544.91*x)	58,856.01	y = -2272.1 + (3050.9*x)	20.04
14-Feb-21	D3	1N	1	11:42	13:26	1:44:00	0.00	0.00			y = -2272.1 + (3050.9*x)	0.00
14-Feb-21	D3	1N	1	11:42	13:28	1:46:00	0.00	0.00			y = -2272.1 + (3050.9*x)	0.00
14-Feb-21	D3	1N	2	11:42	13:30	1:48:00	0.00	0.00			y = -2272.1 + (3050.9*x)	0.00
14-Feb-21	D3	1N	2	11:42	13:32	1:50:00	0.00	0.00			y = -2272.1 + (3050.9*x)	0.00
14-Feb-21	D3	2N	1	11:52	13:35	1:43:00	0.00	0.00			y = -2272.1 + (3050.9*x)	0.00

Date	Day	Sam-ple	Repli-cation	Samp-ling Time	Analy-sis Time	Time Differ-ence	Area	Maximum Height	Equation of Max Height vs Time for Extrapolation	Max height from extrapolation (t=60)	Calibration (Max Height vs Fe (II) Conc)	Fe (II) (nm) (t=60)
14-Feb-21	D3	2N	1	11:52	13:37	1:45:00	0.00	0.00			y = -2272.1 + (3050.9*x)	0.00
14-Feb-21	D3	2N	2	11:52	13:39	1:47:00	0.00	0.00			y = -2272.1 + (3050.9*x)	0.00
14-Feb-21	D3	2N	2	11:52	13:41	1:49:00	0.00	0.00			y = -2272.1 + (3050.9*x)	0.00
14-Feb-21	D3	1C	1	11:21	13:43	2:22:00	51,486.27	9,408.00	y = 97845.54 - (615.81*x)	60,896.94	y = -2272.1 + (3050.9*x)	20.71
14-Feb-21	D3	1C	1	11:21	13:45	2:24:00	49,769.14	10,112.00	y = 97845.54 - (615.81*x)	60,896.94	y = -2272.1 + (3050.9*x)	20.71
14-Feb-21	D3	1C	2	11:21	13:47	2:26:00	64,700.32	10,000.00	y = 92693.90 - (548.81*x)	59,765.30	y = -2272.1 + (3050.9*x)	20.33
14-Feb-21	D3	1C	2	11:21	13:49	2:28:00	71,264.04	13,904.00	y = 92693.90 - (548.81*x)	59,765.30	y = -2272.1 + (3050.9*x)	20.33
14-Feb-21	D3	2C	1	11:33	13:52	2:19:00	64,750.59	9,508.00	y = exp (11.03607 - 0.01295*x)	28,540.23	y = -2272.1 + (3050.9*x)	10.10
14-Feb-21	D3	2C	1	11:33	13:54	2:21:00	64,846.10	10,568.00	y = exp (11.03607 - 0.01295*x)	28,540.23	y = -2272.1 + (3050.9*x)	10.10
14-Feb-21	D3	2C	2	11:33	13:56	2:23:00	72,182.79	11,132.00	y = 91550.61 - (544.91*x)	58,856.01	y = -2272.1 + (3050.9*x)	20.04
14-Feb-21	D3	2C	2	11:33	13:58	2:25:00	70,927.75	14,780.00	y = 91550.61 - (544.91*x)	58,856.01	y = -2272.1 + (3050.9*x)	20.04
14-Feb-21	D3	1N	1	11:42	14:00	2:18:00	0.00	0.00			y = -2272.1 + (3050.9*x)	0.00
14-Feb-21	D3	1N	1	11:42	14:02	2:20:00	0.00	0.00			y = -2272.1 + (3050.9*x)	0.00
14-Feb-21	D3	1N	2	11:42	14:04	2:22:00	0.00	0.00			y = -2272.1 + (3050.9*x)	0.00
14-Feb-21	D3	1N	2	11:42	14:07	2:25:00	0.00	0.00			y = -2272.1 + (3050.9*x)	0.00
14-Feb-21	D3	2N	1	11:52	14:09	2:17:00	0.00	0.00			y = -2272.1 + (3050.9*x)	0.00
14-Feb-21	D3	2N	1	11:52	14:11	2:19:00	0.00	0.00			y = -2272.1 + (3050.9*x)	0.00
14-Feb-21	D3	2N	2	11:52	14:13	2:21:00	0.00	0.00			y = -2272.1 + (3050.9*x)	0.00
14-Feb-21	D3	2N	2	11:52	14:15	2:23:00	0.00	0.00			y = -2272.1 + (3050.9*x)	0.00
15-Feb-21	D4	1C	1	11:13	13:06	1:53:00	97,866.03	25352	y = exp (11.11947 - 0.01228*x)	32,295.07	y = -541.6 + (2052.6*x)	16.00
15-Feb-21	D4	1C	2	11:13	13:11	1:58:00	100,811.30	21236	y = 29340 - (68.65*x)	25,221.00	y = -541.6 + (2052.6*x)	12.55
15-Feb-21	D4	1N	1	11:32	13:21	1:49:00	0.00	0.00			y = -541.6 + (2052.6*x)	0.00
15-Feb-21	D4	1N	1	11:32	13:24	1:52:00	0.00	0.00			y = -541.6 + (2052.6*x)	0.00
15-Feb-21	D4	1N	2	11:32	13:26	1:54:00	0.00	0.00			y = -541.6 + (2052.6*x)	0.00
15-Feb-21	D4	1N	2	11:32	13:28	1:56:00	0.00	0.00			y = -541.6 + (2052.6*x)	0.00

Date	Day	Sam-ple	Repli-cation	Samp-ling Time	Analy-sis Time	Time Differ-ence	Area	Maximum Height	Equation of Max Height vs Time for Extrapolation	Max height from extrapolation (t=60)	Calibration (Max Height vs Fe (II) Conc)	Fe (II) (nm) (t=60)
15-Feb-21	D4	2N	1	11:41	13:30	1:49:00	0.00	0.00			y = -541.6 + (2052.6*x)	0.00
15-Feb-21	D4	2N	1	11:41	13:32	1:51:00	0.00	0.00			y = -541.6 + (2052.6*x)	0.00
15-Feb-21	D4	2N	2	11:41	13:34	1:53:00	0.00	0.00			y = -541.6 + (2052.6*x)	0.00
15-Feb-21	D4	2N	2	11:41	13:36	1:55:00	0.00	0.00			y = -541.6 + (2052.6*x)	0.00
15-Feb-21	D4	1C	1	11:13	13:38	2:25:00	50,480.41	7244	y = exp (11.11947 - 0.01228*x)	32,295.07	y = -541.6 + (2052.6*x)	16.00
15-Feb-21	D4	1C	1	11:13	13:41	2:28:00	46,355.37	9184	y = exp (11.11947 - 0.01228*x)	32,295.07	y = -541.6 + (2052.6*x)	16.00
15-Feb-21	D4	1C	2	11:13	13:43	2:30:00	81,372.96	19036	y = 29340 - (68.65*x)	25,221.00	y = -541.6 + (2052.6*x)	12.55
15-Feb-21	D4	2C	1	11:22	13:47	2:25:00	36,335.22	12652	y = 29304.9 - (114.8*x)	22,416.90	y = -541.6 + (2052.6*x)	11.19
15-Feb-21	D4	2C	2	11:22	13:53	2:31:00	40,547.15	9608	y = 17191.56 - (50.22*x)	14,178.36	y = -541.6 + (2052.6*x)	7.17
15-Feb-21	D4	1N	1	11:32	13:55	2:23:00	0.00	0.00			y = -541.6 + (2052.6*x)	0.00
15-Feb-21	D4	1N	1	11:32	13:58	2:26:00	0.00	0.00			y = -541.6 + (2052.6*x)	0.00
15-Feb-21	D4	1N	2	11:32	14:00	2:28:00	0.00	0.00			y = -541.6 + (2052.6*x)	0.00
15-Feb-21	D4	1N	2	11:32	14:02	2:30:00	0.00	0.00			y = -541.6 + (2052.6*x)	0.00
15-Feb-21	D4	2N	1	11:41	14:04	2:23:00	0.00	0.00			y = -541.6 + (2052.6*x)	0.00
15-Feb-21	D4	2N	1	11:41	14:06	2:25:00	0.00	0.00			y = -541.6 + (2052.6*x)	0.00
15-Feb-21	D4	2N	2	11:41	14:08	2:27:00	0.00	0.00			y = -541.6 + (2052.6*x)	0.00
15-Feb-21	D4	2N	2	11:41	14:10	2:29:00	0.00	0.00			y = -541.6 + (2052.6*x)	0.00
15-Feb-21	D4	2C	2	11:22	14:38	3:16:00	27,768.81	7348	y = 17191.56 - (50.22*x)	14,178.36	y = -541.6 + (2052.6*x)	7.17
15-Feb-21	D4	1C	1	11:13	14:40	3:27:00	29,062.14	6616	y = exp (11.11947 - 0.01228*x)	32,295.07	y = -541.6 + (2052.6*x)	16.00
15-Feb-21	D4	1C	2	11:13	14:42	3:29:00	52,616.60	14988	y = 29340 - (68.65*x)	25,221.00	y = -541.6 + (2052.6*x)	12.55
15-Feb-21	D4	2C	1	11:22	14:46	3:24:00	18,608.32	5876	y = 29304.9 - (114.8*x)	22,416.90	y = -541.6 + (2052.6*x)	11.19
16-Feb-21	D5	1C	1	11:16	12:33	1:17:00	1,252,569.08	229132	y = 313936 - (1618*x)	216,856.00	y = -123178 + (8395*x)	40.50
16-Feb-21	D5	2C	1	11:26	12:37	1:11:00	446,509.15	85124	y = 170233.34 - (1205.11*x)	97,926.74	y = -123178 + (8395*x)	26.34
16-Feb-21	D5	1N	2	11:39	12:46	1:07:00	0.00	0.00			y = -123178 + (8395*x)	0.00
16-Feb-21	D5	1N	2	11:39	12:48	1:09:00	0.00	0.00			y = -123178 + (8395*x)	0.00

Date	Day	Sam-ple	Repli-cation	Samp-ling Time	Analy-sis Time	Time Differ-ence	Area	Maximum Height	Equation of Max Height vs Time for Extrapolation	Max height from extrapolation (t=60)	Calibration (Max Height vs Fe (II) Conc)	Fe (II) (nm) (t=60)
16-Feb-21	D5	2N	1	11:58	12:49	0:51:00	0.00	0.00			y = -123178 + (8395*x)	0.00
16-Feb-21	D5	2N	1	11:58	12:51	0:53:00	0.00	0.00			y = -123178 + (8395*x)	0.00
16-Feb-21	D5	2N	2	11:58	12:52	0:54:00	0.00	0.00			y = -123178 + (8395*x)	0.00
16-Feb-21	D5	2N	2	11:58	12:54	0:56:00	0.00	0.00			y = -123178 + (8395*x)	0.00
16-Feb-21	D5	1C	1	11:16	12:55	1:39:00	733,035.19	132136	y = 313936 - (1618*x)	216,856.00	y = -123178 + (8395*x)	40.50
16-Feb-21	D5	1C	1	11:16	12:57	1:41:00	667,451.51	93540	y = 313936 - (1618*x)	216,856.00	y = -123178 + (8395*x)	40.50
16-Feb-21	D5	2C	1	11:26	13:03	1:37:00	271,203.60	52300	y = 170233.34 - (1205.11*x)	97,926.74	y = -123178 + (8395*x)	26.34
16-Feb-21	D5	2C	2	11:26	13:04	1:38:00	319,242.35	56236	y = exp (11.1223 - 0.005144*x)	49,696.96	y = -123178 + (8395*x)	20.59
16-Feb-21	D5	2C	2	11:26	13:06	1:40:00	357,130.51	64128	y = exp (11.1223 - 0.005144*x)	49,696.96	y = -123178 + (8395*x)	20.59
16-Feb-21	D5	1N	1	11:39	13:07	1:28:00	0.00	0.00			y = -123178 + (8395*x)	0.00
16-Feb-21	D5	1N	1	11:39	13:09	1:30:00	0.00	0.00			y = -123178 + (8395*x)	0.00
16-Feb-21	D5	1N	2	11:39	13:10	1:31:00	0.00	0.00			y = -123178 + (8395*x)	0.00
16-Feb-21	D5	1N	2	11:39	13:12	1:33:00	0.00	0.00			y = -123178 + (8395*x)	0.00
16-Feb-21	D5	2N	1	11:58	13:14	1:16:00	0.00	0.00			y = -123178 + (8395*x)	0.00
16-Feb-21	D5	2N	1	11:58	13:15	1:17:00	0.00	0.00			y = -123178 + (8395*x)	0.00
16-Feb-21	D5	2N	2	11:58	13:17	1:19:00	0.00	0.00			y = -123178 + (8395*x)	0.00
16-Feb-21	D5	2N	2	11:58	13:18	1:20:00	0.00	0.00			y = -123178 + (8395*x)	0.00
16-Feb-21	D5	1C	1	11:16	13:20	2:04:00	720,713.55	135184	y = 313936 - (1618*x)	216,856.00	y = -123178 + (8395*x)	40.50
16-Feb-21	D5	1C	1	11:16	13:21	2:05:00	722,384.87	128732	y = 313936 - (1618*x)	216,856.00	y = -123178 + (8395*x)	40.50
16-Feb-21	D5	2C	1	11:26	13:26	2:00:00	205,587.69	27860	y = 170233.34 - (1205.11*x)	97,926.74	y = -123178 + (8395*x)	26.34
16-Feb-21	D5	2C	1	11:26	13:27	2:01:00	156,934.12	22760	y = 170233.34 - (1205.11*x)	97,926.74	y = -123178 + (8395*x)	26.34
16-Feb-21	D5	2C	2	11:26	13:29	2:03:00	157,735.53	23276	y = exp (11.1223 - 0.005144*x)	49,696.96	y = -123178 + (8395*x)	20.59
16-Feb-21	D5	2C	2	11:26	13:30	2:04:00	189,413.82	37244	y = exp (11.1223 - 0.005144*x)	49,696.96	y = -123178 + (8395*x)	20.59
16-Feb-21	D5	1N	1	11:39	13:32	1:53:00	0.00	0.00			y = -123178 + (8395*x)	0.00
16-Feb-21	D5	1N	1	11:39	13:33	1:54:00	0.00	0.00			y = -123178 + (8395*x)	0.00

Date	Day	Sam-ple	Repli-cation	Samp-ling Time	Analy-sis Time	Time Differ-ence	Area	Maximum Height	Equation of Max Height vs Time for Extrapolation	Max height from extrapolation (t=60)	Calibration (Max Height vs Fe (II) Conc)	Fe (II) (nm) (t=60)
16-Feb-21	D5	1N	2	11:39	13:35	1:56:00	0.00	0.00			y = -123178 + (8395*x)	0.00
16-Feb-21	D5	1N	2	11:39	13:36	1:57:00	0.00	0.00			y = -123178 + (8395*x)	0.00
16-Feb-21	D5	2N	1	11:58	13:38	1:40:00	0.00	0.00			y = -123178 + (8395*x)	0.00
16-Feb-21	D5	2N	1	11:58	13:39	1:41:00	0.00	0.00			y = -123178 + (8395*x)	0.00
16-Feb-21	D5	2N	2	11:58	13:41	1:43:00	0.00	0.00			y = -123178 + (8395*x)	0.00
16-Feb-21	D5	2N	2	11:58	13:42	1:44:00	0.00	0.00			y = -123178 + (8395*x)	0.00
17-Feb-21	D6	1C	1	11:19	12:44	1:25:00	200,493.27	33484	y = 39739.86 - (88.22*x)	34446.66	y = -3941.0 + (630.2*x)	60.91
17-Feb-21	D6	1C	1	11:19	12:46	1:27:00	182,432.47	31864	y = 39739.86 - (88.22*x)	34446.66	y = -3941.0 + (630.2*x)	60.91
17-Feb-21	D6	1C	1	11:19	12:48	1:29:00	174,454.11	30556	y = 39739.86 - (88.22*x)	34446.66	y = -3941.0 + (630.2*x)	60.91
17-Feb-21	D6	1C	2	11:19	12:50	1:31:00	215,821.66	32496	y = 41796.24 - (99.06*x)	35852.64	y = -3941.0 + (630.2*x)	63.14
17-Feb-21	D6	1C	2	11:19	12:52	1:33:00	227,697.06	32700	y = 41796.24 - (99.06*x)	35852.64	y = -3941.0 + (630.2*x)	63.14
17-Feb-21	D6	2C	1	11:27	12:55	1:28:00	131,439.38	23968	y = 51281.82 - (282.34*x)	34341.42	y = -3941.0 + (630.2*x)	60.75
17-Feb-21	D6	2C	1	11:27	12:57	1:30:00	140,677.80	24788	y = 51281.82 - (282.34*x)	34341.42	y = -3941.0 + (630.2*x)	60.75
17-Feb-21	D6	2C	1	11:27	12:59	1:32:00	158,724.88	29200	y = 51281.82 - (282.34*x)	34341.42	y = -3941.0 + (630.2*x)	60.75
17-Feb-21	D6	2C	2	11:27	13:01	1:34:00	68,326.73	12872	y = exp (10.96890 - 0.01597x)	22263.41439	y = -3941.0 + (630.2*x)	41.58
17-Feb-21	D6	2C	2	11:27	13:03	1:36:00	67,596.08	12520	y = exp (10.96890 - 0.01597x)	22263.41439	y = -3941.0 + (630.2*x)	41.58
17-Feb-21	D6	1N	1	11:42	13:05	1:23:00	0.00	0.00				0.00
17-Feb-21	D6	1N	1	11:42	13:07	1:25:00	0.00	0.00				0.00
17-Feb-21	D6	1N	1	11:42	13:09	1:27:00	0.00	0.00				0.00
17-Feb-21	D6	1N	2	11:42	13:12	1:30:00	0.00	0.00				0.00
17-Feb-21	D6	1N	2	11:42	13:14	1:32:00	0.00	0.00				0.00
17-Feb-21	D6	2N	1	11:53	13:16	1:23:00	0.00	0.00				0.00
17-Feb-21	D6	2N	1	11:53	13:18	1:25:00	0.00	0.00				0.00
17-Feb-21	D6	2N	2	11:53	13:20	1:27:00	0.00	0.00				0.00
17-Feb-21	D6	2N	2	11:53	13:22	1:29:00	0.00	0.00				0.00

Date	Day	Sam-ple	Repli-cation	Samp-ling Time	Analy-sis Time	Time Differ-ence	Area	Maximum Height	Equation of Max Height vs Time for Extrapolation	Max height from extrapolation (t=60)	Calibration (Max Height vs Fe (II) Conc)	Fe (II) (nm) (t=60)
17-Feb-21	D6	1C	1	11:19	13:24	2:05:00	163,350.33	30248	y = 39739.86 - (88.22*x)	34446.66	y = -3941.0 + (630.2*x)	60.91
17-Feb-21	D6	1C	1	11:19	13:26	2:07:00	155,672.35	28408	y = 39739.86 - (88.22*x)	34446.66	y = -3941.0 + (630.2*x)	60.91
17-Feb-21	D6	1C	1	11:19	13:29	2:10:00	137,632.52	27152	y = 39739.86 - (88.22*x)	34446.66	y = -3941.0 + (630.2*x)	60.91
17-Feb-21	D6	1C	2	11:19	13:31	2:12:00	196,100.95	32480	y = 41796.24 - (99.06*x)	35852.64	y = -3941.0 + (630.2*x)	63.14
17-Feb-21	D6	1C	2	11:19	13:33	2:14:00	174,363.83	24932	y = 41796.24 - (99.06*x)	35852.64	y = -3941.0 + (630.2*x)	63.14
17-Feb-21	D6	2C	1	11:27	13:35	2:08:00	94,032.26	14784	y = 51281.82 - (282.34*x)	34341.42	y = -3941.0 + (630.2*x)	60.75
17-Feb-21	D6	2C	1	11:27	13:37	2:10:00	91,098.80	14480	y = 51281.82 - (282.34*x)	34341.42	y = -3941.0 + (630.2*x)	60.75
17-Feb-21	D6	2C	1	11:27	13:39	2:12:00	89,284.28	14128	y = 51281.82 - (282.34*x)	34341.42	y = -3941.0 + (630.2*x)	60.75
17-Feb-21	D6	2C	2	11:27	13:41	2:14:00	46,059.18	7396	y = exp (10.96890 - 0.01597x)	22263.41439	y = -3941.0 + (630.2*x)	41.58
17-Feb-21	D6	2C	2	11:27	13:44	2:17:00	37,671.11	6044	y = exp (10.96890 - 0.01597x)	22263.41439	y = -3941.0 + (630.2*x)	41.58
17-Feb-21	D6	1N	1	11:42	13:46	2:04:00	0.00	0.00				0.00
17-Feb-21	D6	1N	1	11:42	13:48	2:06:00	0.00	0.00				0.00
17-Feb-21	D6	1N	1	11:42	13:50	2:08:00	0.00	0.00				0.00
17-Feb-21	D6	1N	2	11:42	13:52	2:10:00	0.00	0.00				0.00
17-Feb-21	D6	1N	2	11:42	13:54	2:12:00	0.00	0.00				0.00
17-Feb-21	D6	2N	1	11:53	13:56	2:03:00	0.00	0.00				0.00
17-Feb-21	D6	2N	1	11:53	13:58	2:05:00	0.00	0.00				0.00
17-Feb-21	D6	2N	2	11:53	14:01	2:08:00	0.00	0.00				0.00
17-Feb-21	D6	2N	2	11:53	14:03	2:10:00	0.00	0.00				0.00
18-Feb-21	D7	1C	1	11:16	12:15	0:59:00	19,857.04	4068	y = 6966.131 - (48.240*x)	4071.731	y = -1578.89 + (44.49*x)	127.01
18-Feb-21	D7	1C	1	11:16	12:16	1:00:00	19,243.05	4004	y = 6966.131 - (48.240*x)	4071.731	y = -1578.89 + (44.49*x)	127.01
18-Feb-21	D7	1C	1	11:16	12:18	1:02:00	18,850.74	4100	y = 6966.131 - (48.240*x)	4071.731	y = -1578.89 + (44.49*x)	127.01
18-Feb-21	D7	1C	2	11:16	12:19	1:03:00	14,283.30	2980	y = exp (8.537517 - 0.009540x)	5054.209301	y = -1578.89 + (44.49*x)	149.09
18-Feb-21	D7	1C	2	11:16	12:21	1:05:00	14,933.48	2560	y = exp (8.537517 - 0.009540x)	5054.209301	y = -1578.89 + (44.49*x)	149.09
18-Feb-21	D7	2C	1	11:29	12:22	0:53:00	16,130.42	2420	y = 3124.464 - (13.773*x)	2298.084	y = -1578.89 + (44.49*x)	87.14

Date	Day	Sam-ple	Repli-cation	Samp-ling Time	Analy-sis Time	Time Differ-ence	Area	Maximum Height	Equation of Max Height vs Time for Extrapolation	Max height from extrapolation (t=60)	Calibration (Max Height vs Fe (II) Conc)	Fe (II) (nm) (t=60)
18-Feb-21	D7	2C	1	11:29	12:24	0:55:00	14,441.58	2336	y = 3124.464 - (13.773*x)	2298.084	y = -1578.89 + (44.49*x)	87.14
18-Feb-21	D7	2C	2	11:29	12:25	0:56:00	11,435.56	1804	y = 2472.526 - (12.504*x)	1722.286	y = -1578.89 + (44.49*x)	74.20
18-Feb-21	D7	2C	2	11:29	12:27	0:58:00	10,510.81	1712	y = 2472.526 - (12.504*x)	1722.286	y = -1578.89 + (44.49*x)	74.20
18-Feb-21	D7	1C	2	11:16	12:49	1:33:00	12,998.90	2176	y = exp (8.537517 - 0.009540x)	5054.209301	y = -1578.89 + (44.49*x)	149.09
18-Feb-21	D7	1C	2	11:16	12:51	1:35:00	11,478.77	2004	y = exp (8.537517 - 0.009540x)	5054.209301	y = -1578.89 + (44.49*x)	149.09
18-Feb-21	D7	2C	1	11:29	13:00	1:31:00	10,198.37	1948	y = 3124.464 - (13.773*x)	2298.084	y = -1578.89 + (44.49*x)	87.14
18-Feb-21	D7	2C	1	11:29	13:02	1:33:00	9,772.51	1772	y = 3124.464 - (13.773*x)	2298.084	y = -1578.89 + (44.49*x)	87.14
18-Feb-21	D7	2C	2	11:29	13:04	1:35:00	6,964.97	1324	y = 2472.526 - (12.504*x)	1722.286	y = -1578.89 + (44.49*x)	74.20
18-Feb-21	D7	2C	2	11:29	13:06	1:37:00	6,849.78	1224	y = 2472.526 - (12.504*x)	1722.286	y = -1578.89 + (44.49*x)	74.20
18-Feb-21	D7	1C	1	11:16	13:10	1:54:00	6,442.11	1476	y = 6966.131 - (48.240*x)	4071.731	y = -1578.89 + (44.49*x)	127.01
18-Feb-21	D7	1C	1	11:16	13:12	1:56:00	6,110.44	1356	y = 6966.131 - (48.240*x)	4071.731	y = -1578.89 + (44.49*x)	127.01
20-Feb-21	D9	2C	2	11:20	12:36	1:16:00	3,492,775.12	655360	y = exp (13.922841 - 0.006384x)	759,033.35	y = -123426 + (10347*x)	85.29
20-Feb-21	D9	2C	2	11:20	12:37	1:17:00	3,381,085.87	794008	y = exp (13.922841 - 0.006384x)	759,033.35	y = -123426 + (10347*x)	85.29
20-Feb-21	D9	2C	2	11:20	12:39	1:19:00	3,328,068.22	602796	y = exp (13.922841 - 0.006384x)	759,033.35	y = -123426 + (10347*x)	85.29
20-Feb-21	D9	2C	1	11:20	12:41	1:21:00	730,137.95	142232	y = exp (13.31377 - 0.01898x)	193,875.21	y = -123426 + (10347*x)	30.67
20-Feb-21	D9	2C	1	11:20	12:42	1:22:00	624,605.45	116196	y = exp (13.31377 - 0.01898x)	193,875.21	y = -123426 + (10347*x)	30.67
20-Feb-21	D9	1C	1	11:12	12:44	1:32:00	746,949.17	123276	y = exp (12.819220 - 0.011552x)	184,628.32	y = -123426 + (10347*x)	29.77
20-Feb-21	D9	1C	1	11:12	12:45	1:33:00	825,448.40	130112	y = exp (12.819220 - 0.011552x)	184,628.32	y = -123426 + (10347*x)	29.77
20-Feb-21	D9	1C	2	11:12	12:47	1:35:00	2,143,904.28	368820	y = exp (13.258939 - 0.004119x)	447,664.34	y = -123426 + (10347*x)	55.19
20-Feb-21	D9	1C	2	11:12	12:48	1:36:00	2,299,897.21	408556	y = exp (13.258939 - 0.004119x)	447,664.34	y = -123426 + (10347*x)	55.19
20-Feb-21	D9	2C	2	11:20	13:01	1:41:00	2,723,335.70	537432	y = exp (13.922841 - 0.006384x)	759,033.35	y = -123426 + (10347*x)	85.29
20-Feb-21	D9	2C	2	11:20	13:03	1:43:00	2,824,092.65	627184	y = exp (13.922841 - 0.006384x)	759,033.35	y = -123426 + (10347*x)	85.29
20-Feb-21	D9	2C	1	11:20	13:04	1:44:00	493,577.12	86108	y = exp (13.31377 - 0.01898x)	193,875.21	y = -123426 + (10347*x)	30.67
20-Feb-21	D9	2C	1	11:20	13:06	1:46:00	431,609.83	79552	y = exp (13.31377 - 0.01898x)	193,875.21	y = -123426 + (10347*x)	30.67
20-Feb-21	D9	1C	1	11:12	13:07	1:55:00	653,260.74	103248	y = exp (12.819220 - 0.011552x)	184,628.32	y = -123426 + (10347*x)	29.77

Date	Day	Sam-ple	Repli-cation	Samp-ling Time	Analy-sis Time	Time Differ-ence	Area	Maximum Height	Equation of Max Height vs Time for Extrapolation	Max height from extrapolation (t=60)	Calibration (Max Height vs Fe (II) Conc)	Fe (II) (nm) (t=60)
20-Feb-21	D9	1C	1	11:12	13:09	1:57:00	561,593.34	90824	y = exp (12.819220 - 0.011552x)	184,628.32	y = -123426 + (10347*x)	29.77
20-Feb-21	D9	1C	2	11:12	13:10	1:58:00	2,020,295.17	330764	y = exp (13.258939 - 0.004119x)	447,664.34	y = -123426 + (10347*x)	55.19
20-Feb-21	D9	1C	2	11:12	13:12	2:00:00	2,161,633.01	369880	y = exp (13.258939 - 0.004119x)	447,664.34	y = -123426 + (10347*x)	55.19
21-Feb-21	D10	1C	1	11:17	12:40	1:23:00	2,439,392.63	530252	y = 1347003 - (9840*x)	756,603.00	y = -58172 + (11518*x)	70.74
21-Feb-21	D10	1C	2	11:17	12:42	1:25:00	2,441,217.47	451208	y = exp (13.71506 - 0.01105*x)	466,055.50	y = -58172 + (11518*x)	45.51
21-Feb-21	D10	1C	2	11:17	12:45	1:28:00	1,657,478.11	263240	y = exp (13.71506 - 0.01105*x)	466,055.50	y = -58172 + (11518*x)	45.51
21-Feb-21	D10	2C	1	11:26	12:47	1:21:00	2,920,336.94	655360	y = 1446178.9 - (9870.5*x)	853,948.90	y = -58172 + (11518*x)	79.19
21-Feb-21	D10	2C	1	11:26	12:49	1:23:00	2,999,826.85	617036	y = 1446178.9 - (9870.5*x)	853,948.90	y = -58172 + (11518*x)	79.19
21-Feb-21	D10	2C	2	11:26	12:51	1:25:00	1,930,336.65	287764	y = 878481.2 - (6473.6*x)	490,065.20	y = -58172 + (11518*x)	47.60
21-Feb-21	D10	2C	2	11:26	12:53	1:27:00	2,610,114.04	357404	y = 878481.2 - (6473.6*x)	490,065.20	y = -58172 + (11518*x)	47.60
21-Feb-21	D10	1C	1	11:17	13:23	2:06:00	959,335.79	107116	y = 1347003 - (9840*x)	756,603.00	y = -58172 + (11518*x)	70.74
21-Feb-21	D10	1C	2	11:17	13:25	2:08:00	1,269,147.52	223948	y = exp (13.71506 - 0.01105*x)	466,055.50	y = -58172 + (11518*x)	45.51
21-Feb-21	D10	2C	1	11:26	13:29	2:03:00	1,830,629.96	248456	y = 1446178.9 - (9870.5*x)	853,948.90	y = -58172 + (11518*x)	79.19
21-Feb-21	D10	2C	1	11:26	13:31	2:05:00	1,382,322.45	197200	y = 1446178.9 - (9870.5*x)	853,948.90	y = -58172 + (11518*x)	79.19
21-Feb-21	D10	2C	2	11:26	13:34	2:08:00	249,426.31	54376	y = 878481.2 - (6473.6*x)	490,065.20	y = -58172 + (11518*x)	47.60
21-Feb-21	D10	2C	2	11:26	13:36	2:10:00	213,250.59	30716	y = 878481.2 - (6473.6*x)	490,065.20	y = -58172 + (11518*x)	47.60
22-Feb-21	D11	1N	1	11:14	12:14	1:00:00	4,982.20	480	y = exp (8.514256 - 0.043102*x)	375.45	y = 68.74 + (1007.66*x)	0.30
22-Feb-21	D11	1N	1	11:14	12:15	1:01:00	3,494.17	384	y = exp (8.514256 - 0.043102*x)	375.45	y = 68.74 + (1007.66*x)	0.30
22-Feb-21	D11	1N	1	11:14	12:17	1:03:00	2,321.51	312	y = exp (8.514256 - 0.043102*x)	375.45	y = 68.74 + (1007.66*x)	0.30
22-Feb-21	D11	1N	2	11:14	12:18	1:04:00	907.90	188	y = exp (5.587371 - 0.007822*x)	167.01	y = 68.74 + (1007.66*x)	0.10
22-Feb-21	D11	1N	2	11:14	12:20	1:06:00	616.13	144	y = exp (5.587371 - 0.007822*x)	167.01	y = 68.74 + (1007.66*x)	0.10
22-Feb-21	D11	2N	1	11:25	12:21	0:56:00	526.34	172	y = exp (5.881918 - 0.012107*x)	173.38	y = 68.74 + (1007.66*x)	0.10
22-Feb-21	D11	2N	1	11:25	12:23	0:58:00	467.22	188	y = exp (5.881918 - 0.012107*x)	173.38	y = 68.74 + (1007.66*x)	0.10
22-Feb-21	D11	2N	2	11:25	12:24	0:59:00	755.45	188	y = 211.4194 - (0.4516*x)	184.32	y = 68.74 + (1007.66*x)	0.11
22-Feb-21	D11	2N	2	11:25	12:26	1:01:00	707.85	180	y = 211.4194 - (0.4516*x)	184.32	y = 68.74 + (1007.66*x)	0.11

Date	Day	Sam-ple	Repli-cation	Samp-ling Time	Analy-sis Time	Time Differ-ence	Area	Maximum Height	Equation of Max Height vs Time for Extrapolation	Max height from extrapolation (t=60)	Calibration (Max Height vs Fe (II) Conc)	Fe (II) (nm) (t=60)
22-Feb-21	D11	1N	1	11:14	12:27	1:13:00	476.73	152	y = exp (8.514256 - 0.043102*x)	375.45	y = 68.74 + (1007.66*x)	0.30
22-Feb-21	D11	1N	1	11:14	12:29	1:15:00	448.61	160	y = exp (8.514256 - 0.043102*x)	375.45	y = 68.74 + (1007.66*x)	0.30
22-Feb-21	D11	1N	2	11:14	12:30	1:16:00	346.55	140	y = exp (5.587371 - 0.007822*x)	167.01	y = 68.74 + (1007.66*x)	0.10
22-Feb-21	D11	1N	2	11:14	12:32	1:18:00	289.10	140	y = exp (5.587371 - 0.007822*x)	167.01	y = 68.74 + (1007.66*x)	0.10
22-Feb-21	D11	2N	1	11:25	12:33	1:08:00	483.32	160	y = exp (5.881918 - 0.012107*x)	173.38	y = 68.74 + (1007.66*x)	0.10
22-Feb-21	D11	2N	1	11:25	12:35	1:10:00	393.37	152	y = exp (5.881918 - 0.012107*x)	173.38	y = 68.74 + (1007.66*x)	0.10
22-Feb-21	D11	2N	2	11:25	12:36	1:11:00	533.36	180	y = 211.4194 - (0.4516*x)	184.32	y = 68.74 + (1007.66*x)	0.11
22-Feb-21	D11	1N	1	11:14	12:39	1:25:00	203.00	148	y = exp (8.514256 - 0.043102*x)	375.45	y = 68.74 + (1007.66*x)	0.30
22-Feb-21	D11	1N	1	11:14	12:41	1:27:00	152.84	136	y = exp (8.514256 - 0.043102*x)	375.45	y = 68.74 + (1007.66*x)	0.30
22-Feb-21	D11	2N	1	11:25	12:47	1:22:00	180.17	132	y = exp (5.881918 - 0.012107*x)	173.38	y = 68.74 + (1007.66*x)	0.10
22-Feb-21	D11	1N	2	11:14	12:52	1:38:00	155.54	128	y = exp (5.587371 - 0.007822*x)	167.01	y = 68.74 + (1007.66*x)	0.10
22-Feb-21	D11	1N	2	11:14	12:53	1:39:00	196.45	124	y = exp (5.587371 - 0.007822*x)	167.01	y = 68.74 + (1007.66*x)	0.10
24-Feb-21	D13	1N	1	11:25	12:54	1:29:00	7,340.84	1568	y = 27979.6 - (299.2*x)	10,027.60	y = 197.80 + (1047.23*x)	9.39
24-Feb-21	D13	1N	1	11:25	12:55	1:30:00	5,888.28	772	y = 27979.6 - (299.2*x)	10,027.60	y = 197.80 + (1047.23*x)	9.39
24-Feb-21	D13	1N	2	11:25	12:56	1:31:00	2,805.57	660				0.00
24-Feb-21	D13	1N	2	11:25	12:57	1:32:00	2,238.25	608				0.00
24-Feb-21	D13	1C	1	11:16	12:58	1:42:00	2,236,781.91	250224				0.00
24-Feb-21	D13	1C	1	11:16	12:59	1:43:00	2,711,624.96	298420				0.00
24-Feb-21	D13	1C	2	11:16	13:00	1:44:00	3,771,779.95	372064				0.00
24-Feb-21	D13	1C	2	11:16	13:01	1:45:00	4,567,669.80	652092				0.00
26-Feb-21	D15	1N	1	11:09	13:04	1:55:00	3,090.20	2252	y = 19981.88 - (153.46*x)	10,774.28	y = 197.80 + (1047.23*x)	10.10
26-Feb-21	D15	1N	2	11:09	13:05	1:56:00	8,298.57	4640	y = 39115.03 - (301.68*x)	21,014.23	y = 197.80 + (1047.23*x)	19.88
26-Feb-21	D15	1N	2	11:09	13:06	1:57:00	10,040.33	3212	y = 39115.03 - (301.68*x)	21,014.23	y = 197.80 + (1047.23*x)	19.88
26-Feb-21	D15	1N	1	11:09	13:07	1:58:00	3,703.23	2164	y = 19981.88 - (153.46*x)	10,774.28	y = 197.80 + (1047.23*x)	10.10
26-Feb-21	D15	1N	1	11:09	13:08	1:59:00	3,722.73	1536	y = 19981.88 - (153.46*x)	10,774.28	y = 197.80 + (1047.23*x)	10.10

Date	Day	Sam-ple	Repli-cation	Samp-ling Time	Analy-sis Time	Time Differ-ence	Area	Maximum Height	Equation of Max Height vs Time for Extrapolation	Max height from extrapolation (t=60)	Calibration (Max Height vs Fe (II) Conc)	Fe (II) (nm) (t=60)
26-Feb-21	D15	1N	2	11:09	13:09	2:00:00	7,154.00	2492	y = 39115.03 - (301.68*x)	21,014.23	y = 197.80 + (1047.23*x)	19.88
26-Feb-21	D15	1N	2	11:09	13:10	2:01:00	7,192.01	3172	y = 39115.03 - (301.68*x)	21,014.23	y = 197.80 + (1047.23*x)	19.88
26-Feb-21	D15	1N	1	11:09	13:11	2:02:00	3,063.26	1208	y = 19981.88 - (153.46*x)	10,774.28	y = 197.80 + (1047.23*x)	10.10
26-Feb-21	D15	1N	2	11:09	13:13	2:04:00	5,233.49	1748	y = 39115.03 - (301.68*x)	21,014.23	y = 197.80 + (1047.23*x)	19.88
26-Feb-21	D15	1N	2	11:09	13:14	2:05:00	3,219.95	1312	y = 39115.03 - (301.68*x)	21,014.23	y = 197.80 + (1047.23*x)	19.88
01-Mar-21	D18	1N	1	11:20	12:01	0:41:00	4,331,195.70	471252	y = 672821 - (4168*x)	422,741.00	y = -125398.3 + (11483.0*x)	47.73
01-Mar-21	D18	1N	2	11:20	12:03	0:43:00	5,373,898.93	538568	y = 651788.9 - (2650.6*x)	492,752.90	y = -125398.3 + (11483.0*x)	53.83
01-Mar-21	D18	1C	1	11:10	12:06	0:56:00	2,663,116.41	256280	y = 534358 - (5726*x)	190,798.00	y = -125398.3 + (11483.0*x)	27.54
01-Mar-21	D18	1C	1	11:10	12:08	0:58:00	1,851,453.66	183760	y = 534358 - (5726*x)	190,798.00	y = -125398.3 + (11483.0*x)	27.54
01-Mar-21	D18	1C	1	11:10	12:09	0:59:00	1,690,800.53	163348	y = 534358 - (5726*x)	190,798.00	y = -125398.3 + (11483.0*x)	27.54
01-Mar-21	D18	1C	2	11:10	12:11	1:01:00	2,242,067.33	195572	y = 243151.9 - (789.6*x)	195,775.90	y = -125398.3 + (11483.0*x)	27.97
01-Mar-21	D18	1C	2	11:10	12:12	1:02:00	2,381,494.54	193720	y = 243151.9 - (789.6*x)	195,775.90	y = -125398.3 + (11483.0*x)	27.97
01-Mar-21	D18	1N	1	11:20	12:14	0:54:00	3,849,390.94	490720	y = 672821 - (4168*x)	422,741.00	y = -125398.3 + (11483.0*x)	47.73
01-Mar-21	D18	1N	1	11:20	12:15	0:55:00	3,999,533.60	466464	y = 672821 - (4168*x)	422,741.00	y = -125398.3 + (11483.0*x)	47.73
01-Mar-21	D18	1N	2	11:20	12:17	0:57:00	4,349,282.80	491080	y = 651788.9 - (2650.6*x)	492,752.90	y = -125398.3 + (11483.0*x)	53.83
01-Mar-21	D18	1N	2	11:20	12:18	0:58:00	4,655,556.53	506772	y = 651788.9 - (2650.6*x)	492,752.90	y = -125398.3 + (11483.0*x)	53.83
01-Mar-21	D18	1C	1	11:10	12:21	1:11:00	1,338,353.73	136920	y = 534358 - (5726*x)	190,798.00	y = -125398.3 + (11483.0*x)	27.54
01-Mar-21	D18	1C	2	11:10	12:23	1:13:00	2,058,203.60	183596	y = 243151.9 - (789.6*x)	195,775.90	y = -125398.3 + (11483.0*x)	27.97
01-Mar-21	D18	1C	2	11:10	12:24	1:14:00	2,220,870.13	186524	y = 243151.9 - (789.6*x)	195,775.90	y = -125398.3 + (11483.0*x)	27.97
01-Mar-21	D18	1N	1	11:20	12:26	1:06:00	3,250,841.87	362592	y = 672821 - (4168*x)	422,741.00	y = -125398.3 + (11483.0*x)	47.73
01-Mar-21	D18	1N	2	11:20	12:29	1:09:00	3,807,080.00	469052	y = 651788.9 - (2650.6*x)	492,752.90	y = -125398.3 + (11483.0*x)	53.83
03-Mar-21	D20	N	1	11:07	11:40	0:33:00	5,385,387.76	601668	y = 800004 - (7218*x)	366,924.00	y = -192977 + (14329*x)	39.07
03-Mar-21	D20	N	1	11:07	11:41	0:34:00	4,782,571.63	514860	y = 800004 - (7218*x)	366,924.00	y = -192977 + (14329*x)	39.07
03-Mar-21	D20	N	2	11:07	11:43	0:36:00	4,875,986.95	430672	y = 506833 - (4102*x)	260,713.00	y = -192977 + (14329*x)	31.66

Date	Day	Sam-ple	Repli-cation	Samp-ling Time	Analy-sis Time	Time Differ-ence	Area	Maximum Height	Equation of Max Height vs Time for Extrapolation	Max height from extrapolation (t=60)	Calibration (Max Height vs Fe (II) Conc)	Fe (II) (nm) (t=60)
03-Mar-21	D20	N	2	11:07	11:44	0:37:00	3,831,537.37	279060	y = 506833 - (4102*x)	260,713.00	y = -192977 + (14329*x)	31.66
03-Mar-21	D20	N	2	11:07	12:00	0:53:00	3,962,173.98	293884	y = 506833 - (4102*x)	260,713.00	y = -192977 + (14329*x)	31.66
03-Mar-21	D20	N	1	11:07	12:11	1:04:00	3,263,377.66	293884	y = 800004 - (7218*x)	366,924.00	y = -192977 + (14329*x)	39.07
03-Mar-21	D20	N	1	11:07	12:12	1:05:00	3,155,179.92	374840	y = 800004 - (7218*x)	366,924.00	y = -192977 + (14329*x)	39.07
04-Mar-21	D21	C	1	11:15	12:17	1:02:00	5,372,628.98	578388	y = 1277639 - (10912*x)	622,919.00	y = -142550 + (12785*x)	59.87
04-Mar-21	D21	C	1	11:15	12:18	1:03:00	5,018,703.17	566212	y = 1277639 - (10912*x)	622,919.00	y = -142550 + (12785*x)	59.87
04-Mar-21	D21	C	2	11:15	12:20	1:05:00	4,795,499.16	500772	y = 841049.7 - (5032.1*x)	539,123.70	y = -142550 + (12785*x)	53.32
04-Mar-21	D21	C	2	11:15	12:21	1:06:00	4,622,915.53	511856	y = 841049.7 - (5032.1*x)	539,123.70	y = -142550 + (12785*x)	53.32
04-Mar-21	D21	N	1	11:25	12:23	0:58:00	5,370,228.06	724064	y = 1164091 - (8080*x)	679,291.00	y = -142550 + (12785*x)	64.28
04-Mar-21	D21	N	1	11:25	12:24	0:59:00	5,380,972.77	655360	y = 1164091 - (8080*x)	679,291.00	y = -142550 + (12785*x)	64.28
04-Mar-21	D21	N	2	11:25	12:26	1:01:00	5,177,831.64	655360	y = 683005.4 - (443.8*x)	656,377.40	y = -142550 + (12785*x)	62.49
04-Mar-21	D21	N	2	11:25	12:27	1:02:00	4,757,895.51	655360	y = 683005.4 - (443.8*x)	656,377.40	y = -142550 + (12785*x)	62.49
04-Mar-21	D21	C	1	11:15	12:29	1:14:00	4,889,834.70	534592	y = 1277639 - (10912*x)	622,919.00	y = -142550 + (12785*x)	59.87
04-Mar-21	D21	C	1	11:15	12:30	1:15:00	4,209,508.04	463296	y = 1277639 - (10912*x)	622,919.00	y = -142550 + (12785*x)	59.87
04-Mar-21	D21	C	1	11:15	12:32	1:17:00	3,965,093.63	452028	y = 1277639 - (10912*x)	622,919.00	y = -142550 + (12785*x)	59.87
04-Mar-21	D21	C	2	11:15	12:33	1:18:00	4,187,493.93	462980	y = 841049.7 - (5032.1*x)	539,123.70	y = -142550 + (12785*x)	53.32
04-Mar-21	D21	C	2	11:15	12:35	1:20:00	4,149,939.88	444180	y = 841049.7 - (5032.1*x)	539,123.70	y = -142550 + (12785*x)	53.32
04-Mar-21	D21	N	1	11:25	12:36	1:11:00	5,158,451.94	599524	y = 1164091 - (8080*x)	679,291.00	y = -142550 + (12785*x)	64.28
04-Mar-21	D21	N	1	11:25	12:38	1:13:00	4,828,630.21	568432	y = 1164091 - (8080*x)	679,291.00	y = -142550 + (12785*x)	64.28
04-Mar-21	D21	N	2	11:25	12:39	1:14:00	4,885,633.86	655360	y = 683005.4 - (443.8*x)	656,377.40	y = -142550 + (12785*x)	62.49
04-Mar-21	D21	N	2	11:25	12:41	1:16:00	4,913,772.64	644780	y = 683005.4 - (443.8*x)	656,377.40	y = -142550 + (12785*x)	62.49
04-Mar-21	D21	C	1	11:15	12:45	1:30:00	2,492,491.51	259052	y = 1277639 - (10912*x)	622,919.00	y = -142550 + (12785*x)	59.87
04-Mar-21	D21	C	2	11:15	12:48	1:33:00	2,354,282.49	363212	y = 841049.7 - (5032.1*x)	539,123.70	y = -142550 + (12785*x)	53.32
05-Mar-21	D22	1N	1	11:05	12:04	0:59:00	5,006,184.50	556712	y = 1052534 - (8404*x)	548,294.00	y = -44089 + (12014*x)	49.31
05-Mar-21	D22	1N	2	11:05	12:05	1:00:00	4,945,037.75	560780	y = 1070227 - (8495*x)	560,527.00	y = -44089 + (12014*x)	50.33

Date	Day	Sam-ple	Repli-cation	Samp-ling Time	Analy-sis Time	Time Differ-ence	Area	Maximum Height	Equation of Max Height vs Time for Extrapolation	Max height from extrapolation (t=60)	Calibration (Max Height vs Fe (II) Conc)	Fe (II) (nm) (t=60)
05-Mar-21	D22	1N	2	11:05	12:07	1:02:00	5,368,244.79	405772	y = 1070227 - (8495*x)	560,527.00	y = -44089 + (12014*x)	50.33
05-Mar-21	D22	2N	1	11:15	12:08	0:53:00	4,649,580.39	417228	y = exp (13.617999 - 0.013223*x)	371,245.56	y = -44089 + (12014*x)	34.57
05-Mar-21	D22	2N	1	11:15	12:10	0:55:00	4,338,010.58	397372	y = exp (13.617999 - 0.013223*x)	371,245.56	y = -44089 + (12014*x)	34.57
05-Mar-21	D22	1N	1	11:05	12:18	1:13:00	4,914,919.17	655360	y = 1052534 - (8404*x)	548,294.00	y = -44089 + (12014*x)	49.31
05-Mar-21	D22	1N	2	11:05	12:21	1:16:00	5,265,263.65	420604	y = 1070227 - (8495*x)	560,527.00	y = -44089 + (12014*x)	50.33
05-Mar-21	D22	1N	2	11:05	12:22	1:17:00	4,393,829.55	419920	y = 1070227 - (8495*x)	560,527.00	y = -44089 + (12014*x)	50.33
05-Mar-21	D22	2N	1	11:15	12:24	1:09:00	3,514,676.17	313796	y = exp (13.617999 - 0.013223*x)	371,245.56	y = -44089 + (12014*x)	34.57
05-Mar-21	D22	1N	2	11:05	12:38	1:33:00	4,545,671.30	594272	y = 1070227 - (8495*x)	560,527.00	y = -44089 + (12014*x)	50.33
05-Mar-21	D22	1N	1	11:05	12:39	1:34:00	3,396,592.42	262580	y = 1052534 - (8404*x)	548,294.00	y = -44089 + (12014*x)	49.31
05-Mar-21	D22	2N	1	11:15	12:42	1:27:00	2,311,705.27	265824	y = exp (13.617999 - 0.013223*x)	371,245.56	y = -44089 + (12014*x)	34.57
08-Mar-21	D25	1C	1	11:19	12:30	1:11:00	2,888,323.14	252964	y = 345870.8 - (1334.8*x)	265,782.80	y = -139510 + (12803*x)	31.66
08-Mar-21	D25	1C	1	11:19	12:31	1:12:00	2,812,746.62	242584	y = 345870.8 - (1334.8*x)	265,782.80	y = -139510 + (12803*x)	31.66
08-Mar-21	D25	1C	1	11:19	12:33	1:14:00	2,859,944.49	252756	y = 345870.8 - (1334.8*x)	265,782.80	y = -139510 + (12803*x)	31.66
08-Mar-21	D25	1C	2	11:19	12:34	1:15:00	3,030,186.70	253312	y = 313737.02 - (829.87*x)	263,944.82	y = -139510 + (12803*x)	31.51
08-Mar-21	D25	1C	2	11:19	12:36	1:17:00	3,019,917.06	247448	y = 313737.02 - (829.87*x)	263,944.82	y = -139510 + (12803*x)	31.51
08-Mar-21	D25	1N	1	11:37	12:40	1:03:00	2,188,514.57	354328	y = exp (14.2031 - 0.0257*x)	315,243.30	y = -139510 + (12803*x)	35.52
08-Mar-21	D25	1N	1	11:37	12:42	1:05:00	1,993,028.75	290636	y = exp (14.2031 - 0.0257*x)	315,243.30	y = -139510 + (12803*x)	35.52
08-Mar-21	D25	1C	2	11:19	12:55	1:36:00	2,343,570.73	234856	y = 313737.02 - (829.87*x)	263,944.82	y = -139510 + (12803*x)	31.51
08-Mar-21	D25	1C	1	11:19	12:58	1:39:00	2,182,475.55	213372	y = 345870.8 - (1334.8*x)	265,782.80	y = -139510 + (12803*x)	31.66
08-Mar-21	D25	2C	1	11:27	13:02	1:35:00	2,941,311.37	291256	y = 507400.0 - (2286.2*x)	370,228.00	y = -139510 + (12803*x)	39.81
08-Mar-21	D25	1N	2	11:37	13:06	1:29:00	2,914,171.21	259272	y = exp (13.4967 - 0.010096*x)	396,703.33	y = -139510 + (12803*x)	41.88
08-Mar-21	D25	1N	2	11:37	13:08	1:31:00	2,977,070.42	263940	y = exp (13.4967 - 0.010096*x)	396,703.33	y = -139510 + (12803*x)	41.88
08-Mar-21	D25	1N	2	11:37	13:10	1:33:00	3,034,084.95	297444	y = exp (13.4967 - 0.010096*x)	396,703.33	y = -139510 + (12803*x)	41.88
08-Mar-21	D25	1N	1	11:37	13:13	1:36:00	1,416,634.01	116124	y = exp (14.2031 - 0.0257*x)	315,243.30	y = -139510 + (12803*x)	35.52
08-Mar-21	D25	1N	1	11:37	13:15	1:38:00	1,430,233.06	113388	y = exp (14.2031 - 0.0257*x)	315,243.30	y = -139510 + (12803*x)	35.52

Date	Day	Sam-ple	Repli-cation	Samp-ling Time	Analy-sis Time	Time Differ-ence	Area	Maximum Height	Equation of Max Height vs Time for Extrapolation	Max height from extrapolation (t=60)	Calibration (Max Height vs Fe (II) Conc)	Fe (II) (nm) (t=60)
08-Mar-21	D25	2N	1	11:45	13:17	1:32:00	2,331,546.23	199900	y = exp (12.7811 - 0.005731*x)	252,009.99	y = -139510 + (12803*x)	30.58
08-Mar-21	D25	2N	1	11:45	13:19	1:34:00	2,286,404.39	225008	y = exp (12.7811 - 0.005731*x)	252,009.99	y = -139510 + (12803*x)	30.58
08-Mar-21	D25	2C	1	11:27	13:21	1:54:00	2,285,711.18	235852	y = 507400.0 - (2286.2*x)	370,228.00	y = -139510 + (12803*x)	39.81
08-Mar-21	D25	2C	1	11:27	13:23	1:56:00	2,449,790.71	252092	y = 507400.0 - (2286.2*x)	370,228.00	y = -139510 + (12803*x)	39.81
08-Mar-21	D25	1C	2	11:19	13:27	2:08:00	1,993,873.27	207448	y = 313737.02 - (829.87*x)	263,944.82	y = -139510 + (12803*x)	31.51
08-Mar-21	D25	1C	2	11:19	13:30	2:11:00	1,925,091.51	204876	y = 313737.02 - (829.87*x)	263,944.82	y = -139510 + (12803*x)	31.51
08-Mar-21	D25	1N	1	11:37	13:32	1:55:00	1,067,836.52	83632	y = exp (14.2031 - 0.0257*x)	315,243.30	y = -139510 + (12803*x)	35.52
08-Mar-21	D25	1N	2	11:37	13:36	1:59:00	1,960,967.90	235616	y = exp (13.4967 - 0.010096*x)	396,703.33	y = -139510 + (12803*x)	41.88
08-Mar-21	D25	2N	1	11:45	13:38	1:53:00	2,199,023.55	181844	y = exp (12.7811 - 0.005731*x)	252,009.99	y = -139510 + (12803*x)	30.58

Remarks:

Sample 1C = Sample from control treatment from replication 1

Sample 2C = Sample from control treatment control from replication 2

Sample 1N = Sample from nitrate-added treatment from replication 1

Sample 2N = Sample from nitrate-added treatment from replication 2

Replication column means measurement repetition from each samples

Appendix 2: ICP-MS Results

Number	No.	Sample Name	Date	Day	Sample	Replication	Sampling Time	Acidifying Time	Mn ug/L	Mn RSD (%)	Fe ug/L	Fe RSD (%)
2021-2946	1	D0-1C-1	11/2/21	0	1C	1	10:45:00	13:31:00	18	0.9	43	2.1
2021-2947	2	D0-1C-2	11/2/21	0	1C	2	10:45:00	13:31:00	28	1.2	54	1.2
2021-2948	3	D0-1C-3	11/2/21	0	1C	3	10:45:00	13:31:00	27	0.7	52	0.7
2021-2949	4	D0-2C-1	11/2/21	0	2C	1	10:55:00	13:36:00	28	0.4	55	0.1
2021-2950	5	D0-2C-2	11/2/21	0	2C	2	10:55:00	13:36:00	29	1.3	56	1.3
2021-2951	6	D0-2C-3	11/2/21	0	2C	3	10:55:00	13:36:00	29	0.5	60	1.3
2021-2952	7	D1-1C-1	12/2/21	1	1C	1	11:23:00	14:53:00	31	0.5	48	2.2
2021-2953	8	D1-1C-2	12/2/21	1	1C	2	11:23:00	14:53:00	42	0.8	55	0.6
2021-2954	9	D1-2C-1	12/2/21	1	2C	1	11:35:00	15:16:00	37	1.2	51	1.1
2021-2955	10	D1-2C-2	12/2/21	1	2C	2	11:35:00	15:16:00	37	1.1	53	1.5
2021-2956	11	D1-1N-1	12/2/21	1	1N	1	11:47:00	15:45:00	48	0.6	54	1.5
2021-2957	12	D1-1N-2	12/2/21	1	1N	2	11:47:00	15:45:00	49	1.5	54	1.2
2021-2958	13	D1-2N-1	12/2/21	1	2N	1	12:00:00	15:45:00	42	1.1	55	1.1
2021-2959	14	D1-2N-2	12/2/21	1	2N	2	12:00:00	15:45:00	47	0.3	54	1.5
2021-2960	15	D2-1C-1	13/2/21	2	1C	1	11:22:00	13:58:00	47	0.6	90	1.3
2021-2961	16	D2-1C-2	13/2/21	2	1C	2	11:22:00	13:58:00	56	0.2	93	0.7
2021-2962	17	D2-2C-1	13/2/21	2	2C	1	11:30:00	13:58:00	58	1.2	85	1.2
2021-2963	18	D2-2C-2	13/2/21	2	2C	2	11:30:00	13:58:00	58	0.5	93	0.7
2021-2964	19	D2-1N-1	13/2/21	2	1N	1	11:38:00	13:58:00	53	0.7	141	0.6
2021-2965	20	D2-1N-2	13/2/21	2	1N	2	11:38:00	13:58:00	64	0.8	113	0.8

Number	No.	Sample Name	Date	Day	Sample	Replication	Sampling Time	Acidifying Time	Mn ug/L	Mn RSD (%)	Fe ug/L	Fe RSD (%)
	QC 50 000x								4.2	0.4	4.8	1.0
	QC 1000x								188	1.0	189	0.6
2021-2966	21	D2-2N-1	13/2/21	2	2N	1	11:45:00	13:58:00	58	1.2	84	0.8
2021-2967	22	D2-2N-2	13/2/21	2	2N	2	11:45:00	13:58:00	54	1.1	100	1.4
2021-2968	23	D3-1C-1	14/2/21	3	1C	1	11:21:00	13:28:00	62	0.4	115	0.7
2021-2969	24	D3-1C-2	14/2/21	3	1C	2	11:21:00	13:28:00	50	0.3	103	1.0
2021-2970	25	D3-2C-1	14/2/21	3	2C	1	11:33:00	13:36:00	65	1.1	106	1.0
2021-2971	26	D3-2C-2	14/2/21	3	2C	2	11:33:00	13:36:00	65	0.3	106	0.7
2021-2972	27	D3-1N-1	14/2/21	3	1N	1	11:42:00	13:40:00	61	1.1	73	1.8
2021-2973	28	D3-1N-2	14/2/21	3	1N	2	11:42:00	13:40:00	69	1.1	61	1.8
2021-2974	29	D3-2N-1	14/2/21	3	2N	1	11:52:00	13:49:00	77	0.3	57	1.2
2021-2975	30	D3-2N-2	14/2/21	3	2N	2	11:52:00	13:49:00	78	1.3	60	1.2
2021-2976	31	D4-1C-1	15/2/21	4	1C	1	11:13:00	13:08:00	44	0.9	101	1.1
2021-2977	32	D4-1C-2	15/2/21	4	1C	2	11:13:00	13:08:00	54	1.0	102	1.4
2021-2978	33	D4-2C-1	15/2/21	4	2C	1	11:22:00	13:08:00	76	0.6	97	1.1
2021-2979	34	D4-2C-2	15/2/21	4	2C	2	11:22:00	13:08:00	80	0.9	91	0.4
2021-2980	35	D4-1N-1	15/2/21	4	1N	1	11:32:00	13:10:00	63	0.5	56	1.7
2021-2981	36	D4-1N-2	15/2/21	4	1N	2	11:32:00	13:10:00	75	0.9	57	1.5
2021-2982	37	D4-2N-1	15/2/21	4	2N	1	11:41:00	13:10:00	86	0.7	60	0.7
2021-2983	38	D4-2N-2	15/2/21	4	2N	2	11:41:00	13:10:00	83	0.2	55	1.2
2021-2984	39	D5-1C-1	16/2/21	5	1C	1	11:16:00	12:37:00	75	0.5	154	1.1

Number	No.	Sample Name	Date	Day	Sample	Replication	Sampling Time	Acidifying Time	Mn ug/L	Mn RSD (%)	Fe ug/L	Fe RSD (%)
2021-2985	40	D5-1C-2	16/2/21	5	1C	2	11:16:00	12:37:00	67	0.6	154	0.5
	QC 50 000x								4.6	0.5	5.3	0.4
	QC 1000x								203	0.7	206	1.1
2021-2986	41	D5-2C-1	16/2/21	5	2C	1	11:26:00	12:37:00	75	0.9	129	0.5
2021-2987	42	D5-2C-2	16/2/21	5	2C	2	11:26:00	12:37:00	79	0.7	124	0.6
2021-2988	43	D5-1N-1	16/2/21	5	1N	1	11:39:00	12:39:00	80	0.2	50	1.0
2021-2989	44	D5-1N-2	16/2/21	5	1N	2	11:39:00	12:39:00	86	0.7	52	2.1
2021-2990	45	D5-2N-1	16/2/21	5	2N	1	11:58:00	12:39:00	85	1.6	52	1.0
2021-2991	46	D5-2N-2	16/2/21	5	2N	2	11:58:00	12:39:00	85	1.0	56	0.4
2021-2992	47	D6-1C-1	17/2/21	6	1C	1	11:19:00	11:27:00	78	0.8	185	0.7
2021-2993	48	D6-1C-2	17/2/21	6	1C	2	11:19:00	11:27:00	95	0.3	170	0.8
2021-2994	49	D6-2C-1	17/2/21	6	2C	1	11:27:00	11:27:00	101	0.2	169	0.7
2021-2995	50	D6-2C-2	17/2/21	6	2C	2	11:27:00	11:27:00	103	0.4	134	0.8
2021-2996	51	D6-1N-1	17/2/21	6	1N	1	11:42:00	11:28:00	86	0.7	57	1.1
2021-2997	52	D6-1N-2	17/2/21	6	1N	2	11:42:00	11:28:00	93	0.7	51	1.3
2021-2998	53	D6-2N-1	17/2/21	6	2N	1	11:53:00	11:28:00	97	0.9	53	1.2
2021-2999	54	D6-2N-2	17/2/21	6	2N	2	11:53:00	11:28:00	99	0.3	55	0.8
2021-3000	55	D7-1C-1	18/2/21	7	1C	1	11:16:00	12:08:00	85	0.9	193	0.9
2021-3001	56	D7-1C-2	18/2/21	7	1C	2	11:16:00	12:08:00	99	1.0	221	0.7
2021-3002	57	D7-2C-1	18/2/21	7	2C	1	11:29:00	12:08:00	103	0.5	183	0.9
2021-3003	58	D7-2C-2	18/2/21	7	2C	2	11:29:00	12:08:00	106	0.7	156	0.9

Number	No.	Sample Name	Date	Day	Sample	Replication	Sampling Time	Acidifying Time	Mn ug/L	Mn RSD (%)	Fe ug/L	Fe RSD (%)
2021-3004	59	D8-1C-1	19/2/21	8	1C	1	11:15:00	13:50:00	82	1.1	232	1.0
2021-3005	60	D8-1C-2	19/2/21	8	1C	2	11:15:00	13:50:00	101	0.7	252	0.6
	QC 50 000x								4.5	0.6	5.2	0.9
	QC 1000x								203	0.9	206	1.0
2021-3006	61	D8-2C-1	19/2/21	8	2C	1	11:23:00	13:50:00	98	0.5	253	0.9
2021-3007	62	D8-2C-2	19/2/21	8	2C	2	11:23:00	13:50:00	103	0.6	263	0.7
2021-3008	63	D8-1N-1	19/2/21	8	1N	1	11:33:00	13:50:00	83	1.1	54	1.3
2021-3009	64	D8-1N-2	19/2/21	8	1N	2	11:33:00	13:50:00	94	0.5	52	1.1
2021-3010	65	D8-2N-1	19/2/21	8	2N	1	11:40:00	13:50:00	103	0.5	57	1.2
2021-3011	66	D8-2N-2	19/2/21	8	2N	2	11:40:00	13:50:00	106	1.1	56	1.1
2021-3012	67	D9-1C-1	20/2/21	9	1C	1	11:12:00	12:24:00	73	0.8	183	0.5
2021-3013	68	D9-1C-2	20/2/21	9	1C	2	11:12:00	12:24:00	83	1.0	218	0.8
2021-3014	69	D9-2C-1	20/2/21	9	2C	1	11:20:00	12:24:00	104	1.1	139	1.0
2021-3015	70	D9-2C-2	20/2/21	9	2C	2	11:20:00	12:24:00	105	1.0	264	1.0
2021-3016	71	D10-1C-1	21/2/21	10	1C	1	11:17:00	12:28:00	92	0.7	207	1.6
2021-3017	72	D10-1C-2	21/2/21	10	1C	2	11:17:00	12:28:00	95	0.6	172	0.5
2021-3018	73	D10-2C-1	21/2/21	10	2C	1	11:26:00	12:28:00	107	0.9	212	1.0
2021-3019	74	D10-2C-2	21/2/21	10	2C	2	11:26:00	12:28:00	109	0.7	249	0.5
2021-3020	75	D11-1N-1	22/2/21	11	1N	1	11:14:00	12:07:00	86	0.4	118	0.6
2021-3021	76	D11-1N-2	22/2/21	11	1N	2	11:14:00	12:07:00	101	1.1	128	0.7
2021-3022	77	D11-2N-1	22/2/21	11	2N	1	11:25:00	12:07:00	98	0.6	110	1.2

Number	No.	Sample Name	Date	Day	Sample	Replication	Sampling Time	Acidifying Time	Mn ug/L	Mn RSD (%)	Fe ug/L	Fe RSD (%)
2021-3023	78	D11-2N-2	22/2/21	11	2N	2	11:25:00	12:07:00	97	0.6	110	0.4
2021-3024	79	D13-1C-1	24/2/21	13	1C	1	11:16:00	11:54:00	119	1.6	238	1.1
2021-3025	80	D13-1C-2	24/2/21	13	1C	2	11:16:00	11:54:00	122	0.7	271	0.5
	QC 50 000x								4.6	0.8	5.3	1.1
	QC 1000x								207	0.6	208	0.6
2021-3026	81	D13-1N-1	24/2/21	13	1N	1	11:25:00	11:54:00	89	0.4	138	0.7
2021-3027	82	D13-1N-2	24/2/21	13	1N	2	11:25:00	11:54:00	96	0.8	126	0.6
2021-3028	83	D15-1N-1	26/2/21	15	1N	1	11:09:00	11:40:00	78	1.1	128	1.2
2021-3029	84	D15-1N-2	26/2/21	15	1N	2	11:09:00	11:40:00	95	0.3	138	0.4
2021-3030	85	D18-1C-1	1/3/21	18	1C	1	11:10:00	11:50:00	118	0.9	209	0.9
2021-3031	86	D18-1C-2	1/3/21	18	1C	2	11:10:00	11:50:00	125	0.7	226	0.3
2021-3032	87	D18-1N-1	1/3/21	18	1N	1	11:20:00	11:50:00	89	0.8	179	1.2
2021-3033	88	D18-1N-2	1/3/21	18	1N	2	11:20:00	11:50:00	103	0.4	217	0.9
2021-3034	89	D20-1N-1	3/3/21	20	1N	1	11:07:00	11:33:00	104	0.8	203	0.7
2021-3035	90	D20-1N-2	3/3/21	20	1N	2	11:07:00	11:33:00	107	1.0	235	0.3
2021-3036	91	D21-1C-1	4/3/21	21	1C	1	11:15:00	11:52:00	114	0.4	191	0.7
2021-3037	92	D21-1C-2	4/3/21	21	1C	2	11:15:00	11:52:00	122	0.6	221	0.3
2021-3038	93	D21-1N-1	4/3/21	21	1N	1	11:25:00	11:52:00	107	0.2	214	0.7
2021-3039	94	D21-1N-2	4/3/21	21	1N	2	11:25:00	11:52:00	110	0.2	242	0.4
2021-3040	95	D22-1N-1	5/3/21	22	1N	1	11:05:00	11:52:00	104	0.7	224	1.1
2021-3041	96	D22-1N-2	5/3/21	22	1N	2	11:05:00	11:52:00	104	1.4	249	0.7

Number	No.	Sample Name	Date	Day	Sample	Replication	Sampling Time	Acidifying Time	Mn ug/L	Mn RSD (%)	Fe ug/L	Fe RSD (%)
2021-3042	97	D22-2N-1	5/3/21	22	2N	1	11:15:00	11:52:00	107	0.6	255	0.3
2021-3043	98	D25-1C-1	8/3/21	25	1C	1	11:19:00	12:22:00	119	0.6	198	0.4
2021-3044	99	D25-1C-2	8/3/21	25	1C	2	11:19:00	12:22:00	121	0.4	251	0.2
2021-3045	100	D25-2C-1	8/3/21	25	2C	1	11:27:00	12:22:00	122	0.7	261	0.4
	QC 50 000x								4.5	0.4	5.2	0.7
2021-3046	101	D25-1N-1	8/3/21	25	1N	1	11:37:00	12:22:00	104	1.1	193	1.0
2021-3047	102	D25-1N-2	8/3/21	25	1N	2	11:37:00	12:22:00	102	0.7	226	0.6
2021-3048	103	D25-2N-1	8/3/21	25	2N	1	11:45:00	12:22:00	107	0.5	214	0.4
2021-3049	104	Seawater1	24/3/21		Blank	1			2.2	3.0	61	1.4
2021-3050	105	Seawater2	24/3/21		Blank	2			*0.23*	10.8	49	1.0
2021-3051	106	Seawater3	24/3/21		Blank	3			*0.27*	11.0	48	1.6
2021-3052	107	Seawater4	24/3/21		Blank	4			0.59	5.8	49	1.1
2021-3053	108	Seawater5	24/3/21		Blank	5			0.50	4.8	51	1.6
2021-3054	109	NASS1	24/3/21		Standard	1			2.1	3.7	39	1.4
2021-3055	110	NASS2	24/3/21		Standard	2			2.1	3.6	39	0.9
2021-3056	111	NASS3	24/3/21		Standard	3			2.0	2.8	39	0.5
2021-3057	112	NASS4	24/3/21		Standard	4			2.0	4.8	40	0.9
2021-3058	113	NASS5	24/3/21		Standard	5			2.0	6.7	39	2.8
LOD									0.003		0.006	
LOQ (LOD * 3,3)									0.009		0.019	
LOD (corrected for the 30x dilution)									0.08		0.17	

LOQ (corrected for the 30x dilution)							0.28	0.56

Remarks:

Sample 1C = Sample from control treatment from replication 1

Sample 2C = Sample from control treatment control from replication 2

Sample 1N = Sample from nitrate-added treatment from replication 1

Sample 2N = Sample from nitrate-added treatment from replication 2

Replication column means measurement repetition from each samples

Appendix 3: H_2S Measurement

Treatment	Replication	Date	Day	Dilution	Absorbance	Transmittance (%)	Background Abs	Background Transmittance (%)	Final Abs	Sulfide (μM)
C	1	11-Feb-21	0	1	0.397	40.1	0.187	65	0.21	7.77
C	2	11-Feb-21	0	1	0.36	43.6	0.213	61.2	0.147	5.02
N	1	11-Feb-21	0	1	0.397	40.1	0.187	65	0.21	7.77
N	2	11-Feb-21	0	1	0.36	43.6	0.213	61.2	0.147	5.02
C	1	12-Feb-21	1	1	0.77	16.8	0.245	56.9	0.525	21.51
C	2	12-Feb-21	1	1	0.669	21.4	0.283	52	0.386	15.45
N	1	12-Feb-21	1	1	0.593	25	0.301	50	0.292	11.35
N	2	12-Feb-21	1	1	0.578	26.4	0.316	48.3	0.262	10.04
N	1	13-Feb-21	2	1	0.464	34.4	0.166	68.2	0.298	11.61
N	2	13-Feb-21	2	1	0.396	40.2	0.157	69.7	0.239	9.03
C	1	13-Feb-21	2	10	0.302	49.9	0.011	97.6	0.291	113.02
C	2	13-Feb-21	2	10	0.342	45.5	0.009	97.8	0.333	131.35
N	1	14-Feb-21	3	1	0.338	45.9	0.246	56.7	0.092	2.62
N	2	14-Feb-21	3	1	0.37	42.7	0.283	52.1	0.087	2.40
C	1	14-Feb-21	3	10	0.392	40.5	0.023	94.9	0.369	147.06
C	2	14-Feb-21	3	10	0.404	39.4	0.024	94.6	0.38	151.86
N	1	15-Feb-21	4	1	0.27	53.7	0.278	52.8	-0.008	0.00
N	2	15-Feb-21	4	1	0.326	46.9	0.264	54.4	0.062	1.31
C	1	15-Feb-21	4	10	0.468	34	0.031	93.1	0.437	176.73
C	2	15-Feb-21	4	10	0.534	29.3	0.023	94.8	0.511	209.02
N	1	16-Feb-21	5	1	0.264	54.5	0.288		-0.024	0.00
N	2	16-Feb-21	5	1	0.296	50.6	0.221	60.1	0.075	1.88
C	1	16-Feb-21	5	10	0.546	28.4	0.039	91.4	0.507	207.28
C	2	16-Feb-21	5	10	0.613	24.4	0.046	89.9	0.567	233.46
N	1	17-Feb-21	6	1	0.267	54.1	0.242	57.3	0.025	0.00

Treatment	Replication	Date	Day	Dilution	Absorbance	Transmittance (%)	Background Abs	Background Transmittance (%)	Final Abs	Sulfide (μM)
N	2	17-Feb-21	6	1	0.267	54	0.282	52.2	-0.015	0.00
C	1	17-Feb-21	6	10	0.863	83.7	0.044	90.5	0.819	343.43
C	2	17-Feb-21	6	10	0.8	15.9	0.047	89.7	0.753	314.63
C	1	18-Feb-21	7	100	0.187	65	0.005	98.8	0.182	654.56
C	2	18-Feb-21	7	100	0.203	62.7	0.004	99.1	0.199	728.75
N	1	19-Feb-21	8	1	0.352	44.5	0.336	46.2	0.016	0.00
N	2	19-Feb-21	8	1	0.411	38.5	0.338	46	0.073	1.79
C	1	19-Feb-21	8	100	0.449	35.6	0.003	99.4	0.446	1,806.60
C	2	19-Feb-21	8	100	0.423	37.7	0.004	99	0.419	1,688.78
C	1	20-Feb-21	9	100	0.563	27.3	0.004	99	0.559	2,299.70
C	2	20-Feb-21	9	100	0.573	26.7	0.006	98.7	0.567	2,334.61
C	1	21-Feb-21	10	100	0.573	26.7	0.003	99.3	0.57	2,347.70
C	2	21-Feb-21	10	100	0.578	26.4	0.005	98.8	0.573	2,360.80
N	1	22-Feb-21	11	1	0.301	41.6	0.268	53.9	0.033	0.04
N	2	22-Feb-21	11	1	0.396	40.2	0.273	53.3	0.123	3.97
N	1	24-Feb-21	13	1	0.487	32.6	0.273	53.3	0.214	7.94
C	1	24-Feb-21	13	100	0.602	25	0.005	98.8	0.597	2,465.53
N	1	26-Feb-21	15	1	0.888	12.9	0.381	41.6	0.507	20.73
N	1	01-Mar-21	18	10	0.864	13.5	0.038	91.7	0.826	346.48
C	1	01-Mar-21	18	100	0.603	24.9	0.005	98.9	0.598	2,469.89
N	1	03-Mar-21	20	100	0.386	41.1	0.004	99.1	0.382	1,527.32
C	1	04-Mar-21	21	100	0.563	27.4	0.006	98.7	0.557	2,290.98
N	1	04-Mar-21	21	100	0.514	30.6	0.004	99	0.51	2,085.88
N	1	05-Mar-21	22	100	0.51	30.9	0.003	99.4	0.507	2,072.79
N	2	05-Mar-21	22	100	0.471	33.8	0.004	99.1	0.467	1,898.24
C	1	08-Mar-21	25	100	0.666	21.6	0.004	99	0.662	2,749.17

Treatment	Replication	Date	Day	Dilution	Absorbance	Transmittance (%)	Background Abs	Background Transmittance (%)	Final Abs	Sulfide (μM)
C	2	08-Mar-21	25	100	0.646	22.6	0.013	97.1	0.633	2,622.62
N	1	08-Mar-21	25	100	0.588	25.9	0.003	99.2	0.585	2,413.16
N	2	08-Mar-21	25	100	0.584	26.1	0.003	99.3	0.581	2,395.71

Appendix 4: pH, Redox Potential, and Dissolved O2

Treatment	Replication	Date	Day	DO (mg/L)	Redox Potential (mV)	pH
C	1	11-Feb-21	0	7	16.4	7.33
C	2	11-Feb-21	0	6.8	13.7	7.2
N	1	11-Feb-21	0	7	16.4	7.33
N	2	11-Feb-21	0	6.8	13.7	7.2
C	1	12-Feb-21	1	1.2	-198.2	6.65
C	2	12-Feb-21	1	1.1	-169	6.78
N	1	12-Feb-21	1	0.4	-140.6	6.78
N	2	12-Feb-21	1	1.1	-111.6	6.67
N	1	13-Feb-21	2	0.6	-38	6.85
N	2	13-Feb-21	2	0.7	-33.3	6.59
C	1	13-Feb-21	2	0.9	-226.3	6.72
C	2	13-Feb-21	2	0.6	-199.4	6.63
N	1	14-Feb-21	3	1.4	-28.4	6.42
N	2	14-Feb-21	3	1.5	-48.9	6.37
C	1	14-Feb-21	3	1.3	-216.2	6.29
C	2	14-Feb-21	3	1.1	-217.2	6.21
N	1	15-Feb-21	4	1.5	1.8	6.24
N	2	15-Feb-21	4	1.7	11.3	6.3
C	1	15-Feb-21	4	1.5	-202.5	6.15
C	2	15-Feb-21	4	1.7	-208.6	6.11
N	1	16-Feb-21	5	2.3	-5	6.37
N	2	16-Feb-21	5	2.1	18.2	6.34
C	1	16-Feb-21	5	1.7	-205.7	6.12
C	2	16-Feb-21	5	1.7	-198.6	6.24
N	1	17-Feb-21	6	2	7.1	6.38
N	2	17-Feb-21	6	1.6	19.5	6.25
C	1	17-Feb-21	6	1.6	-208.4	6.24
C	2	17-Feb-21	6	1.3	-213.7	6.22
C	1	18-Feb-21	7	1.6	-220.3	6.23
C	2	18-Feb-21	7	1.4	-219.1	6.28
N	1	19-Feb-21	8	1.6	-54.6	6.3
N	2	19-Feb-21	8	1.3	-118.3	6.27
C	1	19-Feb-21	8	1.6	-245.5	6.24
C	2	19-Feb-21	8	1.2	-242.6	6.14
C	1	20-Feb-21	9	2.6	-253.3	6.21
C	2	20-Feb-21	9	1.4	-264.8	6.11
C	1	21-Feb-21	10	1.6	-267	6.15
C	2	21-Feb-21	10	1.3	-272.2	6.16
N	1	22-Feb-21	11	0.8	-112.1	6.96
N	2	22-Feb-21	11	0.4	-154.5	7.02

Treatment	Replication	Date	Day	DO (mg/L)	Redox Potential (mV)	pH
N	1	24-Feb-21	13	0.7	-213.8	6.74
C	1	24-Feb-21	13	0.9	-265.9	6.02
N	1	26-Feb-21	15	0.8	-222.2	6.75
N	1	01-Mar-21	18	0.8	-294.6	6.58
C	1	01-Mar-21	18	2.2	-297.3	5.97
N	1	03-Mar-21	20	0.7	-350.3	6.49
C	1	04-Mar-21	21	1.2	-305.6	5.98
N	1	04-Mar-21	21	0.9	-325.1	6.47
N	1	05-Mar-21	22	1.3	-292.2	6.38
N	2	05-Mar-21	22	0.6	-359.3	6.46
C	1	08-Mar-21	25	1.4	-309.3	5.92
C	2	08-Mar-21	25	1.3	-312.7	6.02
N	1	08-Mar-21	25	0.9	-320.9	6.42
N	2	08-Mar-21	25	1	-375.1	6.42

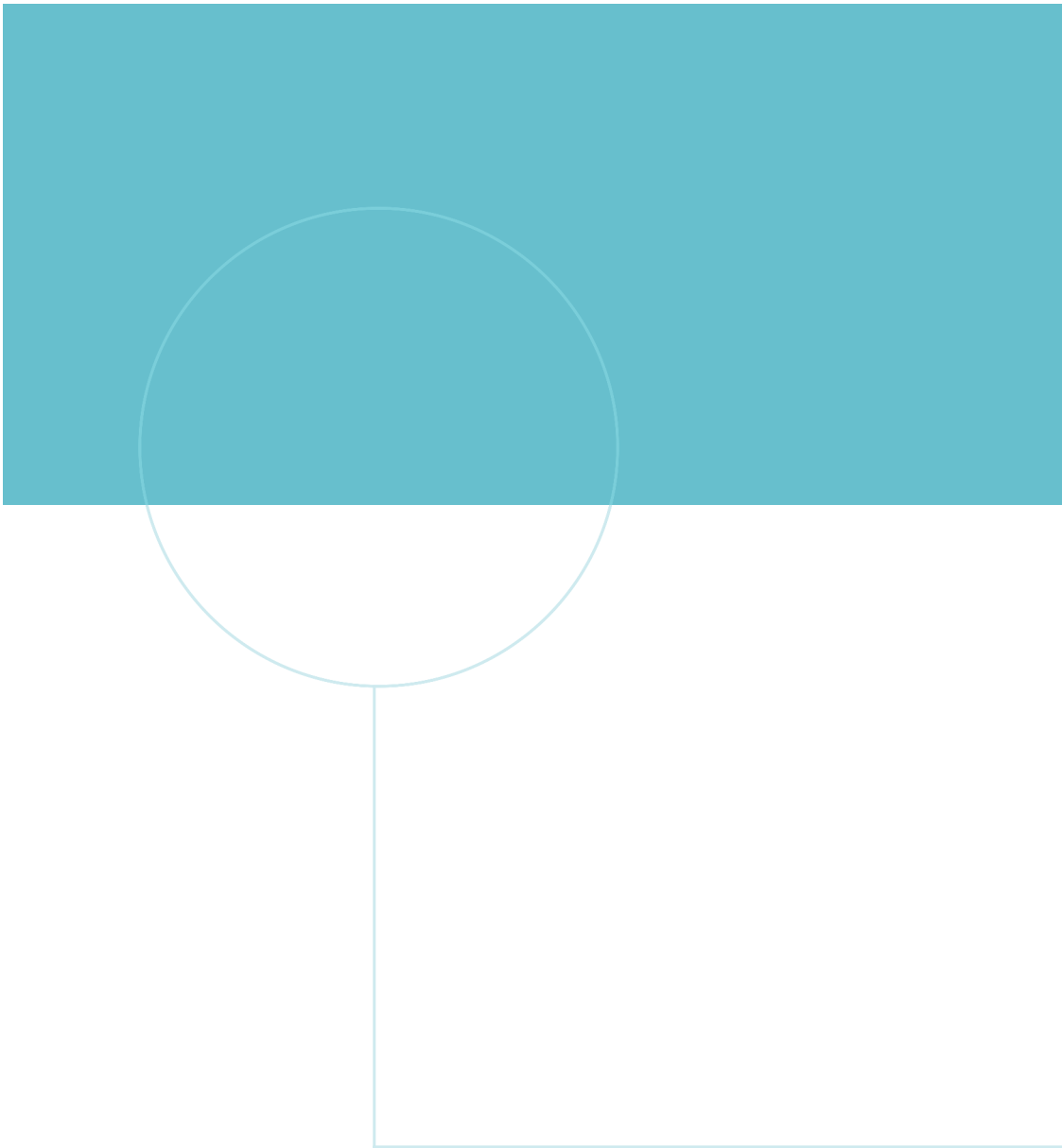

NTNU

Norwegian University of
Science and Technology